Charles University in Prague

Faculty of Mathematics and Physics

Luminescence and scintillation properties of phosphate glasses doped by Ce^{3+} and Tb^{3+} ions

Ph.D. thesis

Natalia Solovieva

Supervisor: **Ing. M. Nikl, CSc.**

Section: **F6 – Quantum optics and optoelectronics**

2007

Contents

Introduction

Scintillators are the principal elements of various kinds of high-energy radiation detectors. The increasing demand for scintillators in applications motivates the search for new scintillation materials. One of the interesting and promising types of such materials are scintillation glasses. The undoubted advantage of glasses is the low cost of their production, easy shaping and great variability of composition. At the same time, glass scintillation materials often suffer from a lower light yield than that of traditional single crystal scintillators. The further development of scintillation glasses aimed at the enhancement of their light yield requires a deeper understanding of the underlying microphysical processes of energy transfer and storage.

This dissertation is devoted to the energy transfer phenomena in phosphate glasses doped with Tb^{3+} or Ce^{3+} ions and enriched with Gd^{3+} ions. Based on a series of experiments, their main optical, luminescence and scintillation characteristics are collected and systemized, and then adequate theoretical models of the underlying energy transfer processes are selected.

The main text of the dissertation consists of six chapters, which are followed by the conclusions, the mathematical appendix, the list of references, and the list of the related publications of the author. Chapter 1 introduces the concept of scintillator, lists the key scintillator characteristics, and outlines possible ways of increasing the scintillation light yield. Chapter 2 reviews the existing models of energy transfer as a basic phenomenon in luminescent materials. Chapter 3 extends this review by narrowing the focus on Ce^{3+}-doped and Tb^{3+}-doped Gd^{3+}-enriched phosphate glasses. Chapter 4 provides technical details of the experiments. Chapters 5 and 6 present the experimental results and their discussion. Two different series of samples are examined here, which are referred to as the glasses of "the first" (Chapters 5) and "second" (Chapters 6) generations.

Chapter 1

Scintillators and their characteristics

A scintillation material is a kind of converter that transforms the energy of one high energy photon (X-ray, γ-ray) or particle (proton, electron, neutron, α-particle, etc.) into a number of UV/visible photons, which are easily detectable with a conventional photomultiplier tube, semiconductor detector, etc. (Fig. 1) [nikl2006]

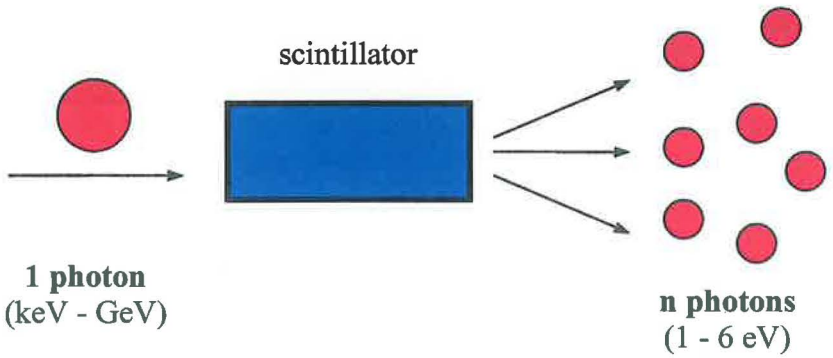

Fig. 1. Energy conversion in a scintillator

The scintillation method is widely used for the detection of different kinds of ionizing radiation. Inorganic scintillators find various applications in devices for high energy physics, tomography in medicine, safety precautions, astrophysics, well logging, etc. [rodnyi1997, ishii1991, grabmaier1993, grabmaier1994, andryushchenko2003, plastino2002, porras2002, gorin2002, schippers2002, schmidt2002, novotny2001, fouassier1997, melcher1991, barbon1996]

The scintillation process can be divided into three subprocesses (Fig. 2):

1) *Conversion* of high energy photon into electron-hole pairs and their thermalisation;
2) *Transport* of thermalised electron-hole pairs (or excitons) toward emission centers;
3) *Radiative de-excitation* of the emission centers.

The efficiency of a scintillator can be expressed as

$$\eta = \beta S Q, \tag{1}$$

where β, S, and Q denote the efficiencies of the conversion, transport, and radiative de-excitation respectively.

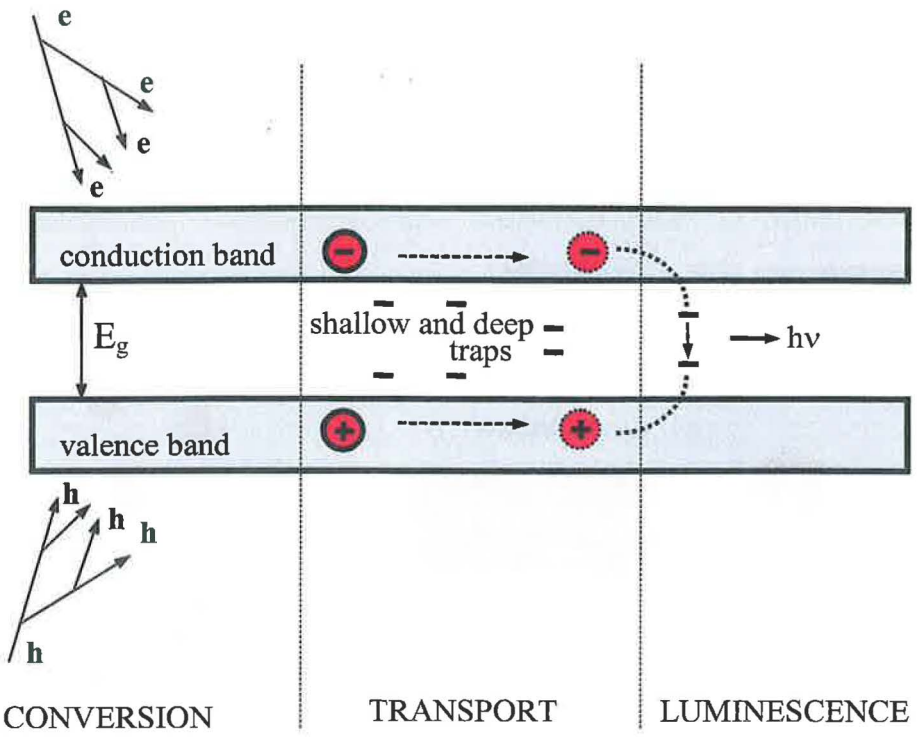

Fig. 2. Three stages of the scintillation process. *Conversion* is a very short process (a few picoseconds) that includes interaction of a high-energy photon with a material (photoeffect, Compton effect, pair production), creation of hot electron-hole pairs and their thermalization. *Transport* includes migration of electron-hole pairs (excitons) through the material, which is troubled with possible (repeated) trapping at defects, nonradiative recombination etc. *Luminescence* means trapping of opposite sign charge carriers at the luminescence centres and their radiative recombination.

The efficiency η is rather a theoretical concept. There are a few measurable scintillation characteristics that can be used in practice [rodnyi1997, nikl2000, nikl2006]. The search for new scintillation materials is guided by five main criteria: high light yield, integral scintillation efficiency, short decay time, low afterglow, and high density. Let us consider these key scintillation characteristics in more detail.

Light yield

The essential feature required of any scintillator is to be an effective and fast converter of ionizing radiation to visible light. Light yield L_R is defined as the number of emitted

(detected) photons N_{ph} per unit of absorbed energy E_γ (usually 1 MeV) within certain time gate (typically 10^2-10^4 ns) after high energy photon arrival:

$$L_R = \frac{N_{ph}}{E_\gamma}. \tag{2}$$

Integral scintillation efficiency

For estimation of this parameter the integral of the whole X-ray excited radioluminescence spectrum (or some separate bands of the spectrum) is calculated.

Duration of scintillation pulse and decay time

In the simplest case when the times of the conversion and transport are negligible with respect to the lifetime of luminescence centers, the intensity of the emission $I(t)$ of the scintillator with one type of luminescent center has the maximum at time $t = 0$ and decays exponentially with *the decay time constant* τ:

$$I(t) = A\exp\left(-\frac{t}{\tau}\right), \tag{3}$$

where A is the intensity at $t = 0$. However, in most of scintillation materials, *two or more decay time* constants can be detected, so that

$$I(t) = \sum A_i \exp\left(-\frac{t}{\tau_i}\right). \tag{4}$$

The presence of components with substantially long decay times (up to hundred microseconds) usually means that delayed recombination process takes place due to retrapping at shallow traps during the transport stage.

As an integral characteristic, a so-called *mean decay time* τ_{mean} is commonly used:

$$\tau_{mean} = \frac{\sum A_i \tau_i^2}{\sum A_i \tau_i}. \tag{5}$$

Another widely used quantity, which is suitable for the characterization of the initial slope of the decay curve, is $\tau_{1/e}$, which is defined as the solution to equation

$$I(\tau_{1/e}) = I(0)/e. \quad (6)$$

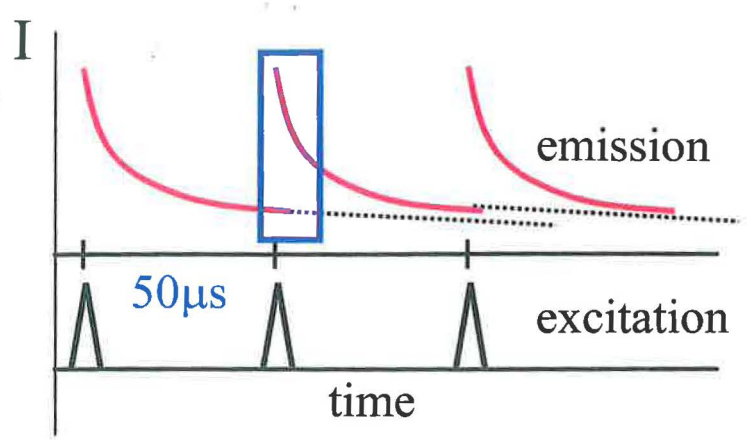

Fig. 3. Increasing of the decay background due to slow decay components

When measuring scintillation decay, it is sometimes impossible to estimate the slow component by the common decomposition into the sum of exponentials by formula (4). This relates to the fact that the frequency of the emission of the radioactive ^{22}Na source is constant, and consequently all the exponential components with decay times at 50 μs and above do not vanish by the next flash, contributing to the background of the next decay curve (Fig. 3). Thus the slow component increases the background. To evaluate the contribution of the slow components to the background, one can use coefficient α, which shows the percentage share of the increased background relative to the amplitude with the substracted initial background (Fig. 4):

$$\alpha = \frac{I_S}{I_{tot}} \cdot 100\%. \quad (7)$$

Afterglow

A scintillator can display a long-time delayed luminescence (milliseconds and up) which is called afterglow. The origin of afterglow is the delayed radiative recombination (luminescence) rising in a scintillator due to the thermal release of the carriers from deeper

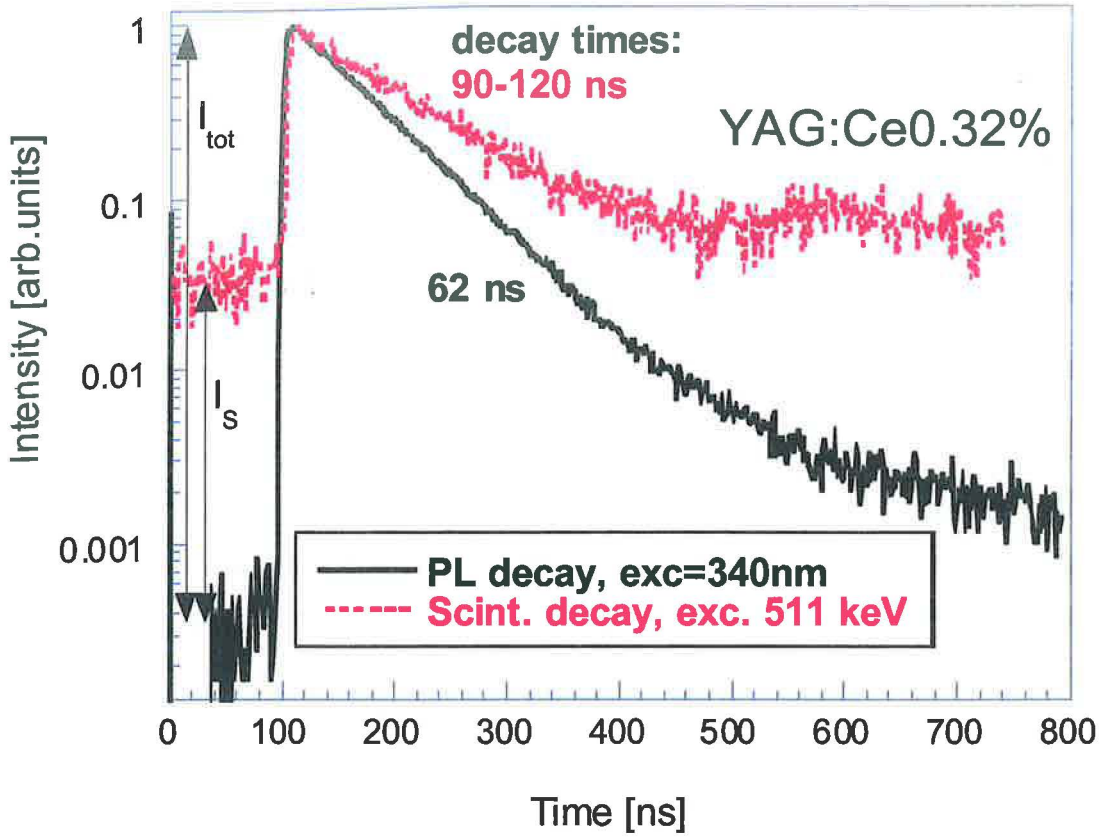

Fig. 4. Normalized photoluminescence (PL) and scintillation decays of YAG:Ce single crystal measured at 500 nm and in spectrally unresolved mode, respectively, under comparable experimental conditions at room temperature. The signal level before the rising edge of PL decay represents the true value of the background due to photo-detector noise.

traps at room temperature. The traps are formed due to defects, imperfections and impurities existing in the crystal as well as those created by irradiation. The residual impurities and point defects can form additional centres of luminescence (phosphorescence) in the crystal. The intensity, spectral composition, and decay time of the afterglow depend on the purity of raw material, manufacturing conditions, post-growth heat treatment, and doses of irradiation.

Density

For gamma-ray detection and spectroscopy, heavy inorganic crystals are most often used. High density materials permit the absorption of the total energy of the gamma quanta within a shorter distance. X-ray stopping power (attenuation coefficient) for a given thickness of a material depends on its density ρ and effective atomic number Z_{eff} [ishii1991]. In the approximation of dominance of photoelectric effect for X-rays and of the atomic mass in proportion to Z, the Z_{eff} for a compound $A_xB_yC_z$ can be given by the following equation:

$$Z_{eff} = [(xM_aZ_a^4 + yM_bZ_b^4 + zM_cZ_c^4)/(xM_a + yM_b + zM_c)]^{1/4}. \quad (8)$$

Here, M_a, M_b and M_c are atomic masses of A, B and C, respectively. Z_a, Z_b and Z_c are atomic numbers of A, B and C, respectively. Considering only the interaction through photoelectric effect the X-ray stopping power appears proportional to ρZ_{eff}^{3-4} [eijk2001].

High energy physics experiments require heavy scintillator materials with densities over 5.5 to 6.0 g/cm^3. For soft X-ray, α-particles and low energy β-rays the density is not required to be large, and the light inorganic scintillators can be used.

Scintillators can exist in the form of crystals, glasses, liquids and gases. Glass scintillator materials have been investigated considerably less compared to single crystal scintillators [ehrt1992, eijk2001]. *Scintillation glasses* are used in the bulk or fiber form for the detection of X-rays and γ-rays or neutrons [zanella1995; dalligna1997, bollinger1962, fairley1978, atkinson1987, dalton1987a]. The advantage of glass as host material is that it can be prepared in various sizes and shapes of high optical quality, and often can be produced with relatively inexpensive manufacturing techniques. Due to its compositional versatility, many physical and spectroscopic properties of scintillating glasses can be tailored (within certain limits) for specific applications. The essential problem of a glass matrix is low transfer efficiency S (see equation (1)), which is the reason for rather low yield observed in glass scintillators compared to single crystal systems.

The low transfer efficiency of glass scintillators is due to a large number of nonradiative energy traps in the irregular glass matrix. Because of these traps, the electron-hole pairs that emerge in the scintillator during the conversion stage have a low chance to reach the activators (the emission centres). There are two ways to solve this problem. First, one can simply increase the concentration of the emission centres, thus making the necessary migration path shorter. However, a high concentration of activators can worsen the glass structure and also gives often rise to concentration quenching phenomenon. Hence the desirable gain in the light yield does not arise. Another way of increasing the light yield of a scintillator is its sensitization known from the crystal luminescence materials. The idea is to improve the energy transfer by building an appropriate energy transportation network. For this purpose one introduces another impurity into the host material. The ions of this new impurity are called sensitizers, and play the role of the intermediate transportation nodes. The ions of the original impurity, the activators, play the role of the destination nodes, and

therefore are often referred to as acceptors. The sensitizers, on the other hand, are also called donors. The role of the donor ions in energy transfer is similar to that of catalysers in chemical reactions: both accelerate and make more efficient the process but do not affect the qualitative result. In this respect, an important property of the donor is that its radiative decay rate should not be greater than the radiative rate of the activator. The process of energy transportation in a scintillator with and without sensitization is illustrated in Fig. 5.

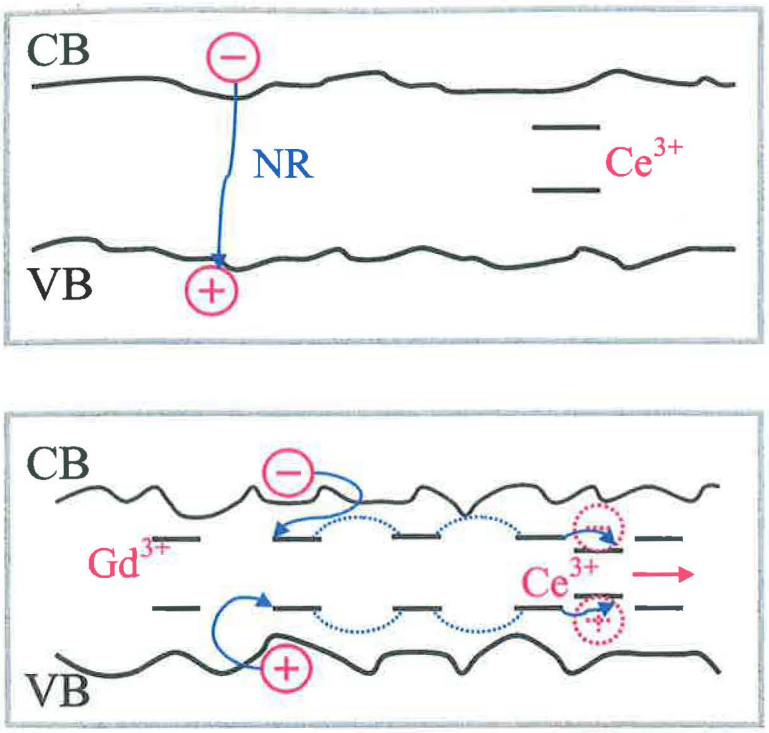

Fig. 5. Transportation of energy in the glass scintillator to the emission centers (Ce^{3+} ions). *Above*: in a nonsensitized glass (NR = nonradiative decay). *Below*: in a glass sensitized with Gd^{3+} ions. (CB = conduction band, VB = valence band).

The technique of energy transfer sensitization has been successfully applied in many phosphor, scintillation and laser crystals [mares1995; mares1997; walsh2000, jia2001, courrol2001, lin2002, sharonov1996, salley2002]. In this work this technique is applied to glasses.

Chapter 2

Energy transfer

2.1 Historical overview

The active development of scintillation materials began after the World War II. To the same time is usually dated the birth of the systematic theory of energy transfer both in scintillators and other kinds of luminescent materials. The pioneering works by Forster [forster1948], Inokuti and Hirayama [inokuti1965], and Dexter [dexter1969] were devoted to the case of static decay, when multi-step energy migration is not possible. Just a few years later two approaches to the modeling of migration-accelerated energy transfer were proposed: the diffusion model by Yokota and Tanimoto [yokota1967] and the "hopping" model by Burshtein [burshtein1972]. These first models of energy migration were largely phenomenological, exploiting analogies from other branches of physics. Huber [huber1979] was one of the first who derived the theory directly from the kinetic equations of the motion of excitons. Classical examples of careful experimental analysis include the work by Weber [weber1971], who considered the diffusion model, and that by Voronko et al. [voronko1976], who studied the hopping mechanism. A special note deserves the experimental and methodological work by Blasse and coworkers, who have made the theory much closer to the experimenters (e.g., see [kellendonk1982, vries1988a, blasse1994]). The most detailed review on the theory of energy transfer remains to be [burshtein1984]. (See also [burshtein1985] for a shorter version.)

2.2 Qualitative picture of energy transfer

The simplest case of energy transfer in a scintillator is shown in Fig. 6. The energy transfer takes place here between two ions, which represent two types of luminescent centers. The centre that transfers its energy to another centre, is called *donor* (D), whereas the other centre is referred to as *acceptor* (A). The energy level schemes of such centers are shown on Fig. 7, where D and A denote the ground states of the ions, and D^* and A^* denote the excited states. Let us suppose that the distance is so short that the centers D and A have a non-vanishing interaction with each other. If D is in the excited state and A in the ground state, the relaxed

excited state of D may nonradiatively transfer its energy to A. This process can be written as follows:

$$D + A + h\nu_{exc} \rightarrow D^* + A \rightarrow D + A^* \rightarrow D + A + h\nu_{em}.$$

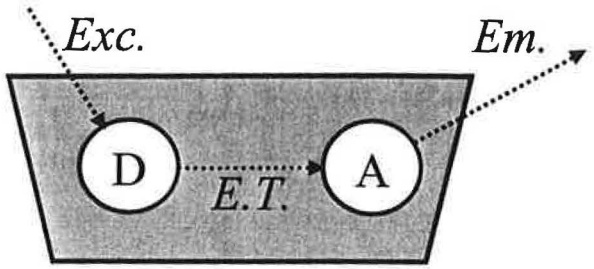

Fig. 6. Energy transfer process in the simplest case: after the donor ion D is excited by external light, it transfers its excitation energy (E.T.) to the acceptor ion A, which emits the energy back to the outer space [blasse1994]

This expression describes three stages of energy transfer process:

1) The donor absorbs a photon of energy and arrives at an excited state;
2) The donor transfers its energy to the acceptor that results by returning of the donor to the ground state and coming of the acceptor to an excited state;
3) The acceptor comes back to the ground state emitting a photon of light.

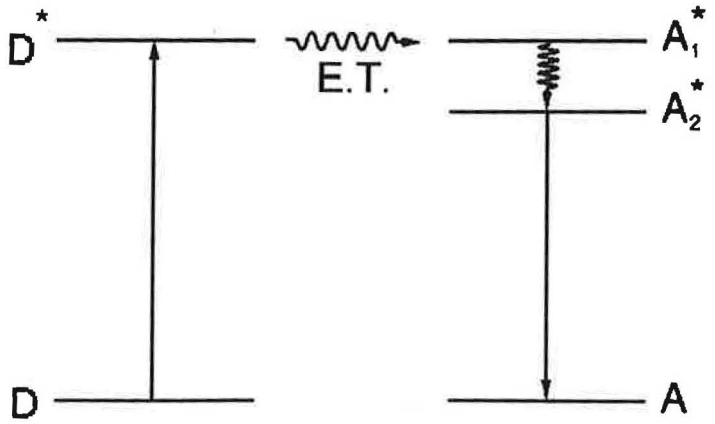

Fig. 7. Energy transfer from D to A. The $D \rightarrow D^*$ transition is the absorption (or excitation), the $A_2^* \rightarrow A$ transition is the emission. The level A_1^*, populated by energy transfer (*E.T.*), decays nonradiatively to the slightly lower A_2^* level. This prevents back transfer. [blasse1994]

For energy transfer occurrence two conditions must be fulfilled [blasse1994]:

1) Resonance conditions: the energy differences between the ground- and excited states of D and A must be equal;
2) Existence of a suitable interaction between both systems. The interaction may be either an exchange interaction (if there is wave function overlap) or an electric or magnetic multipolar interaction.

When the resonance conditions are not satisfied, energy transfer may happen with the assistance of phonons (see Section 2.7)

For the full description of energy transfer process, we must take into account other attendant processes (Fig. 8) After excitation, the donor D may not only transfer its energy to the acceptor A (process (4)), but also may decay radiatively (1) or nonradiatively (2) or transfer energy to another donor ion D (3). Also back energy transfer from the acceptor A to the donor D (5) is possible. The energy transfer from one acceptor to another one (6) can occur only at high concentration of acceptors.

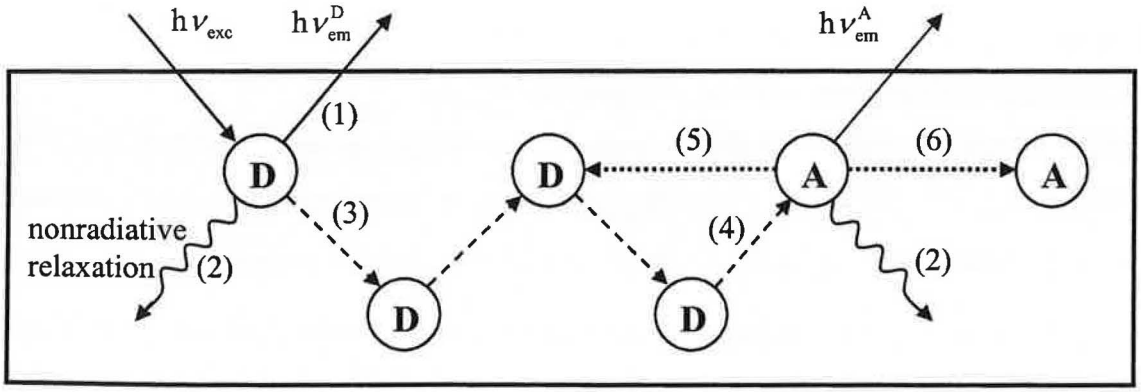

Fig. 8. Schematic representation of the possible luminescence processes in a scintillator with donor D and acceptor A ions. The excited donor D may: (1) emit radiatively; (2) decay nonradiatively; (3) transfer its energy to another D ion; (4) transfer its energy to an A ion; (5) back transfer from to D ion; (6) back transfer to A ion.

2.3 Kinetic equations

The multi-step process of energy transfer illustrated in Fig. 8 can be rigorously formulated by means of kinetic equations. Assume a short-pulse excitation at time $t = 0$. Let us consider the

decay kinetics for donors. If back transfer is ignored, the decay kinetics for donors takes the following form [sakun1972, huber1979]:

$$\frac{dP_d(t)}{dt} = -\left(\frac{1}{\tau_0} + W_{da} + \sum_{d'} W_{dd'}\right) P_d(t) + \sum_{d'} W_{d'd} P_d(t) \tag{9}$$

$$\frac{dQ_a(t)}{dt} = -\frac{1}{\tau_A} Q_a(t) + \sum_{d} W_{da} P_d(t), \tag{10}$$

where $P_d(t)$ and the parameter $1/\tau_A$ is the probability that donor d is exited at time t, and $Q_a(t)$ is the probability that acceptor a is excited at time t. The parameter $1/\tau_0$ and denotes the sum of the radiative and nonradiative decay rates of the donor, $1/\tau_A$ is the analogous parameter for the acceptor, W_{da} is the transfer rate from donor d to acceptor a, $W_{dd'}$ is the transfer rate from donor d to donor d', and $W_{d'd}$ is the transfer rate from donor d' to donor d. The first term on the right-hand side represents the energy loss due to the internal decay of the donor, energy transfer to an acceptor, and energy transfer to another donor respectively. The second term expresses the energy gain due to energy transfers from other donors. The donor decay rate $1/\tau_0$ is assumed to be the same among all the donors, while the transfer rates W_{da}, $W_{dd'}$ and $W_{d'd}$ vary from ion to ion. The donor-donor (D-D) energy transfer is assumed to be symmetric, that is $W_{dd'} = W_{d'd}$, for every pair (d,d'), which is in contrast to the donor-acceptor (D-A) transfer modeled here as a one-way process.

The initial conditions for the first-order differential equations (9) and (10) are

$$P_d(0) = \frac{N_D^*(0)}{N_D} \tag{11}$$

$$Q_a(0) = 0, \tag{12}$$

for all donors d, and acceptors a, where N_D is the number of all donor ions in the sample, and $N_D^*(0)$ is the number of the donors excited at time $t = 0$. These initial conditions encapsulate the assumption that the neighborhoods of the donors exited at time $t = 0$ are representative of the possible local ion configurations. The number of the ions is supposed arbitrarily large. The donors and acceptors are assumed to be independently and uniformly distributed in every finite volume. These distributions are characterized by parameters c_A and c_D, which are the acceptor and donor concentrations respectively. The concentration is understood here as the number of ions in a unit volume.

The ion-ion transfer rates $W_{dd'}$ and W_{da} can be further expanded [forster1948, dexter1953] as

$$W_{dd'} = C_{DD}\, f_{DD}(R), \tag{13}$$

$$W_{da} = C_{DA}\, f_{DA}(R), \tag{14}$$

where R is the distance between the two interacting particles. The subscripts on the right-hand sites do not refer to particular ions A or D but indicate the types of the interacting ions. The form of the function f depends on the type of the ion interaction. In the case of multipolar ion coupling, $f(R) = R^{-s}$, where $s = 6, 8, 10,\ldots$ is a parameter of multipolar coupling ($s = 6$ for dipole-dipole coupling, $s = 8$ for quadrupole-quadrupole coupling, etc.). In the case of exchange coupling, $f(R) = \exp(-2R/L)$, where L is the effective average Bohr radius for the excited and ground states. The coefficients C_{DD} and C_{DA} are important microscopic parameters. Their ratio $Z = C_{DA}/C_{DD}$ measures the relative strength of the D-A and D-D interaction, and plays a crucial role in the theory.

The decay curve of donor luminescence shows the aggregate intensity of luminescence across all the donors as a function of time $I_D(t)$, which is proportional to the number of the excited donors $N_D^*(t)$:

$$I(t) \sim N_D^*(t) = \sum_d P_d(t). \tag{15}$$

The donors loose their excitation for two reasons, which are intradonor decay and energy transfer to acceptors (also known as energy quenching by acceptors). Their effects can be conveniently separated as follows. Let $\{\tilde{P}_d(t)\}$ be the solution to equations (9) when $\tau_0 = \infty$ (that is, the intradonor decay is ignored) and initial conditions (11) such that $N^*{}_D(0) = 1$ (i.e. only one donor is initially excited). Introduce function

$$J(t) = \sum_d \tilde{P}_d(t). \tag{16}$$

In words, $J(t)$ is the proportion of the donors that would be excited at time t if the internal donor decay were absent. One can check that

$$I(t) = I(0)\exp(-\frac{t}{\tau_0})J(t), \tag{17}$$

or, equivalently,

$$N_D^*(t) = N_D^*(0)\exp(-\frac{t}{\tau_0})J(t). \tag{18}$$

Thus, studying energy transfer, we can focus on the function $J(t)$, ignoring the intradonor decay.

It is sometimes convenient to express the function $J(t)$ through the average quenching rate, which is defined as

$$Y(t) = \left(\sum_d X_d P_d(t)\right) \Big/ \left(\sum_d P_d(t)\right) = \sum_X w(X,t)X\,, \tag{19}$$

where

$$X_d = \sum_a W_{da} \tag{20}$$

is the quenching rate of individual donor d, and

$$w(X,t) = \sum_d \left\{ P_d(t) \Big/ \sum_{d'} P_{d'}(t) : X_d = X \right\}, \tag{21}$$

which is simply the probability that an excited donor at time t has quenching rate X. One can check that

$$\frac{dJ(t)}{dt} = -Y(t)J(t)\,. \tag{22}$$

In other words, if $J(t) = \exp(-h(t))$ then $Y(t) = dh(t)/dt$. In particular, $J(t)$ is exponential if, and only if, $Y(t) = const$. A more general case, which is actually always observed in experiments, and is also often justified by the theory, is that $Y(t)$ *does not increase* with t. This is equivalent to saying that $\ln J(t)$ is a convex function. The latter implies that $J(t)$ is convex too. Note also the obvious fact that $Y(t)$ is positive; this implies that $J(t)$ is a decreasing function.

Equation (22) can be rewritten in terms of $N_D^*(t)$:

$$\frac{dN_D^*(t)}{dt} = -\left(Y(t) + \frac{1}{\tau_0}\right) N_D^*(t)\,. \tag{23}$$

Here $Y(t) + 1/\tau_0$ is the average donor decay rate at time t, which is the sum of the average rate of quenching and the internal decay rate of the donor. What was said above about the convexity and decreasingness of $J(t)$ (and $\ln J(t)$) equally applies to $N_D^*(t)$ (resp. $\ln N_D^*(t)$). A typical graph of $N_D^*(t)$ is shown in Fig. 9.

Similarly to the donor decay function, the acceptor decay curve $I_A(t)$ shows the intensity of acceptor luminescence at time t, and is proportional to the total number of excited acceptors at this time:

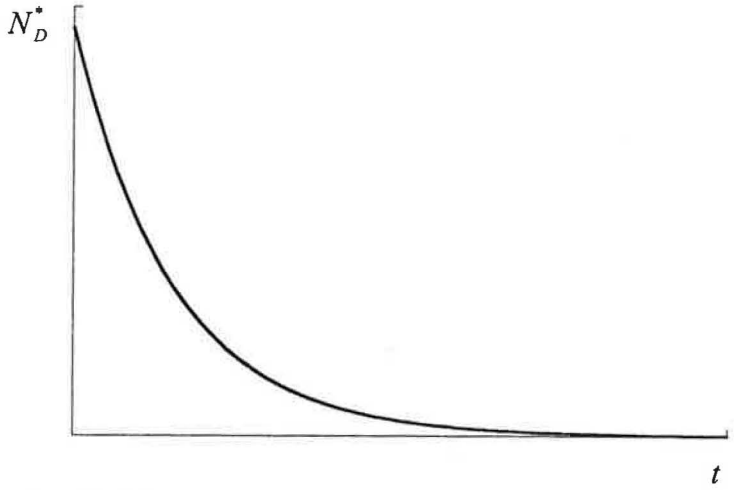

Fig. 9. A typical time dependence of the number of excited donors

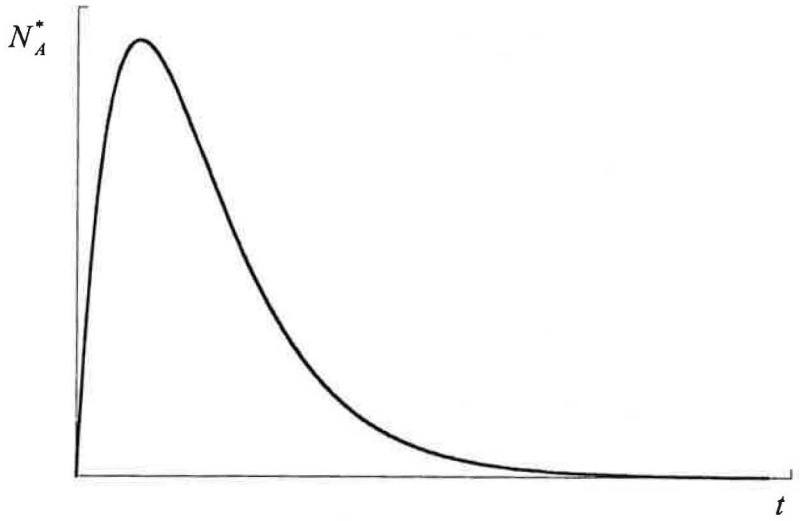

Fig. 10. A typical time dependence of the number of excited acceptors

$$I_A(t) \sim N_A^*(t) = \sum_a Q_a(t). \tag{24}$$

It can be easily checked that $N_A^*(t)$ is the solution to the following single differential equation:

$$\frac{dN_A^*(t)}{dt} = -\frac{1}{\tau_A} N_A^*(t) + \left(-\frac{dN_D^*(t)}{dt} \right) \tag{25}$$

with initial condition

$$N_A^*(0) = 0. \tag{26}$$

Thus, knowing $N_D^*(t)$, one can easily compute $N_A^*(t)$ (or, equivalently, $J(t)$). In particular, all properties of $N_A^*(t)$ can be derived from those of $N_D^*(t)$. A typical graph of $N_A^*(t)$ is presented in Fig. 10.

To understand this picture, consider first the particular case when $N_D^*(t) = \exp(-\delta t)$ (as is in the Stern-Volmer approximation [write1976] or under supermigration (see Section 2.4)). Assuming that $1/\tau_A > \delta$, we can find that

$$N_A^* \sim \exp\left(-\frac{t}{\tau_A}\right) - \exp(-\delta t) \ . \tag{27}$$

Note that the right-hand side is a *difference* of two exponents, and therefore the graph of $N_A^*(t)$ in this case must have the shape like that in Fig. 10.

To explain the shape of the graph of $N_A^*(t)$ in the general case, write equation (25) in the form

$$\frac{dN_A^*(t)}{dt} = -\Phi^{(-)}(t) + \Phi^{(+)}(t), \tag{28}$$

where $\Phi^{(-)}(t)$ and $\Phi^{(+)}(t)$ are respectively the outflow and inflow of energy for the acceptor subsystem at time t. The outflow is actually driven (controlled) by the inflow: $\Phi^{(+)}$ changes N_A^*, and then N_A^* automatically determines $\Phi^{(-)}$. Keeping this in mind, consider the evolution of N_A^*. The light flash at time $t = 0$ excites the donors only; all acceptors at time $t = 0$ are in the ground state. Therefore $N_A^*(0) = \Phi^{(-)}(0) = 0$. Due to the positive energy inflow from the donors ($\Phi^{(+)}(0) > 0$), N_A^* begins to increase. The growth of N_A^* implies the growth of the energy outflow $\Phi^{(-)}$. This growth continues until time t' when the outflow and the inflow become equal: $\Phi^{(-)}(t') = \Phi^{(+)}(t')$. A further increase in N_A^* is impossible without an increase in $\Phi^{(+)}$. But the inflow $\Phi^{(+)}(t)$ is permanently decreasing with t: $d\Phi^{(+)}(t)/dt = d^2N_D^*(t)/dt^2 > 0$ if we accept the hypothesis that $N_D^*(t)$ is convex (i.e. $d^2N_D^*(t)/dt^2 > 0$ for all t). Therefore $N_A^*(t)$ must decrease after t', at least locally. Extending this argument, one can also show that $N_A^*(t)$ will *never* grow again.

Thus, the analysis of both donor and acceptor decay curves reduces to the study of the function $J(t)$. Due to the large number and random location of the ions, the function $J(t)$ is uniquely determined by the ion concentrations c_A and c_D, types of ion interactions expressed

by f_{DA} and f_{DD}, and rate coefficients C_{DA} and C_{DD}. The relationship between $J(t)$ and these parameters will be reviewed in the next two sections.

2.4 Energy transfer by direct donor-acceptor interaction

Assume that no energy transfer between donors is possible, that is $W_{dd'} = W_{d'd} = 0$ in equations (9). Energy can be transferred from donors to acceptors only directly, by one step, as illustrated in Fig 6. This case is known as "static decay" in the literature. It can be easily shown that the decay curve in this case is nonexponential, i.e. $\ln(I(t))$ is a nonlinear function. The nonexponential behaviour of the donor decay function is caused by the variance of the quenching rate

$$X_d = \sum_a W_{da} . \tag{29}$$

This variance is inevitable in disordered systems, where donors may significantly differ from each other in the configuration of acceptors around them.

The "variance effect" can be loosely explained as follows. Imagine that there are only two types of donors, which are "quick" donors with a quenching rate X_1, and "slow" donors with a quenching rate X_2, where $X_1 > X_2$. The average rate of quenching is a weighted sum of the individual rates, $Y = w_1 X_1 + w_2 X_2$. The weights are expressed as $w_1 = N_1^*/N^*$ and $w_2 = N_2^*/N^*$, where N_1^* and N_2^* are the numbers of the exited donors of the "quick" and "slow" types respectively, and $N^* = N_1^* + N_2^*$. These weights represent the distribution of excitation among donors according to their quenching rates. If the weights were constant over time, the average rate would be constant too, and the process would be exponential. But the weights are changing. By definition, the "quick" donors lose their excitation quicker, and therefore the number of the "quick" exited donors decreases faster than the number of the "slow" exited donors. As the result, the contribution of the "quick" donors to the average rate of quenching becomes smaller and smaller over time, so that the average rate becomes lower and lower. For example, if the numbers of "quick" and "slow" exited donors are initially the same, then the initial average rate is $Y = (X_1 + X_2)/2$. But for large times, when the excitation of the "quick" donors is almost exhausted, the average rate of quenching is determined by the "slow" donors: $Y = X_2$.

The kinetic equations simplify for the case of static decay to

$$\frac{dP_d(t)}{dt} = -\left(\frac{1}{\tau_0} + X_d\right)P_d(t), \tag{30}$$

and have a simple solution $P_d(t) = P_d(0)\exp(-t/\tau_0 - tX_d)$, which implies that

$$J(t) = \frac{1}{N_D}\sum_d \exp(-tX_d). \tag{31}$$

This formula may be useful for qualitative judgements. For instance, looking at this formula, one can formally infer that $J(t)$ (and therefore $I(t)$), is not exponential.

The first formulas suitable for quantitative estimates appeared in the pioneering work by Forster [forster1949], where he considered dipole-dipole donor-acceptor interaction with allowed transitions. Dexter [dexter1953] extended his results to the case of forbidden transitions. Formulas for the general case of multipole interactions were obtained by Sveshnikov and Shirokov [sveshnikov1962] (see also the review [burshtein1984]):

$$J(t) = \exp\left(-\frac{4\pi}{3}n_A\Gamma\left(1-\frac{3}{s}\right)(C_{DA}t)^{3/s}\right), \tag{32}$$

where Γ denotes the gamma function. For $s = 6$, which corresponds to dipole-dipole interaction, this simplifies to Forster's formula

$$J(t) = \exp\left(-\gamma\sqrt{t}\right), \tag{33}$$

where

$$\gamma = \frac{4}{3}\pi^{3/2}n_A\sqrt{C_{DA}} \tag{34}$$

Inokuti and Hirayama [inokuti1965] derived an analogous formula for the case of exchange interaction:

$$J(t) = \exp\left(-\frac{\pi}{6}L^3 n_A g(C_{DA}t)\right), \tag{35}$$

where

$$g(z) = -z\int_0^1 \exp(-zy)(\ln y)^3\,dy. \tag{36}$$

The same authors propose a way of numerical evaluation of $g(z)$ for every z. Specifically, they recommend Taylor approximation

$$g(z) = \sum_{m=0}^{\infty}\frac{(-z)^m}{m!(m+1)^4} \tag{37}$$

for $z \le 10$, and the expansion

$$g(z) = (\ln z)^3 - h_1(\ln z)^2 + h_2(\ln z) + h_3 + O(e^{-z}(\ln z)^3 z^{-2}) \tag{38}$$

for z > 10, where

$$\begin{aligned} h_1 &= -3\Gamma'(1) \approx 1.73164699 \\ h_2 &= 3\Gamma''(1) \approx 5.93433597 \\ h_3 &= -\Gamma'''(1) \approx 5.44487446 \end{aligned} \tag{39}$$

Remark. The provided formulas give reliable approximations of $J(t)$ for every t. The absolute accuracy of these approximations is very high. But one should *not* use these formulas for estimating the *derivative* of $J(t)$ if time t is close to 0. For instance, Forster's formula (33) implies that

$$\frac{d}{dt}J(0) = \infty, \tag{40}$$

while in reality this derivative is finite. The reason is that formulas (32)–(35) are derived under the assumption that the distance between any two ions may be arbitrary small. This assumption is a mathematical trick for effective modelling of the randomness in ion locations. But it inevitably distorts the picture of the decay process at its early stage, when the ion interaction takes place almost exclusively between the closest neighbours in the ion array. In the case of multipolar interaction, the ignorance of the minimal distance between ions implies that the energy transfer rate between neighbouring ions is infinite, which explains the absurd equality (40).

2.5 Energy transfer with energy migration over donors

Energy migration between donors makes the picture of energy transfer more complicated. The donor decay kinetics after a short-pulse excitation can be roughly divided into three stages (see also Fig. 11):

1. **Stage of static ordered decay:**

   $\ln J(t) \approx \exp(-\alpha t)$, where $\alpha = -\frac{d}{dt}J(0) < \infty$.

2. **Stage of static disordered decay:**

   $\ln J(t) \approx -\gamma\sqrt{t}$, where γ is given by Forster's formula (34). There is also some evidence [voronko1976] that a better approximation for the decay curve in this stage is $\ln J(t) \approx -\gamma\sqrt{t} + \overline{W}t$, where constant $\overline{W}$ is defined below.

3. **Stage of migration-limited decay:**

$\ln J(t) \approx -\Delta - \overline{W}t$, where Δ and $\overline{W}$ are positive constants. Expressions for $\overline{W}$ will be given below.

These three stages were explicitly formulated already in [voronko1976]. As far as we know, all experiments having been made so far support their existence.

The complexity of the decay process can be explained by the interplay of two opposite effects. The energy transfer from donors to acceptors makes the distribution of energy among donors more and more uneven over time. This is because the "quick" donors (those located close to the acceptors) lose their excitation faster than the "slow" donors (those located far from the acceptors). Because of this, as we saw in the previous section, the average rate of quenching lowers over time. Random energy migration between donors tends to equalize the disturbed energy distribution. This has the effect of energy pump from the "slow" to the "quick" donors. The redistribution of energy resists the decrease of the average rate of quenching.

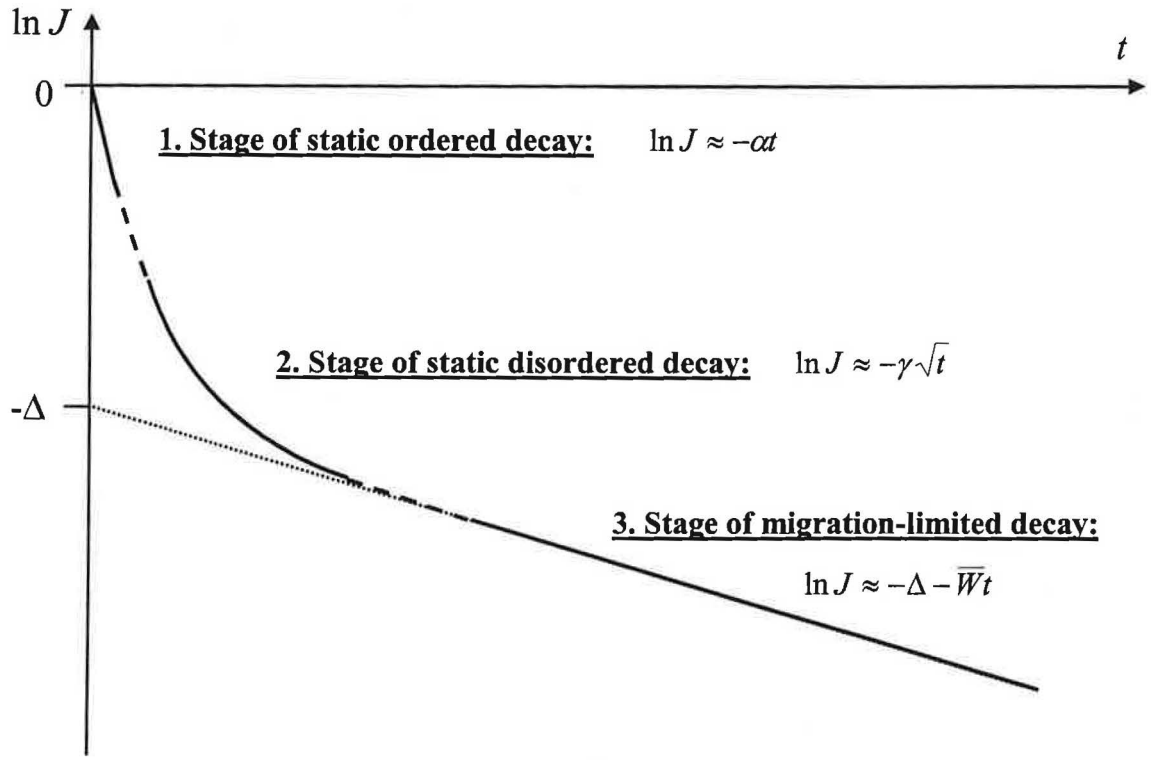

Fig. 11. Three stages of the depopulation of energy after a short-time excitation. Donor emission intensity is $I(t) = I(0)\exp\left(-\frac{t}{\tau_0}\right)J(t)$

Consider this process step by step. Energy quenching in Stages 1 and 2 is mostly due to the direct D–A transfer, as described in the previous section. This fact is reflected in the application of the term "static decay" to these stages. Note that Stage 1 is usually too short to be observed in experiments. But its existence is essential for the general understanding of the process (see Remark at the end of the previous section). Energy migration between donors has only local effects in the Stages 1 and 2; too little time has passed for the global redistribution of energy from "acceptor-poor" to "acceptor-rich" regions. Eventually the struggle of the two opposite effects, the "skewing" of the energy distribution by energy quenching and the "equalization" of the energy distribution by energy migration, brings the system to a stationary state, when the energy distribution among donors does not change anymore. Here Stage 3 begins. The decay process at this stage is exponential, with the average rate of quenching $\overline{W}$.

Unfortunately, there is no unified theory of energy migration that would be equally well elaborated for all possible values of the characteristics of the ion system, which are the microscopic parameters C_{DA} and C_{DD}, the ion concentrations n_A and n_D, and the types of ion interactions embodied in the distance dependences $f_{DA}(R)$ and $f_{DD}(R)$.

First, the theory is best developed for the case when both D–A and D–D ion interactions have the dipole-dipole character, that is $f_{DA}(R) = f_{DD}(R) = 1/R^6$. For the sake of simplicity, the analysis will be restricted to dipole-dipole interactions.

Second, the choice of the theoretical model depends on the value of $Z = C_{DA}/C_{DD}$. Two limiting cases are well studied in the literature (see [burshtein1984] for a detailed review or [vries1988a] for a summary written by an experimenter):

Case Z>>1. The process of energy transfer resembles the process of diffusion. In this case one speaks about *diffusion-limited* energy migration. A classical example is the model by Yokota and Tanimoto [yokota1967].

Case Z<<1. The movement of excitons in the scintillator is similar to the motion of gas molecules. This is the case of a so-called *hopping-limited* energy migration. The first hopping model was proposed by Burshtein [burshtein1972].

For the general case of an arbitrary Z only approximate solutions have been found. For instance, Huber [huber1979] proposes an approximate formula for the Laplace transform of $J(t)$ based on average-t-matrix approximation (ATA).

Third, the theory often assumes that the concentrations n_A and n_D are sufficiently small for the distribution of donors and acceptors to be indeed random.

It is also apparently difficult to derive explicit expressions of the decay curve $I(t)$ on the whole time interval $0 \le t < \infty$. The existing theories of energy transfer usually restrict themselves to the analysis of particular pieces of the curve such as the three stages described above. Note that the borders between the stages are diffuse, and the theory says little about the decay curve in the border areas. Nevertheless, there have been a few attempts to approximate the decay curve in the whole time range. Yokota and Tanimoto [yokota1967] used the method of Padé approximants to derive the formula

$$J(t) = \exp\left[-\frac{4}{3}\pi^{3/2} n_A (C_{DA} t)^{1/2} \left(\frac{1+10.87x+15.50x^2}{1+8.743x}\right)^{3/4}\right], \tag{41}$$

where $x = DC^{-1/3}t^{2/3}$. This formula works for the case of diffusion-limited migration Z>>1. The parameter D is a diffusion constant, which can be expressed through C_{DA} as follows [artamonova1972]:

$$D = \frac{1}{2}\left(\frac{4\pi}{3}\right)^{4/3} n_D^{4/3} C_{DD}. \tag{42}$$

Tachiya and coworkers [tachiya1983, murata1995, iway1998] do not derive an analytical form of the solution. Instead they use a method of approximating the decay curve numerically, which is sufficient for the evaluation of the model parameters. Again, their approach appears restricted for the diffusion-limited case. Vries et al. [vries1988a], based on the results obtained in [bondar1981, bondar1983], interpolate the three stages in the form

$$J(t) = \exp\left(-e^{-t/t_b}\sqrt{t} - \left(1-e^{-t/t_b}\right)\Delta - \overline{W}t\right), \tag{43}$$

where the parameter t_b can be interpreted as the border time between Stage 2 and Stage 3. The authors set $t_b = (\gamma/\overline{W})$, although it seems equally reasonable to use t_b as a free fitting parameter. Vries et al. state that formula (43) provided very good approximations in all cases they studied, including samples with both Z>>1 and Z<<1, outperforming Yokota–Tanimoto formula (41). Thus formula (43) seems to work well for all Z, although it needs a better theoretical ground.

As it was said, Stage 1 is always very short. As for the relative length of Stages 2 and 3, it varies with the relative concentration of the donors, $n_D/(n_D + n_A)$. Let us fix the concentration of acceptors and observe what happens with the increase in the concentration of donors. See Fig. 12. When the concentration of donors is very small, the decay curve is not much different from the static case; almost the entire curve is Stage 2, Stage 3 is invisible

(Fig. 12 (a)). As the number of donors increases, Stage 3 becomes more pronounced (Fig. 12 (b)). Stage 2 becomes shorter and shorter, and in the so-called kinetic limit, when the concentration of donors is very high, it collapses; the entire curve becomes Stage 3 (Fig. 12 (c)).

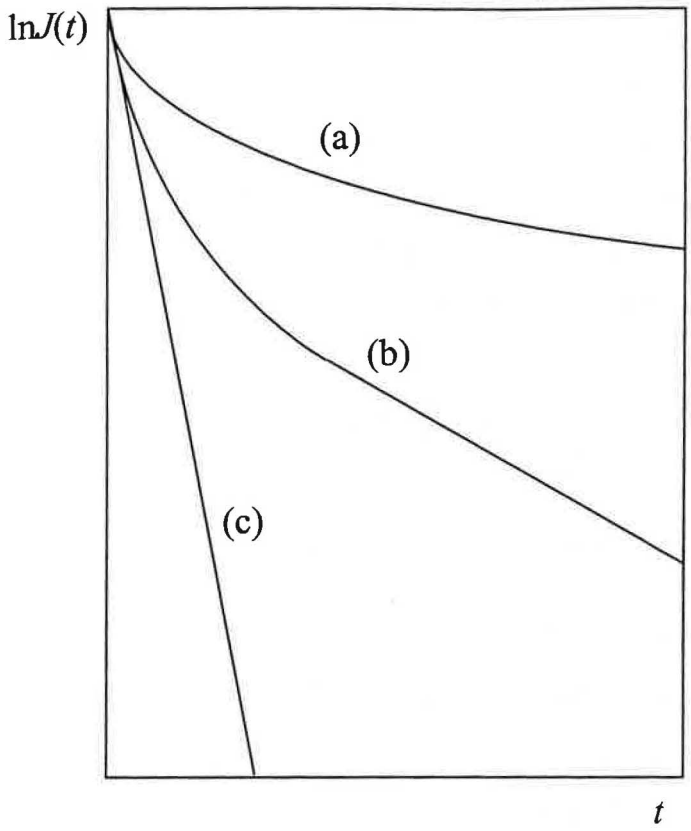

Fig. 12. Change of the shape of ln$J(t)$ with the increase in the donor concentration (the acceptor concentration is fixed):
(a) very low donor concentration ⇒ no energy migration;
(b) moderate donor concentration ⇒ both Stage 2 and 3 are present
(c) very high donor

The phenomenon of the kinetic limit is also known as quick migration, or supermigration in the literature (e.g., see [huber1981a] or [burshtein1984]). To understand this phenomenon, it is useful to think of energy transfer as of a cyclic two-phase process. The first phase is energy quenching, when the donors transfer part of their energy to the acceptors. The second phase is energy migration, when the donors transfer energy to each other. The random energy migration works like a mixer. The mixer tries to distribute the remaining energy after quenching uniformly among all the donors. But its activity is intervened by a new phase of quenching, which obscures the emerging uniformity. Supermigration is a superfast mixer. It manages to complete its task before the new phase of quenching comes. Thus the characteristic feature of supermigration is that the excitation energy is kept always uniformly distributed among the donors. This is possible only if the rate of D-D transfer is much higher than the rate of D-A transfer. Supermigration provides the highest possible decay rate (given

the energy migration is *random*). This rate is approximately given by the formula (see [burshtein1984]):

$$\overline{W} = n_A C_{DA} \int_{R_0}^{\infty} f_{DA}(R) d^3 R, \tag{44}$$

where R_0 is an estimate of the minimal D-A distance. The right-hand side is an approximate expression for $-dJ(0)/dt$, which is the decay rate at Stage 1.

Voronko et al. [voronko1976] established that supermigration may happen only at an extremely high relative donor concentration if energy migration is diffusion-limited. At the same time, if energy migration is hoping-limited, supermigration may take place at relatively low donor concentrations. This statement is confirmed by Burshtein [burshtein1984]. Thus, choosing between the diffusion and hopping mechanisms, one has to choose the hoping one if supermigration is observed.

Consider now the expressions for the asymptotic quenching rate $\overline{W}$ when the relative concentration of donors $c_D = n_D/(n_D + n_A)$ is sufficiently small.

(i) For Z>>1 (diffusion-limited migration, see [yokota1967]),

$$\overline{W} = k_{diff} n_A n_D (C_{DA})^{\frac{1}{4}} (C_{DD})^{\frac{3}{4}}, \tag{45}$$

where the coefficient k_{diff} can be computed by [artamonova1972]

$$k_{diff} = \frac{(4\pi)^2}{3}\left(\frac{1}{2}\right)^{\frac{3}{4}}. \tag{46}$$

This value of k_{diff} is not however commonly accepted. The value of k_{diff} depends on the definition of a so-called diffusion constant D. Fortunately, the different definitions of D imply almost the same values of k_{diff} (see [burshtein1984] for a discussion).

(ii) For Z<<1 (hopping-limited migration, see [burshtein1972,burshtein1984]),

$$\overline{W} = k_{hopp} n_A n_D \sqrt{C_{DA} C_{DD}}, \tag{47}$$

where

$$k_{hopp} = \frac{8\pi^3}{9\sqrt{2}}. \tag{48}$$

Another version of the coefficient is

$$k_{hopp} = \pi\left(\frac{2\pi}{3}\right)^{5/2}, \tag{49}$$

proposed in [huber1979]. Burshtein [burshtein1984] argues that (48) better takes into account the randomness in the spatial distribution of donors.

As the concentration of donors rises, the expressions for $\overline{W}$ change their form. This can be seen from the comparison of (44) and (47). This change is gradual, there is a "transition zone" between the case of "relatively small donor concentration" and supermigration. The formula for $\overline{W}$ that takes into account this transition in the case of hopping-limited migration was found by Huber [huber1981a] (see also burshtein1984):

$$\overline{W} = \pi\left(\frac{2\pi}{3}\right)^{5/2} n_A n_D \sqrt{C_{DA}C_{DD}}\left(1-\frac{2}{\pi}\tan^{-1}\left(\frac{R_0}{R_W}\right)^3\right), \tag{50}$$

where R_0, as before, is the minimal distance between the donor and the acceptor in the sample, and

$$R_w = \sqrt{\frac{3}{2\pi}}\left(\frac{C_{DA}}{C_{DD}}\right) n_D^{-2} \tag{51}$$

is the radius of the so-called black sphere. When $(R_0/R_w)^3 \approx 0$ formula (50) becomes (47) with k_{hopp} given by (48). In the other limiting case $(R_0/R_w)^3 \approx \infty$ formula (50) transforms to the formula for supermigration (44). If energy migration is diffusion-limited, the expression for $\overline{W}$ given by (45) does not change with the growth of the donor concentration as dramatically as in the hopping-limited case. Still, one should be aware that formula (45) may not work well for high donor concentrations.

2.6 Practical procedure of estimating C_{DA} and C_{DD}

Based on the theoretical facts summarized in the two previous sections, one can use the following algorithm to identify the mechanism of energy migration and estimate the microscopic parameters C_{DA} and C_{DD} from the experimental data. As before, we focus on the case of dipole-dipole ion interaction. The ion concentrations n_A and n_D, and the minimal D-A distance R_0 are assumed to be known.

1. Fit the donor decay curve for the sample without acceptor ions by equation

$$I_0(t) = I_0(0)\exp\left(-\frac{t}{\tau_0}\right) \tag{52}$$

find the donor radiative decay time τ_0. The fitting parameters are $I_0(0)$ and τ_0.

2. Consider the donor decay curve for the sample doped with acceptors. Check if this curve is exponential. If yes, quick migration takes place, and consequently the energy migration is

hopping-limited. To estimate the parameter C_{DA} of the donor-acceptor interaction, fit the curve by equation

$$I(t) = I(0)\exp\left(-\left(\frac{1}{\tau_0} + \overline{W}\right)t\right) \tag{53}$$

with the fitting parameters $I(0)$ and $\overline{W}$, and then apply formula (44). The parameter C_{DD} of the donor-donor interaction is impossible to estimate under supermigration.

3. If the decay curve has a clearly distinguishable nonexponential beginning, i.e. quick migration is not detected, estimate the parameters γ and $\overline{W}$. There are two ways of doing this.

   a. One can estimate the nonexponential and exponential parts of the curve separately. For this purpose, one has first to define somehow the border time τ_b between the two parts. Then fit the decay curve by equation

   $$I(t) = I(0)\exp\left(-\gamma\sqrt{t} - Vt\right) \tag{54}$$

   with the fitting parameters $I(0)$, γ and V on the interval $(0, \tau_b)$, and by equation

   $$I(t) = I(\tau_b)\exp\left(-\left(\frac{1}{\tau_0} + \overline{W}\right)t\right) \tag{55}$$

   with the fitting parameters $I(\tau_b)$ and $\overline{W}$ on the interval (τ_b, ∞).

   b. Alternatively, one can estimate the whole decay curve on the time interval $(0,\infty)$ by equation

   $$I(t) = I(0)\exp\left(-\frac{t}{\tau_0} - e^{-t/\tau_b}\gamma\sqrt{t} - \left(1 - e^{-t/\tau_b}\right)\Delta - \overline{W}t\right), \tag{56}$$

   where $\tau_b = \left(\gamma/\overline{W}\right)$, and the fitting parameters are $I(0)$, γ, Δ, and $\overline{W}$.

   Remark. The fitting parameters different from γ and $\overline{W}$ are not used in the further analysis.

4. Having γ in hand, find C_{DA} with formula (34).Then use $\overline{W}$ to calculate two versions of C_{DD}:

   a. Apply (45) to find C_{DD}^{diff}.

   b. Use (50) to calculate C_{DD}^{hopp}. If $(R_0/R_w)^3 \approx 0$, one can recomputed C_{DD}^{hopp} by (47) to obtain a more precise estimate.

If $C_{DA}/C_{DD}^{diff} \gg 1$ then the data fit the diffusion mechanism, and it is legible to set $C_{DD} = C_{DD}^{diff}$. If $C_{DA}/C_{DD}^{hopp} \ll 1$ then the data fit the hopping mechanism, and one can set $C_{DD} = C_{DD}^{hopp}$. If neither $C_{DA}/C_{DD}^{diff} \gg 1$ nor $C_{DA}/C_{DD}^{hopp} \gg 1$ holds then the data suggests neither

hopping nor diffusion mechanism of energy migration; in this case the obtained estimates of C_{DD} are invalid.

Remark. Because of technological reasons, the knowledge of the ion concentrations n_A and n_D may be problematic. It is also a problem for glasses to obtain an estimate of R_0 with the same precision as is common for crystals.

2.7 Phonon-assisted energy transfer

Sometimes the requirement of the equality of level differences is not met, which often takes place in disordered systems. However, in this case energy transfer is possible with the participation of phonons (Fig. 13).

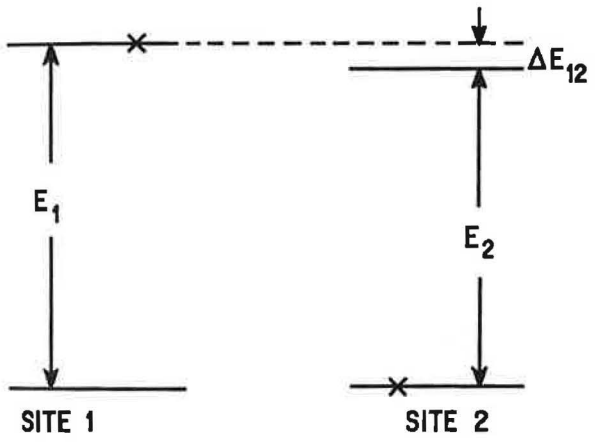

Fig. 13. The electronic energy levels of two sites between which excitation is to be transferred. The crosses symbolize the initial occupations, and the quantity ΔE_{12} the energy mismatch between excitations on sites 1 and 2 [holstein1981]

The various mechanisms of phonon-assisted energy transfer and their dependence on the temperature are described by Holstein et al. [holstein1981]. Phonon-assisted energy transfer requires the presence of ion-ion coupling (multipolar of exchange) to affect spatial transport of excitation. At phonon-assisted excitation transfer, the energy is conserved either due to phonon energy itself (one-phonon process) or due to the difference in phonon energies (two-phonon process, Fig. 14) being equal to the energy mismatch of the participating sites.

Table 1. Approximate temperature dependences of the various phonon-assisted energy transfer mechanisms [tissue1989]

Type of phonon-assisted process	Temperature dependence
One-phonon	T
Two-phonon:	
Two-site, non-resonant	T^3
Raman	T^7
Resonant	$\exp(-\Delta E_{12}/kT)$
One-site, nonresonant	T^7

The temperature dependencies obtained by Holstein et al. [holstein1981] are summarized in Table 1 [tissue1989]. The temperature dependence of the energy transfer rate (the right column) is normally used to determine the type of energy transfer (the left column). This method has been successfully applied in an variety of systems [garcia1999, lacha2004, martin2004, vliet1989a, bujis1988, selzer1977, flach1975, wietfeldt1986].

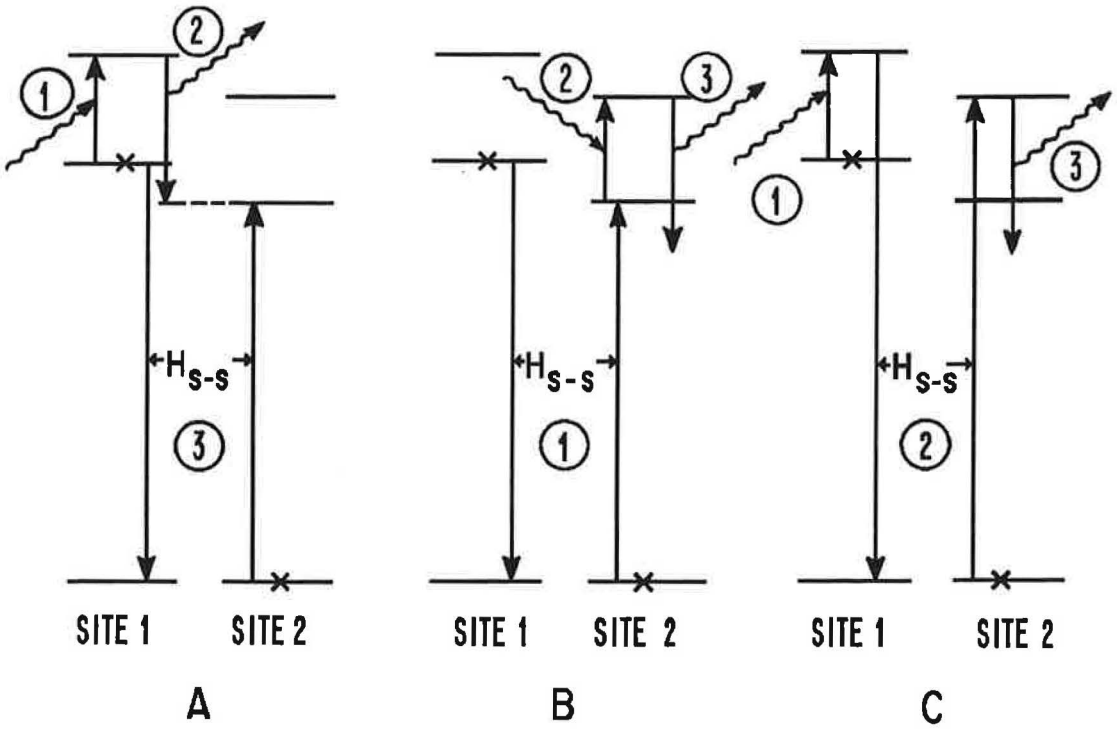

Fig. 14. One-site resonant process. The ion-phonon interaction acts twice, the site-site coupling Hamiltonian once. The circled numbers indicate the order of transitions; the arrows the sense of the transitions. [holstein1981]

Chapter 3

Ce^{3+}- and Tb^{3+}-doped Gd^{3+}-rich phosphate glasses

3.1 Optical properties of emission centres based on the Ce^{3+}, Tb^{3+}, and Gd^{3+} ions

All scintillating glasses must contain activator elements such as lanthanide ions or transition-metal ions. Cerium and terbium are frequently used as the dopant of scintillating glasses [ebendorff2000; bettinelli1996; barbon1996; jouhari1996; devitsin1998; zanella1994; stroud1962; edgar1999; ebendorff1996b; vandeun1999; ebendorff1999a; ebendorff1999b; hosono1998; zanella1995; ebendorff2002; bettinelli1989; hayakawa1996]. Scintillators doped with Ce^{3+} or Tb^{3+} ions show the emission in UV-blue and green-red spectral regions, respectively. While Ce^{3+}-based emission centres expose fast and broad-band photoluminescence with typical decay time about 20-50 ns due to the allowed *5d-4f* transitions of Ce^{3+} ion, much slower decay is typical for Tb^{3+} centres based on forbidden *4f-4f*. The light yield depends on the concentration of the activator elements.

Cerium-activated scintillator material have been known and used for several decades but have received renewed interest for many applications because of the favourable spectroscopic properties of Ce^{3+} and the ability to incorporate Ce^{3+} into many different host materials [eijk1997a, bettinelli1996, eijk1994, francini1997, pedrini1993, mares1996, zanella1994, devitsin1998, graaf2003]. The most attractive properties of Ce^{3+} are

1) its luminescence occurs in the visible - near ultraviolet region, and is well matched to the spectral response of high efficiency photodetectors;
2) the emission involves an allowed electric dipole-dipole transition, and thus is fast for good timing resolution;
3) the luminescence intensity and decay time are stable and insensitive to temperature for most hosts at room temperature;
4) there are no natural long-lived radioactive isotopes;
5) cerium is the least rare of the rare earth elements.

The emission of the Ce^{3+} ($4f^1$) ion corresponds to a *5d-4f* transition. The excited configuration is $5d^1$. The $4f^1$ ground state configuration yields two levels, viz. $^2F_{5/2}$ and $^2F_{7/2}$,

separated by some 2000 cm^{-1} due to spin-orbit coupling. Depending on the site symmetry the $5d^1$ configuration is splitted by the crystal field in 2 to 5 components. The total splitting amounts to some 15000 cm^{-1} (Fig. 15).

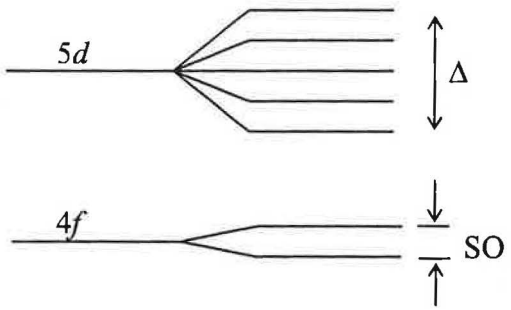

Fig. 15. [blasse1994] The simplified energy level scheme of the Ce^{3+} ion ($4f^1$). On the left hand side only the $4f$ level and the $5d$ level are given without taking into account further interactions. On the right hand side the spin-orbit (SO) coupling has split the $4f$ level into two components (about 2000 cm^{-1} apart), and the crystal field (Δ) has split the $5d$ level into five crystal-field components spanning together some 15000 cm^{-1}.

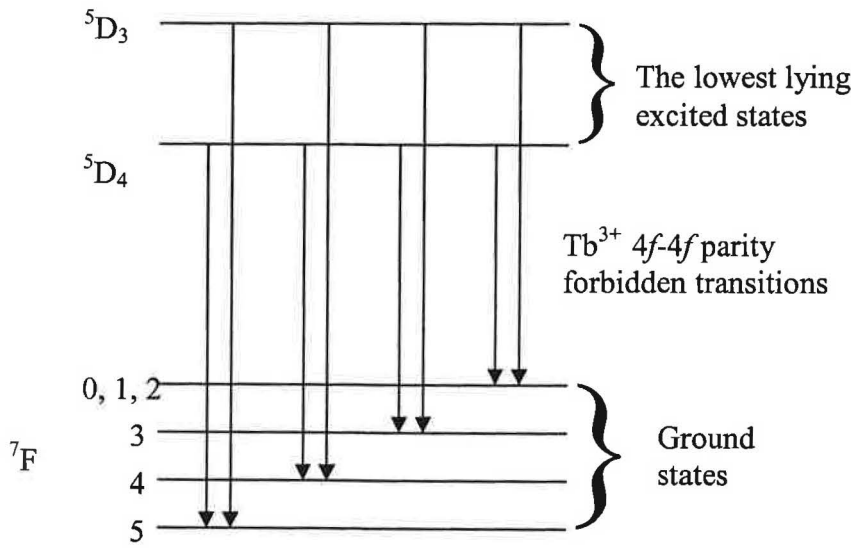

Fig. 16. The simplified energy level scheme of the Tb^{3+} ion ($4f^8$).

The Ce^{3+} ion is one of the few examples of inorganic luminescence centres corresponding to a completely allowed emission transition. The decay time is therefore short (some tens ns). The application of the Ce^{3+} ion in phosphors for index tubes and flying-spot scanners is based upon this property.

The emission of Tb^{3+} ($4f^8$) is due to transitions $^5D_3$-^7F_J or $^5D_4$-^7F_J, which occurs mainly in the violet-blue and green-red, respectively (Fig. 16). Since the J values, involved in the transitions, are high, the crystal field splits the levels into many sublevels, which gives the spectrum its complicated appearance.

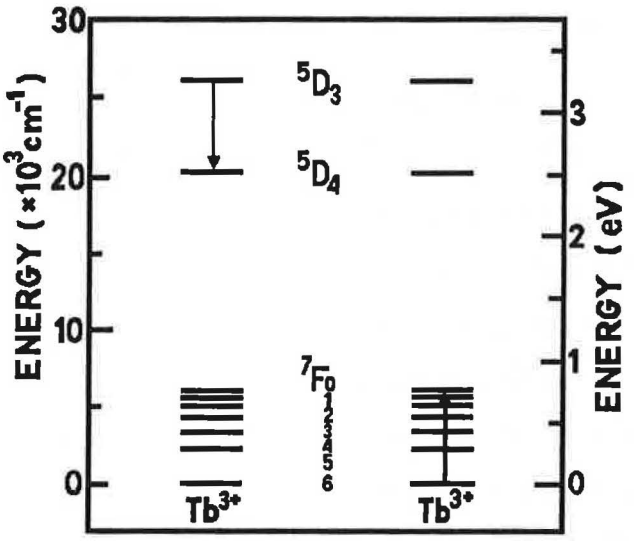

Fig. 17. Schematic energy level diagram of Tb^{3+}. Arrows illustrate cross-relaxation transitions between neighbouring Tb^{3+} ions. [tonooka1991]

The energy difference between the $^5D_3$ and $^5D_4$ levels is equal to that between $^7F_0$ and $^7F_6$, therefore resonant energy transfer between the $^5D_3$-$^5D_4$ transition and $^7F_6$-$^7F_0$ transition are possible as illustrated schematically in Fig. 17 [tonooka1991, hayakawa1996, hayakawa1997; maruyama1997]. This so-called cross-relaxation becomes important with increasing Tb^{3+} concentration due to decreasing average ion distance. As a consequence luminescence from $^5D_4$ state increases predominantly.

The Gd^{3+} ion has $4f^7$ electronic configuration, and the energy gap between the ground state $^8S_{7/2}$ and the first excited term $^6P_{7/2}$ is 32.000 cm^{-1} (Fig. 18). Thus the lowest-energy emission of transition $^6P \rightarrow {}^8S_{7/2}$ occurs at about 312 nm.

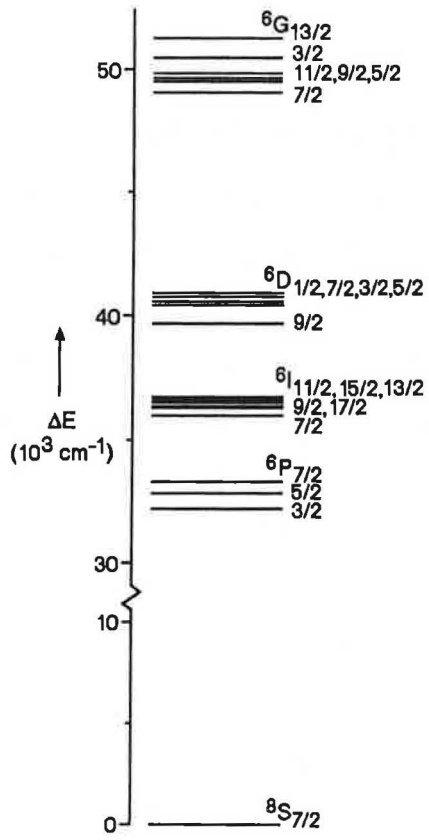

Fig. 18. Energy-level scheme in the range 0-50000 cm^{-1} for Gd^{3+} in fluoride lattices. [wegh1997]

3.2 Energy transfer sensitization in glasses

One important consequence of the energy transfer process is the phenomenon of "sensitized luminescence" in solids [dexter1953]. Sensitized luminescence is potentially of great importance in increasing the light yield of scintillation glasses. In the present case one should construct a chain of donor (Gd^{3+}) levels. An electron-hole pair can move through these levels towards the emission centre (Ce^{3+} or Tb^{3+}). Such concept has been successfully used in crystals [blasse1986, dorenbos1997]

In other words, we have developed a new concept of energy transfer sensitisation in scintillation glass based on nearly resonant energy migration through a rare earth sub-system in the glass matrix followed by a single step transfer to the emission centre. Gd^{3+} ions at sufficiently high concentration enable effective energy migration in the phosphate-based glass matrices followed by single-step transfer towards emission centres created by Ce^{3+} or Tb^{3+} doping.

Validity of the above concept in glass matrix has been evidenced by experimental measurements of excitation and emission spectra, decay kinetics and absorption spectra.

3.3 Doping concentration

Very often the enlargement of light yield can be achieved by increasing the activator concentration. However, a very high concentration of dopant leads to quenching of luminescence. The theory of concentration quenching was described by Dexter [dexter1954]. Also with increasing of doping concentration, the possibility of clustering arises: dimers, trimers, etc. are forming [imbush1981]. In the case of glass matrix, small recrystalized regions can appear. This phenomenon is called devitrification.

The doping concentration is a very important issue for Ce-doped glasses. At higher concentrations of Ce^{3+} ions, an unfavourable combination of low transfer efficiency and quenching of Ce^{3+} emission due to the interaction between closely occurring elementary excitation was noted. Consequently, the glasses do not allow large value of Ce^{3+} ions concentrations and typical values are around a few mol%.

In the systems with weaken crystal field at rather high temperatures bi-directional energy transfer could occur between Gd^{3+} and Ce^{3+} ions, which also decreases light yield of glass scintillator.

3.4. Influence of glass matrix

Rare earth ions occur predominantly in the trivalent state in glasses. Because of their electron configurations, cerium and terbium ions can exist in tetravalent charge state, too [ebendorff2000]. In the most glasses melted by conventional technique in air, the trivalent ions are stable, but sometimes somewhat reducing atmosphere or a post-preparation heat treatment must be used to avoid unwanted tetravalent charge state. Ce^{3+} and Tb^{3+} serve as electron donors, because Ce^{3+} has one electron above the filled *5p* shell and Tb^{3+} has one electron above the half-filled *4f* shell [blasse1994]. Therefore, oxidising melting conditions as well as X-ray and ultraviolet radiation enable the oxidation to Ce^{4+} and Tb^{4+} [ebendrorff1996a, ebendorff1999b, arbuzov1992, arbuzov1992a, stroud1962].

The occurrence of two valences in the case of cerium and terbium ions affects the absorption properties of these ions. The electron donation ability of the lower charge state ions facilitates the excitation of an electron from the *4f* to the *5d* shell. As the result, both *4f*-*5d* transitions of cerium and terbium ions are shifted to lower energy into the ultraviolet range, which is measurable by conventional spectrophotometers compared with rare earth ions, which do not like to be oxidised (Eu^{3+}, Yb^{3+}) [blasse1994, ebendorff1996a, dorenbos2003]. Since *4f*-*5d* absorptions are allowed electronic transitions, they have high intensities and are sensitive to the host glass matrix field [blasse1994].

The energy for the excitation of an electron from the *4f* to the *5d* shell decreases with the increasing electron donor strength of the rare earth ion, i.e. with the increasing capability of the ion to be oxidised. Therefore, the experimentally measured shift of the *4f*-*5d* transitions to lower energy in the order $Tb^{3+}>Ce^{3+}$ suggests a stronger tendency for oxidation in the order $Tb^{3+}<Ce^{3+}$. The energy of a charge-transfer transition from ligands to metal ions decreases with the increasing electron acceptor strength of the metal ion, i.e. with the increasing capability of the ion to be reduced. Therefore, the experimentally measured shift of the charge-transfer transition to lower energy in the order $Ce^{4+}>Tb^{4+}$ suggests a stronger tendency for the reduction in the order $Ce^{4+}<Tb^{4+}$ [ebendorff2000].

These oxidation-reduction tendencies can affect the spectral properties of glasses, and also the bandwidths, traps positions and energetic structure. It is necessary to take into account these facts in the design of new materials.

3.5. Structure of the glass

To analyse the structure of glass, let us accept the hypothesis that the local configuration of ions in the considered glasses is similar to that in the analogous crystals. In Chapter 6 it will be shown that the glass shows the short range order, so this approach can be applied.

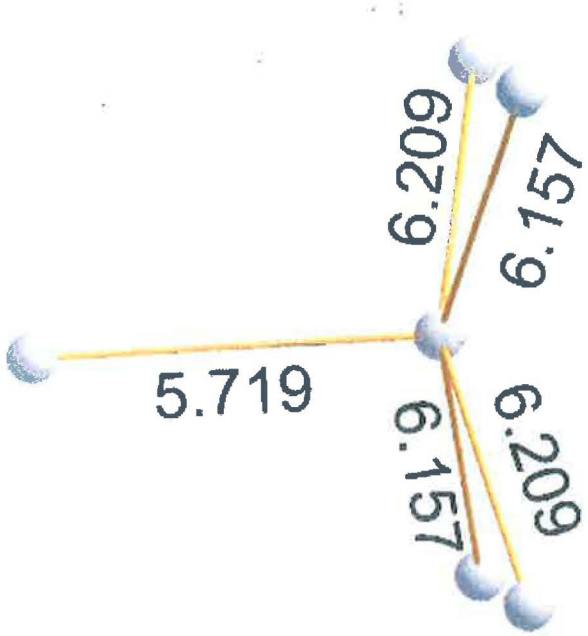

Fig. 19. The minimal distances between Nd ions in the $NaNd(PO_3)_4$ structure

Thus to reveal the local structure of the glass, one of the studied samples, namely the $Na_{50}Gd_{49}Ce_1$-II sample, was crystallized. The measurements of X-ray diffraction revealed that the crystal lattice has the structure of $NaGd(PO_3)_4$ [nitsch2005]. The spatial location of ions in this crystal must be similar to that of $NaNd(PO_3)_4$, since the atomic radii of Gd and Nd are almost the same (resp. 233 pm and 206 pm, see www.webelements.com). The very similar structures for glasses are described in [ilieva2001], the structures for YbP_3O_9 in [hong1974] and for $LiYb(PO_3)_4$ in [zarkouna2004]. The spatial structure of the $NaNd(PO_3)_4$ crystal is graphically illustrated in Fig. 20a-c. It is seen in Fig. 20 that each Nd^{3+} atom (which is replaced with a Gd^{3+}, Ce^{3+} or Tb^{3+} atom in the studied glasses) is surrounded with a thick shell of $(PO_3)^-$ groups. The position of each of these groups relative to the Nd^{3+} atom, and also relative to each other, is quite stable. It is this stability that ensures the existence of the short range order in the glass. The knowledge of the three-dimensional structure (see Fig. 19) allows to estimate the distance between the closest Gd^{3+} ions, $R_0 \approx 6 \cdot 10^{-10}$ m, which will be necessary in Section 5.2 to apply formula (50).

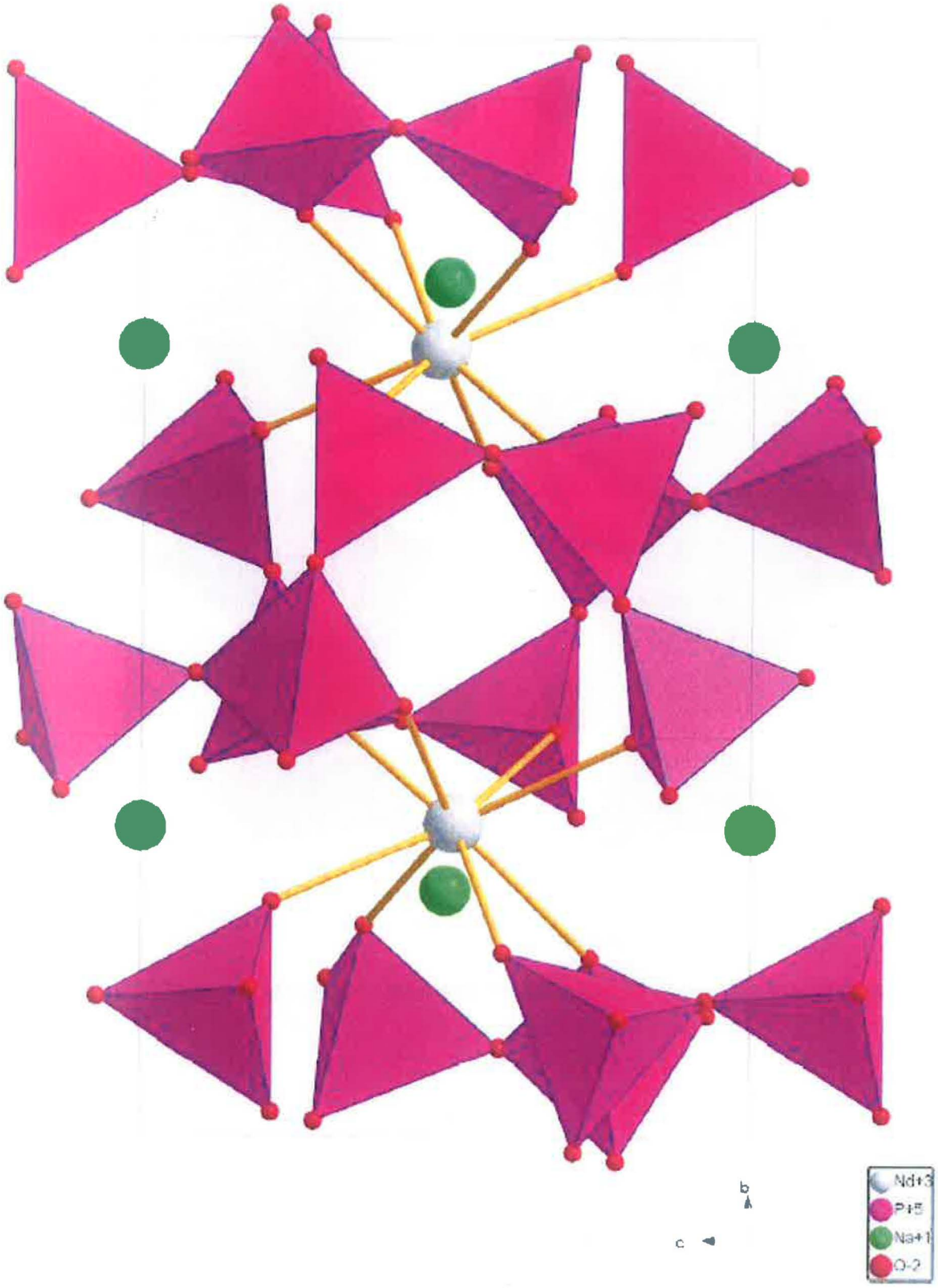

Fig. 20a. The structure of the crystal lattice of $NaNd(PO_3)_4$ in b-c projection

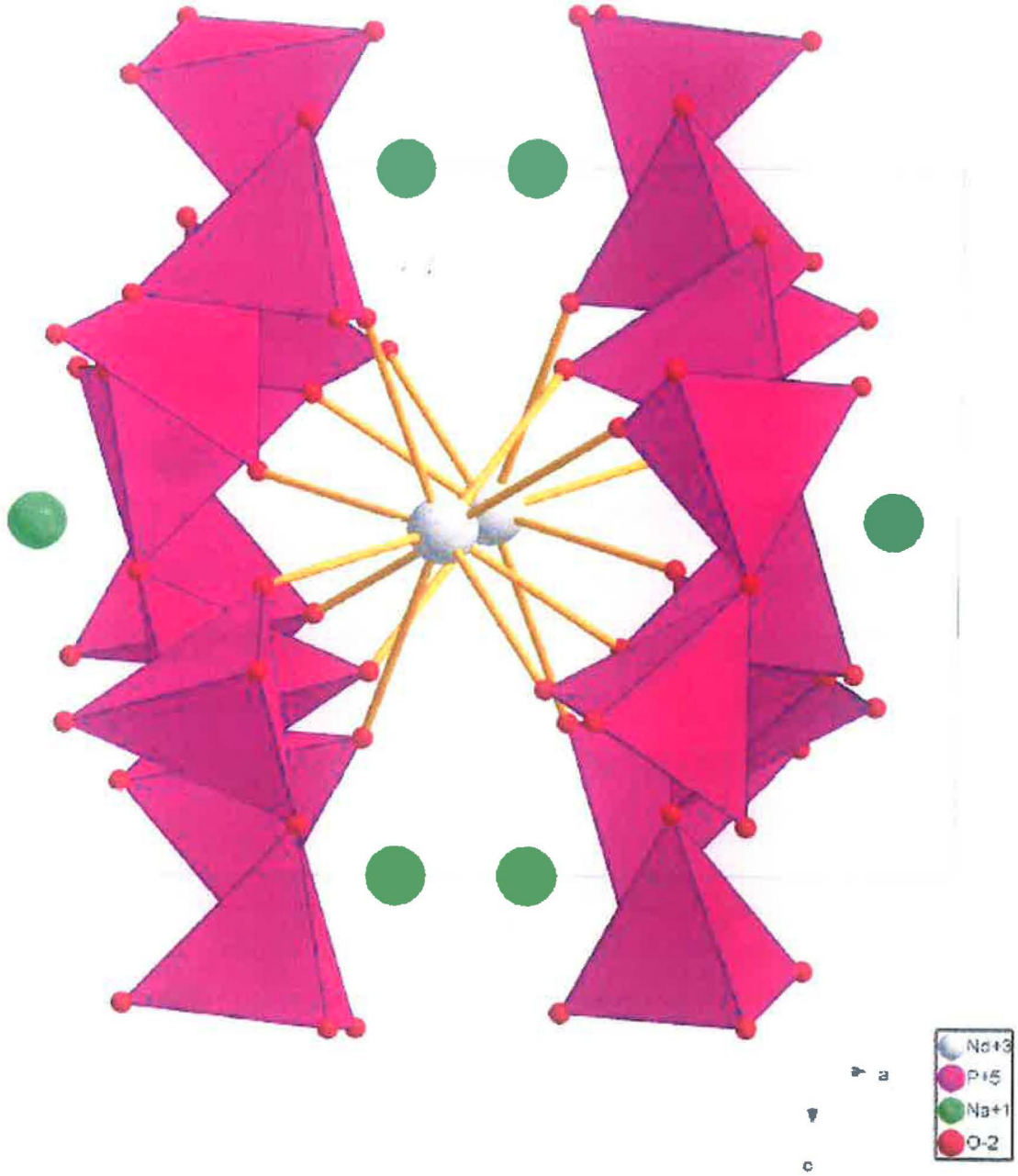

Fig. 20b. The structure of the crystal lattice of $NaNd(PO_3)_4$ in a-c projection

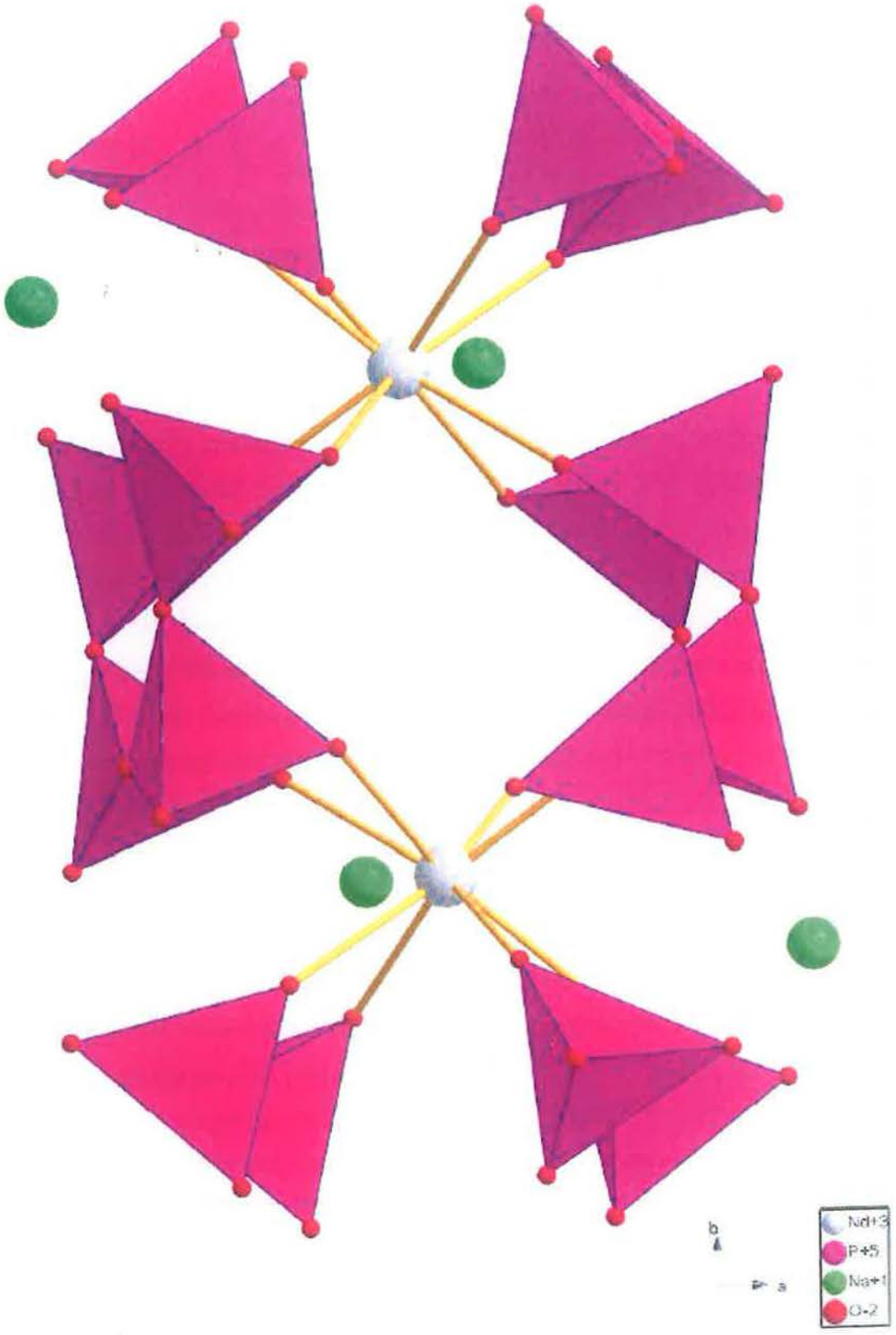

Fig. 20c. The structure of the crystal lattice of $NaNd(PO_3)_4$ in a-b projection

Chapter 4

Experimental

4.1 Experimental techniques

The absorption spectra at RT were measured by the UV-vis-NIR spectrophotometer Shimadzu UV-3101PC. For the measurement of the absorption spectra below RT, the spectrophotometer Specord M 40 (190-900 nm) was used.

The luminescence and scintillation characteristics were obtained by Spectrofluorimeter 199S (Edinburgh Instrument) using photon counting detection. This Spectrofluorimeter is equipped with the steady-state hydrogen and X-ray (35 kV, Mo anticathode) lamps and ^{22}Na radioisotope as the excitation sources. Furthermore, the slow decays in the ms time scale were measured with a Xe microsecond flashlamp and a multichannel analyser in the scaling regime. The fast decay kinetics in the ns range were obtained with hydrogen- or nitrogen-filled nanosecond pulse flashlamp by the using the time-correlated single photon counting method. The same method was also applied for the measurement of scintillation decay with ^{22}Na radioisotope as the excitation source.

Excimer laser (XeCl mixture, f_{rep} = 10 Hz, E_{pulse}(max) = 8 mJ, λ_{em} = 308 nm, FWHM = 10 ns) excited luminescence was measured using a closed cycle cryogenerator (10-300 K). The laser beam was focused on the sample surface in a pencil-shape beam (power density of the order of 10^5 W/mm^2) and the emission was observed at right angle by a monochromator coupled to an optical multichannel analyzer or to a photomultiplier connected to a digital oscilloscope (for details see also [baccaro2000]).

For low temperature measurements two Oxford Instruments cryostats were used: a liquid nitrogen-bath one (for the measurements down to 80 K) and a liquid helium-flow one (for the measurements down to 5 K).

Wavelength resolved thermally stimulated luminescence (TSL) measurements were performed after X-ray irradiation at 10 K (Philips 2274 X-ray tube operated at 20 kV). The detection system was a monochromator coupled to a CCD detector (Jobin-Yvon Spectrum One 3000) operating in the 280-820 nm interval (heating rate of 0.1 K/s).

All the spectra were corrected for the experimental distortions. The decay times were extracted from the decay curves using deconvolution procedures to remove the distortions caused by finite width of the excitation pulse (which are essential mainly in the ns time scale).

For the curve fitting, the computer programs SpectraSolve, Kaleidagraph, Origin, MATLAB and SeDuMi were used.

4.2 Sample preparation

All the samples of the phosphate glasses were prepared in the Chemical Laboratory of the Department of Optical Crystals of the Institute of Physics in Prague.

The Ce^{3+}- and Tb^{3+}-doped Gd-riched phosphate glasses were prepared using $NaPO_3$, $GdPO_4$ and $CePO_4$ or $TbPO_4$ starting powders of the 4-5N purity. Sample compositions are coded as $Na_xGd_yCe_z$, where x,y,z show the molar percentage of the corresponding starting materials in the melt. The content of $GdPO_4$ varied from 15 to 47 mol% in the first generation of glasses and that of the impurity phosphates from 0.1 to 10 mol%. Undoped and Gd-free glasses were also prepared to provide limit compositions. The second generation set of glasses, denoted as $Na_xGd_yCe_z$-II with high concentration of Gd (up to 90 mol%) was prepared using a new improved technology (see Chapter 6).

The mixed constituents were melted in a quartz ampoule at around 1200°C and after homogenization (about 2 h) poured into a graphite crucible. The obtained samples had the volume of a few cubical centimetres. Appropriate postgrowth annealing for about 20 h at 300°C had to be applied to remove thermal stresses before cutting and polishing procedures. Polished plates about 12 × 8 × 1 mm were used for the luminescent measurements and bulks of a few cubical centimetres were applied for measurements of scintillation decay (Fig. 21). All the plates

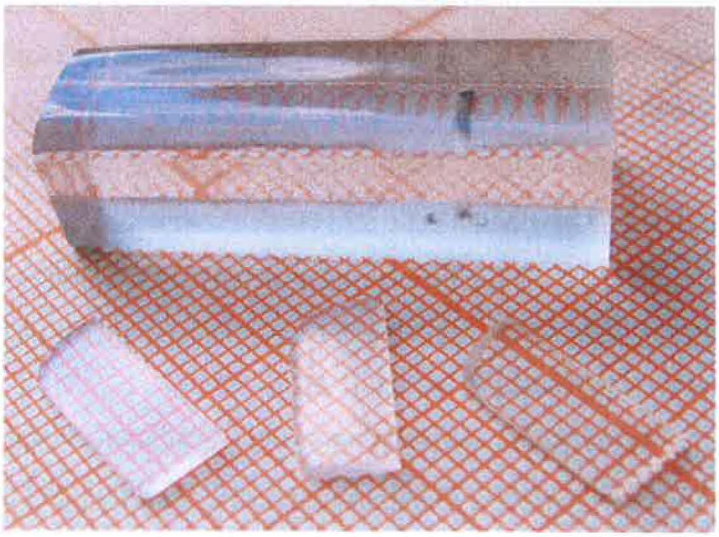

Fig. 21. Photo of the cut and polished samples (a bulk and plates) of NaGd phosphate glasses

Table 2. Densities of some Ce-doped phosphate glasses

Glass composition	Density, g/cm^3
$Na_{69.9}Gd_{30}Ce_{0.1}$	2.95
$Na_{69}Gd_{30}Ce_1$	2.97
$Na_{69}Gd_{30}Tb_1$	2.93
$Na_{60}Gd_{30}Tb_{10}$	2.99
$Na_{90}Gd_9Ce_1$-II	2.64
$Na_{80}Gd_{19}Ce_1$-II	2.77
$Na_{70}Gd_{29}Ce_1$-II	2.83
$Na_{50}Gd_{49}Ce_1$-II	3.07
$Na_{40}Gd_{59}Ce_1$-II	3.00
$Na_{30}Gd_{69}Ce_1$-II	3.04
$Na_{20}Gd_{79}Ce_1$-II	3.19
$Na_{10}Gd_{89}Ce_1$-II	3.25

had the same size and shape, so that we can compare their luminescent characteristics obtained in the same experimental conditions.

The densities of the various Ce-doped scintillation glasses are present in Table 2.

Results

Chapter 5

Ce^{3+}- and Tb^{3+}-doped phosphate glasses

In this chapter the results of measurements of Ce^{3+}- and Tb^{3+}-doped samples are described and the mechanisms of energy transfer in these samples are discussed. In the conclusions the comparison between Ce^{3+}- and Tb^{3+}-doped glasses is provided.

5.1 Ce^{3+}-doped phosphate glasses

Due to *5d-4f* transition of Ce^{3+} ions they can interact at a longer distance. Consequently for effective energy transfer the concentration of Ce^{3+} needs not be too high. In this paragraph,

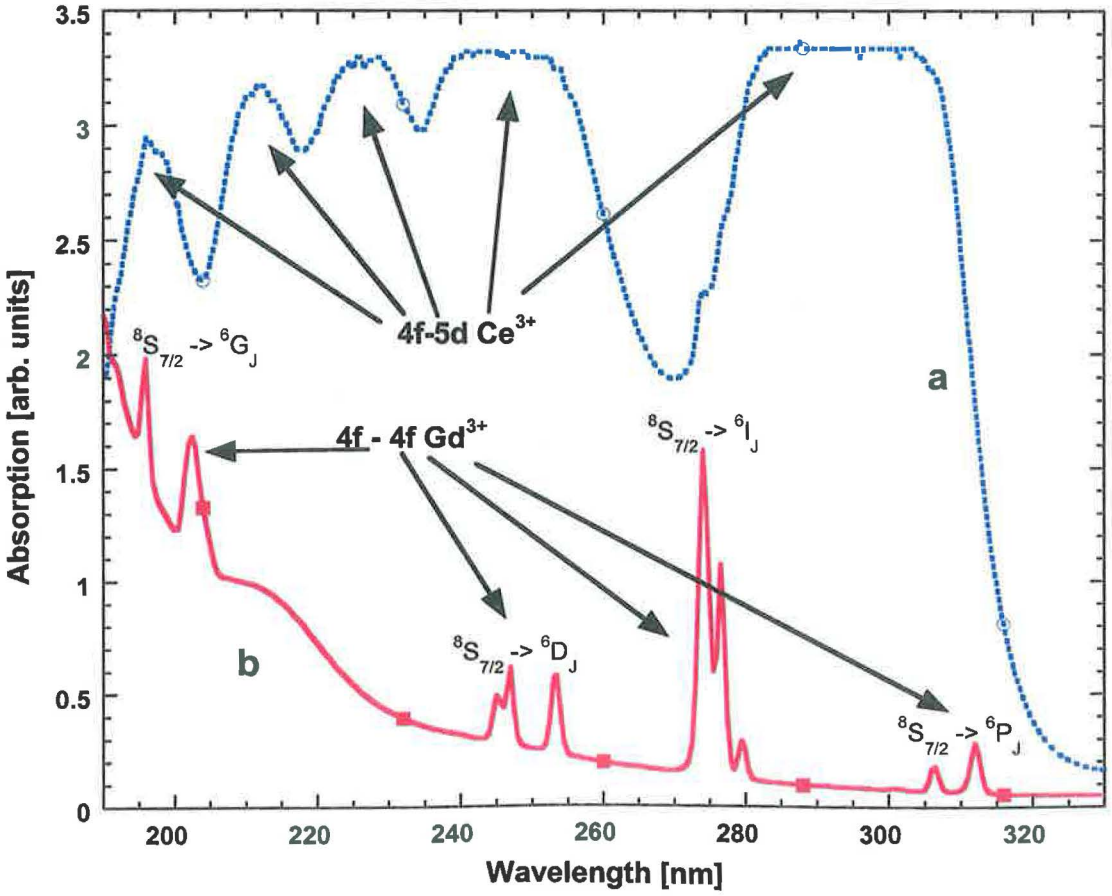

Fig. 22. The absorption spectra of phosphate glasses $Na_{74}Gd_{25}Ce_1$ (a) and $Na_{75}Gd_{25}$ (b) at room temperature. The absorption bands belonging to Ce^{3+} and Gd^{3+} transitions are marked

after common characteristics of optical properties of Ce^{3+}-doped phosphate glasses, we consider energy transfer process in two samples with the Ce^{3+} concentration of 0.1 mol% and 1 mol%.

5.1.1 Results

Absorption spectra

The absorption spectra of $Na_{75}Gd_{25}$ and $Na_{74}Gd_{25}Ce_1$ samples are given in Fig. 22 at room temperature. The transitions related to the Ce^{3+} and Gd^{3+} energy levels are marked in the figure. According to classification of ref. [dorenbos1997], this is the case of intermediate crystal field, in which the lowest $4f^1$-$5d^0$ transition of Ce^{3+} is about the same energy as the lowest $4f^1$-$4f^1$ transition around 312 nm belonging to the Gd^{3+} ion. In such a situtation, at elevated temperatures bi-directional energy transfer could occur between Gd^{3+} and Ce^{3+} ions.

Photo- and radioluminescence spectra

In Fig. 23 excitation and emission spectra related to Ce^{3+} emission centres are given together with X-ray excited emission for the $Na_{74}Gd_{25}Ce_1$ sample. In the latter emission spectrum, also

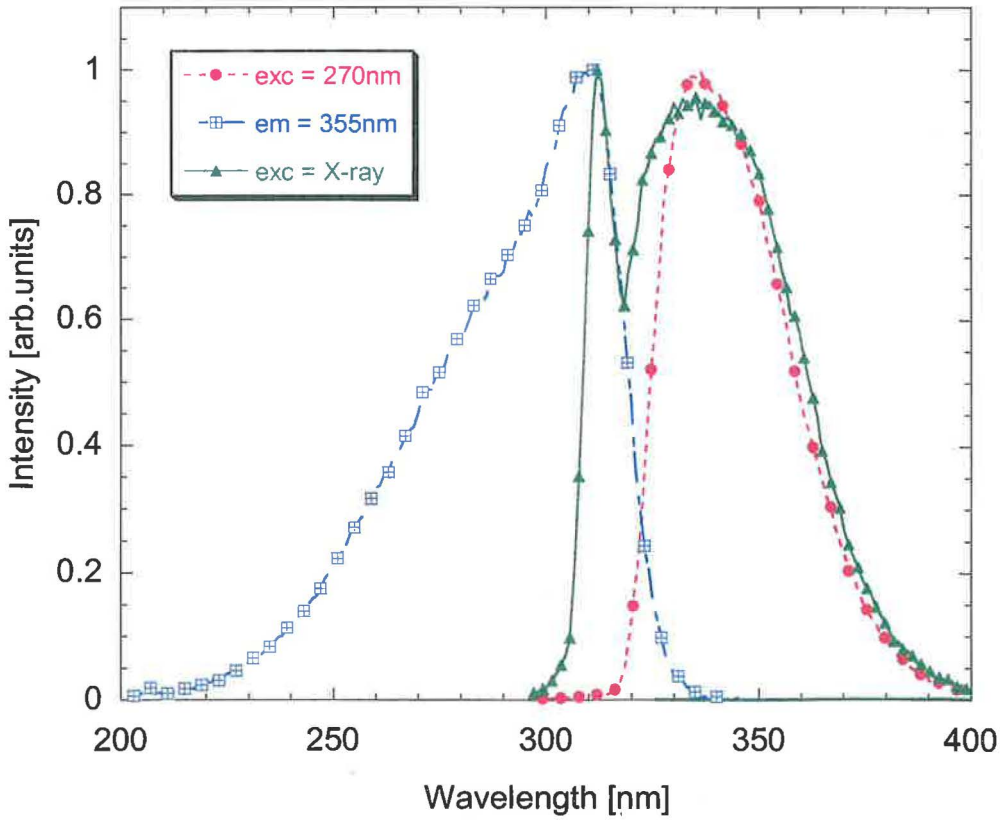

Fig. 23. Excitation ($\lambda_{em.}$ = 355 nm) and emission ($\lambda_{exc.}$ = 270 nm and X-ray) spectra of $Na_{75}Gd_{24}Ce_1$ sample at RT

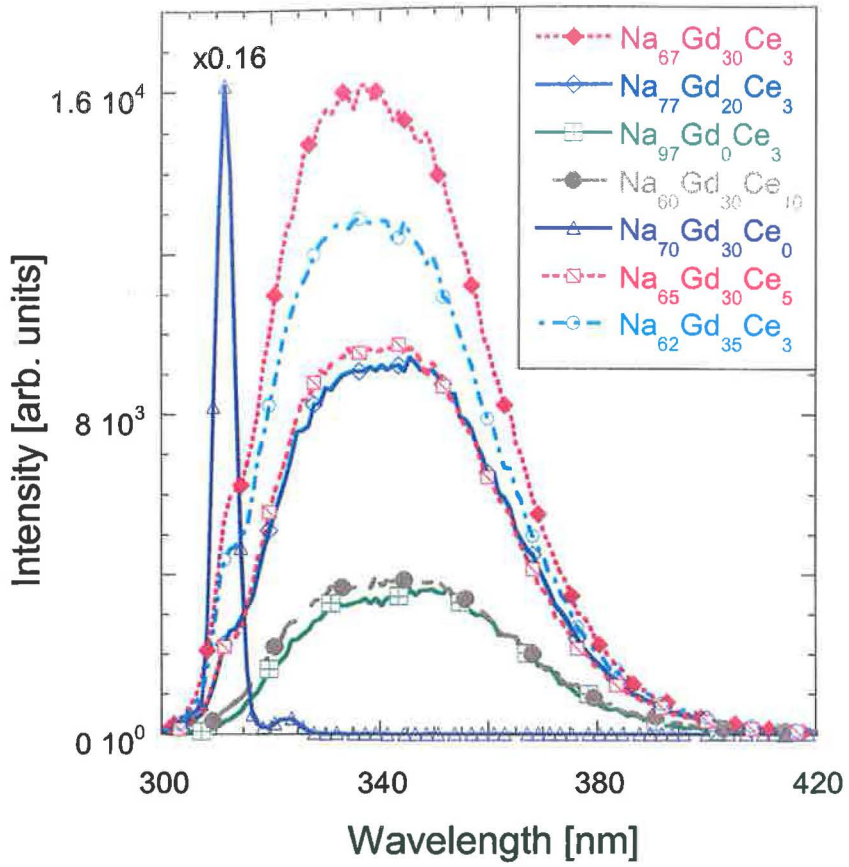

Fig. 24. Radioluminescence spectra of Ce-doped phosphate glasses at RT (X-ray excitation).

the Gd^{3+} emission peak is clearly visible round 312 nm, which is in perfect overlap with the lowest part of Ce^{3+} excitation spektrum. Such overlap is an evidence that efficient energy transfer $Gd^{3+} \rightarrow Ce^{3+}$ can occur.

In Fig. 24 X-ray excited emission spectra of the set of $Na_xGd_yCe_z$ samples are given. The samples are about the same shape and all the measurements were performed in comparable conditions, so that the spectra can be compared in an

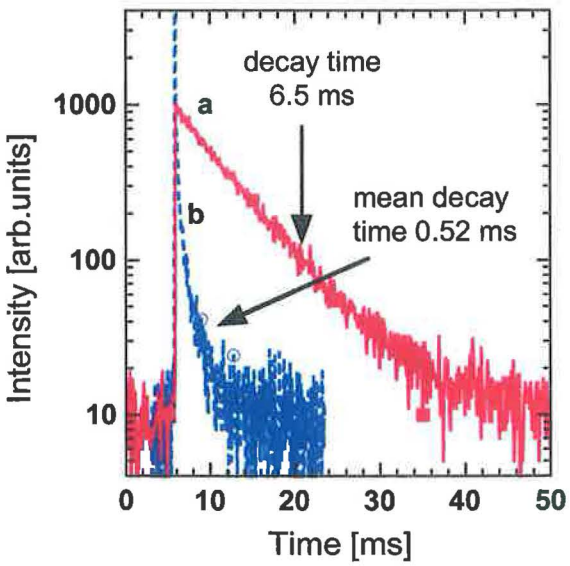

Fig. 25. Photoluminescence decay of Gd^{3+} centres ($\lambda_{exc.}$ = 275 nm, $\lambda_{em.}$ = 312 nm) at RT: a) $Na_{75}Gd_{25}$; b) $Na_{74}Gd_{25}Ce_1$

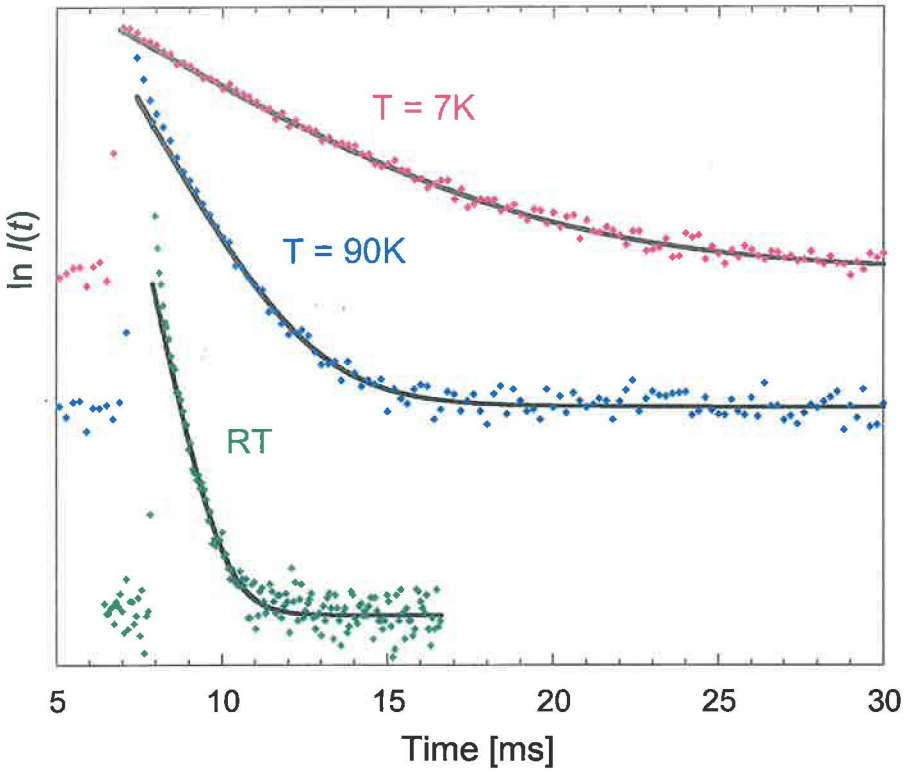

Fig. 26. Photoluminescence decay of $Na_{69}Gd_{30}Ce_1$ glass (λ_{exc} = 275 nm, λ_{em} = 312 nm)

absolute way. We have observed strongly increasing efficiency of Ce^{3+} emission in the Gd^{3+}-containing $Na_{67}Gd_{30}Ce_3$ sample with respect to Gd^{3+}-free $Na_{97}Gd_0Ce_3$ sample, while the Gd^{3+} emission show strong intensity decrease in Ce^{3+}-containing samples (see Fig. 24). Maximum radioluminiscence intensity was achieved for Ce^{3+} concentrations about 3 mol%. Decreased radioluminescence intensity in the case of 5% and 10% Ce^{3+}-doped samples might be related to a (Ce^{3+}-related) concentration quenching, which is known from other material systems as well. Optimum Gd concentration seems to be round 30%, but it could be explained by an imperfect technology of glasses preparation. For improved glasses samples intensity of emission increases with increasing of Gd^{3+} concentration (further see Chapter 6).

Gd^{3+} decay kinetics

The energy transfer $Gd^{3+} \rightarrow Ce^{3+}$ can be evidenced also from the Gd^{3+} emission decay in Fig. 25. While Ce^{3+}-free $Na_{75}Gd_{25}$ sample show undistorted Gd^{3+} decay of single exponential shape and decay time of about 6.5 ms, substantial shortening and non-exponential shape (mean decay time about 0.52 ms) is evident for $Na_{74}Gd_{25}Ce_1$ sample. Such behaviour can be explained by efficient energy transfer from the Gd^{3+}-subsystem towards Ce^{3+} emission centres.

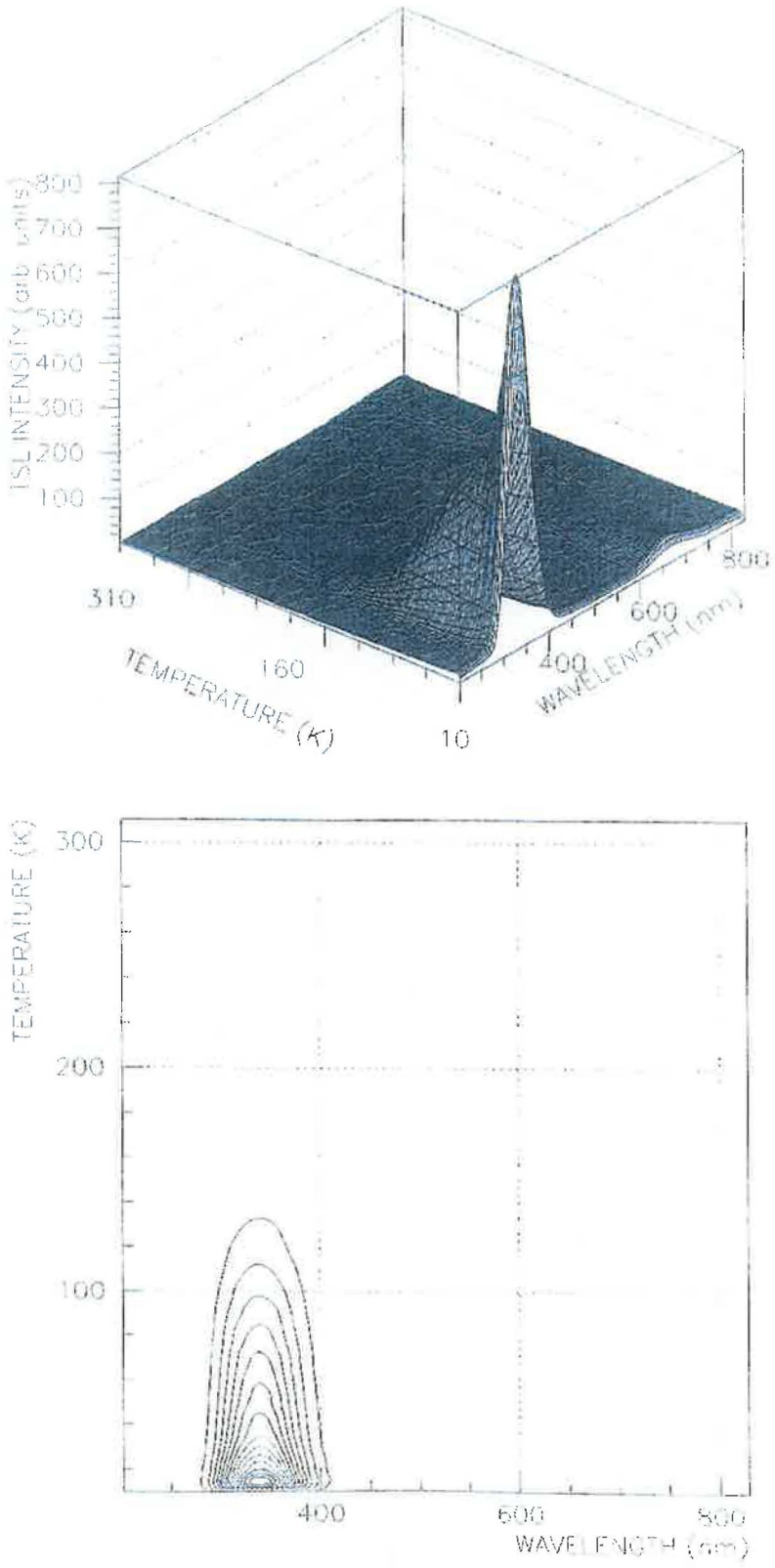

Fig. 27. Wavelength resolved thermally stimulated luminescence measurements on $Na_{74}Gd_{25}Ce_1$ glass after X-ray irradiation at 10 K

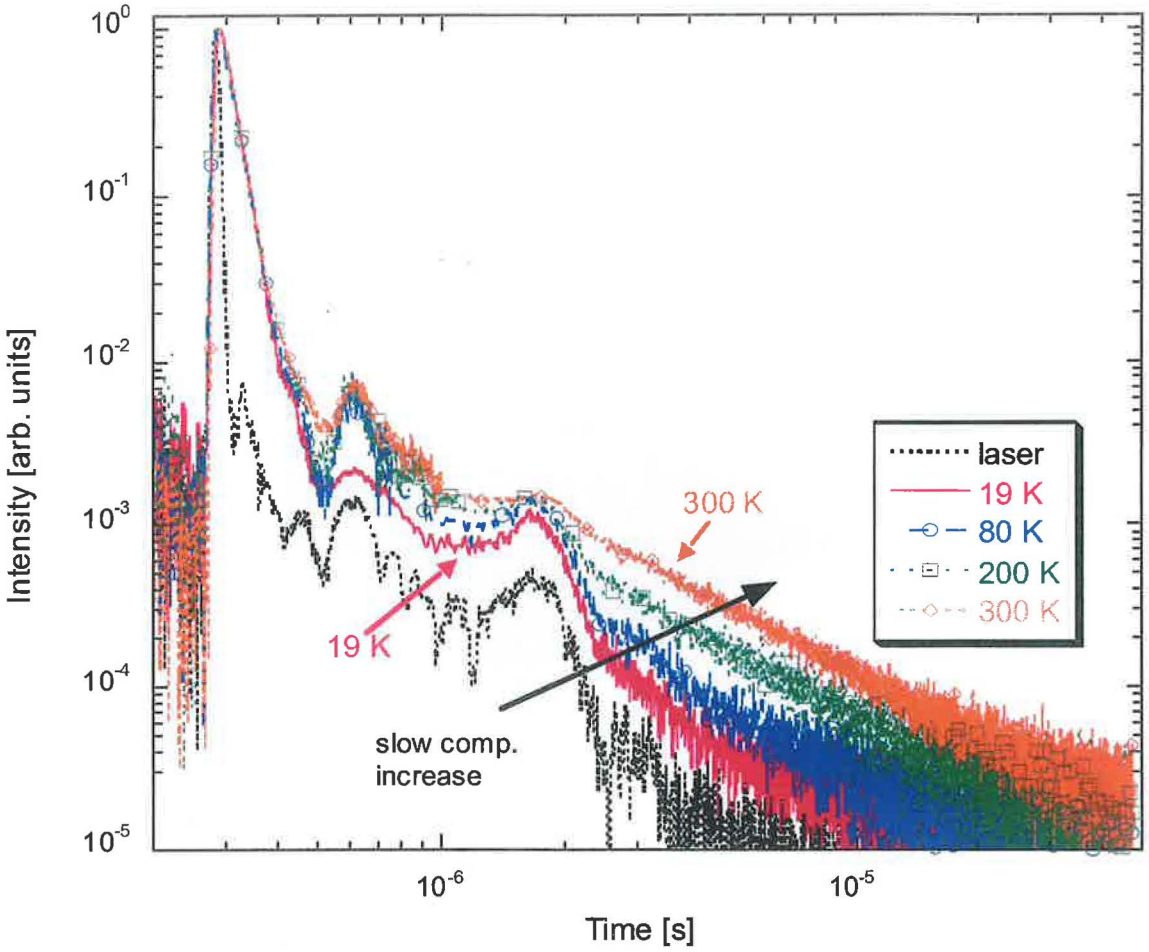

Fig. 28. Photoluminescence decay of $Na_{52}Gd_{45}Ce_3$ phosphate glass (exc. = 308 nm, em = 345 nm).The arrow shows the enhancement of the slow decay components in the μs time scale with elevated temperature.

Strong acceleration of Gd decay kinetics is also observed with increasing of temperature. In Fig. 26 decay curves are presented for the sample $Na_{69}Gd_{30}Ce_1$ at three temperatures. The Gd^{3+} decay kinetics will be analyzed in more detail in Subsection 5.1.2.

Thermally stimulated luminescence

The wavelength distribution of the thermally stimulated luminescence signals within 10-300 K was also investigated. Fig. 27 reports a contour plot of a measurement performed on the $Na_{74}Gd_{35}Ce_1$ sample. Only one band, centered at about 340 nm, is present, which coincides with radioluminescence spectra of Ce^{3+}-doped samples (Fig. 24). Smoothly increasing TSL signal below 140 K points to a broad continuum of shallow electron traps.

Bidirectional energy transfer

The presence of the back energy transfer $Ce^{3+} \rightarrow Gd^{3+}$ is evidenced by Ce^{3+} photoluminescence decay in extended dynamical and time scale and the enhancement of the amplitude of the slow component in the decay kinetics (Fig. 28). The slow components appear due to return of the excitation energy from the acceptor to donor and its further migration through the donor subsystem. So, the migration path is longer:

$Gd^{3+} \rightarrow Gd^{3+} \rightarrow .... \rightarrow Gd^{3+} \rightarrow \mathbf{Ce^{3+}} \rightarrow Gd^{3+} \rightarrow Gd^{3+} \rightarrow ... \rightarrow Gd^{3+} \rightarrow \mathbf{Ce^{3+}} \rightarrow \lambda_{em}\nu$

Strong dependence of slow component intensity on temperature proves thermally stimulated character of this process with an activation energy.

5.1.2 Discussion

The Gd^{3+} decay kinetics (λ_{exc} = 275 nm, λ_{em} = 312 nm) for the Ce^{3+}-doped samples was measured in the wide temperature range from 7 K through 300 K. For the low temperatures between 7 K and 150 K, the kinetics was measured with the time step of 100 μs, and for the higher temperatures from 150 K through 300 K, it was measured with the step of 20 μs because of shortening of the curves (see Fig. 26).

A few of the decay curves are shown in Fig. 26. Note that each curve has a non-exponential beginning and an exponential tail. The presence of the exponential tails accelerated with increasing temperature indicates the existence of energy migration in the donor (Gd^{3+}) subsystem. Moreover, the non-exponential initial part in the presence of an exponential tail suggests that the energy migration is diffusion limited [vries1988].

Another topic to discuss is the role of phonons in the Gd^{3+}-Gd^{3+} energy transfer. This will be described in Subsection 5.1.2.2.

5.1.2.1 Type of energy migration

Let us recall from Section 2.5 that energy migration can be described by a diffusion mechanism if the ratio $Z = C_{DA} / C_{DD}$ is much greater than 1. The values of C_{DA} and C_{DD} can be derived from the parameters γ and $\overline{W}$, which characterize the initial part and the tail of the decay curve, respectively (see Section 2.6). The analysis of the initial part of the decay curve requires the light intensity be measured with a sufficiently small time step. Therefore the estimation of C_{DA} and C_{DD}, and testing the hypothesis of the diffusion-limited mechanism

were based on the data for the temperatures between 150 K and 300 K, where the decay kinetics was measured with the smaller step of 20 μs.

According to the estimation procedure outlined in Section 2.6, the measured decay curves after the subtraction of the background noise were fitted with the least squares method by equation

$$I(t) = \exp\left(-\frac{t}{\tau_0}\right) J(t), \tag{57}$$

where $J(t)$ is given by Bondar's formula (43), and $\tau_0 = 5.8$ ms is the donor (Gd^{3+}) decay time in the acceptor-free sample [babin2003]. The quality of fit was found unsatisfactory. Therefore alternative approaches were developed.

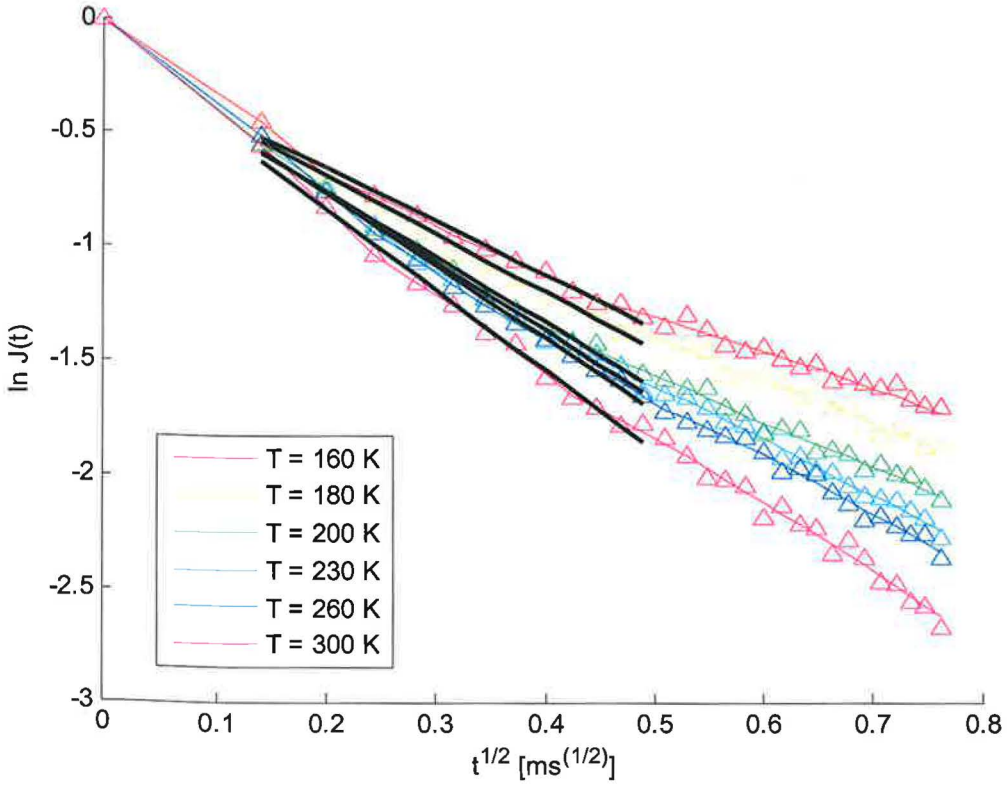

Fig. 29. Fitting of the beginnings of the decay curves (λ_{exc} = 275 nm, λ_{em} = 312 nm) for the $Na_{69}Gd_{30}Ce_1$ sample. Triangles denote the measured data. Colored lines are log-convex approximations (see Appendix A). Bold black lines are the approximations by $-\beta - \gamma\sqrt{t}$

To identify the bounds of Stage 2 (see Fig. 11, Section 2.5) and estimate the parameter γ, for each temperature T = 160 K, 180 K, 200 K, 230 K, 260 K, 300 K, the function $\ln J(t)$, which is the logarithm of the measured decay curve net of the intradonor decay, was plotted

versus $\sqrt{t}$ for small times t (see Fig. 29). Looking at these graphs, one can clearly see initial straight line segments. These segments indicate the parts of the decay curves that are described by equation $\ln J(t) = -\gamma\sqrt{t}$. Having visually determined the bounds of these segments, we fit them by formula

$$-\beta - \gamma\sqrt{t}, \tag{58}$$

using the least squares method. Since the observations at the very early times are likely to be distorted with the direct light from the lamp, thus shifting the observed light intensity upwards, the first data point was omitted. The obtained dependence of γ on the temperature is graphically shown in Fig. 30, and is duplicated in Table 3. Note that the value of γ increases by more than 1.5 times in the considered temperature range from 160 K through 300 K. This persistent and considerable growth of γ is robust to reasonable variations in the number of data points used in the estimation.

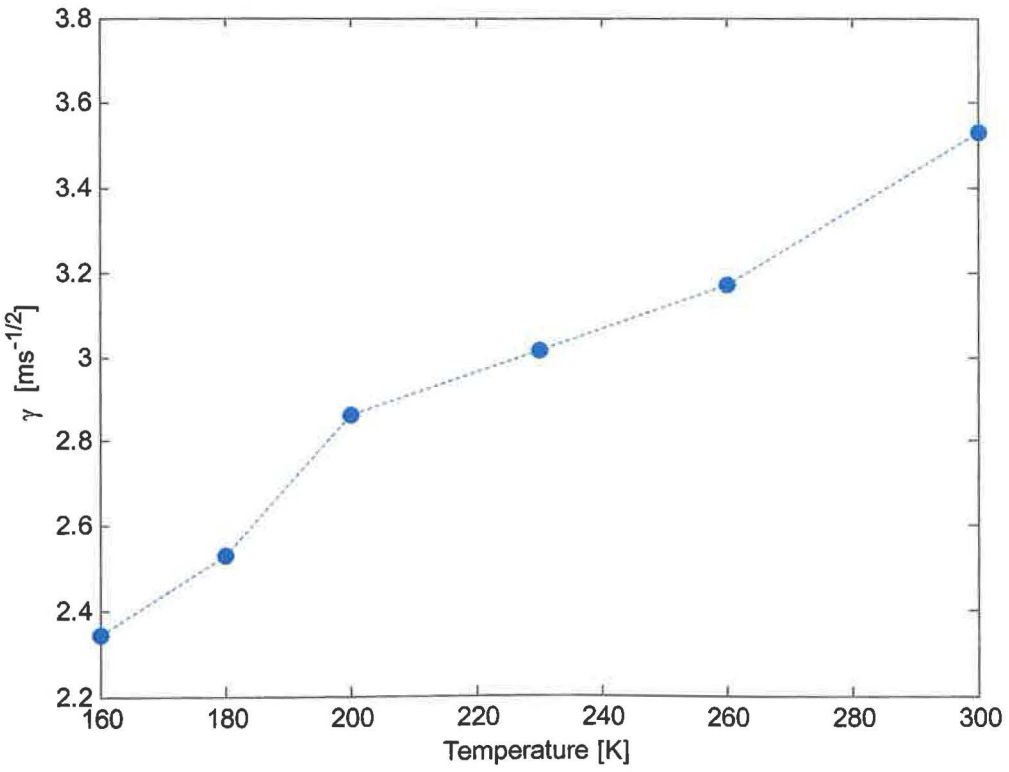

Fig. 30. Temperature dependence of γ for the $Na_{69}Gd_{30}Ce_1$ sample

Table 3. Temperature dependence of the parameters of energy transfer for the $Na_{69}Gd_{30}Ce_1$ sample (the values of C_{DD} are given under the hypothesis of diffusion-limited energy migration)

T [K]	γ [ms$^{-1/2}$]	$\overline{W}$ [ms^{-1}]	C_{DA} [m^6/ms] x 10^{-51}	C_{DD} [m^6/ms] x10^{-55}	$Z=C_{DA}/C_{DD}$
160	2.34 ± 0.20	0.89 ± 0.03	0.05 ± 0.01	0.17 ± 0.02	3024.6
180	2.53 ± 0.24	1.03 ± 0.04	0.06 ± 0.01	0.20 ± 0.02	3051.4
200	2.86 ± 0.19	1.09 ± 0.03	0.08 ± 0.01	0.19 ± 0.02	3909.1
230	3.02 ± 0.26	1.17 ± 0.06	0.08 ± 0.01	0.21 ± 0.03	4123.3
260	3.17 ± 0.21	1.31 ± 0.05	0.09 ± 0.01	0.23 ± 0.02	4030.4
300	3.53 ± 0.27	1.54 ± 0.07	0.12 ± 0.02	0.27 ± 0.03	4311.9

The estimation of the asymptotic rate of quenching $\overline{W}$ was based on a combination of two techniques. The first is fitting of the tail of the decay curve with an exponential function. As it was already pointed out, the problem with this method is the determination of the beginning of the exponential tail. To solve this problem, the entire decay curve was fitted by a log-convex function (see Appendix A). The tail was determined as the point t_0 where the slope of the log-convex approximation becomes indistinguishable from the slope of the exponential fit on the interval $[t_0,\infty)$. The common slope at the time t_0 determines the "raw" asymptotic decay rate W, which is related to $\overline{W}$ by formula

$$W = \frac{1}{\tau_0} + \overline{W}. \tag{59}$$

The found values of $\overline{W}$ are gathered in Table 3.

Having estimated the parameters γ and $\overline{W}$, and assuming diffusion-limited energy migration, one can easily compute the parameters C_{DA} and C_{DD} by solving the system of equations (34) and (45).[1] See Table 3 for the computed values. Note that the ratio $Z = C_{DA} / C_{DD}$ is high, having the order of 10^3 for all the six temperatures. This supports the hypothesis that energy migration in the Ce^{3+}-doped samples is diffusion-limited. On the other hand, assuming hopping-limited migration, we obtained, solving (47), Z of order 10^4-10^5, which is not consistent with required inequality $Z<<1$.

5.1.2.2 Role of phonons in energy transfer

The type of the phonon-assisted energy transfer between Gd^{3+} ions can be identified by the shape of the temperature dependence of C_{DD} ([holstein1981], see Section 2.7 for a review).

[1] The ion concentrations n_A and n_D were calculated under the simplifying assumption that there is no loss of the matter during the glass preparation.

The results of the revious subsection provide the values of C_{DD} for high temperatures only. For lower temperatures, it was impossible to obtain reliable estimates of γ, and therefore it was impossible to estimate C_{DD} using the technique described above. At the same time, the parameter $\overline{W}$, can be estimated for the whole temperature range, and one can try to obtain information about C_{DD} from $\overline{W}$. Under the diffusion-limited migration mechanism, equation (45) implies that

$$\overline{W}^{\frac{4}{3}} \sim C_{DA}^{\frac{1}{3}} \cdot C_{DD.}$$

Let us suppose that C_{DA} does not change with the temperature, or, at least, it grows with the temperature but not faster than C_{DD}. Then one can state that

$$\overline{W}^{\frac{4}{3}} \sim C_{DD}$$

approximately holds. In our case, note in Table that both C_{DA} and C_{DD} significantly grow when the temperature rises from 160 K to 300 K, but their ratios C_{DA}/C_{DD} fluctuates around a constant value. That is, C_{DA} and C_{DD} grow at approximately the same rate for the subrange of high temperatures. Assuming that this holds also for other temperatures, let us accept the statement that C_{DD} is roughly proportional to $\overline{W}^{\frac{4}{3}}$.

The temperature dependencies of $\overline{W}^{\frac{4}{3}}$ are shown in Fig. 31. Following [holstein1981] and [tissue1989], this dependence was fitted with function

$$\left(\overline{W}\right)^{4/3}(T) = m_1 \exp(-m_2/T) + m_3 T + m_4 T^3 + m_5 T^7,$$

where the exponential, linear, and cubic terms represent the effects of the two-phonon resonant, the one-phonon, and the two-phonon two-site non-resonant energy transfer, respectively, and the last term describes the joint effect of the (two-phonon) Raman transfer and the two-phonon one-site non-resonant energy transfer. It was found that only the exponential and linear terms are statistically significant. This implies that Gd^{3+}-Gd^{3+} energy transfer in the considered samples is accomplished dominantly by the two-phonon resonant and one-phonon processes. The one-phonon mechanism for energy transfer is most likely important only at very low temperatures (T < 50 K) [selzer1977, flach1975, wietfeldt1986]. At higher temperatures various two-phonon or Raman processes come into play. The

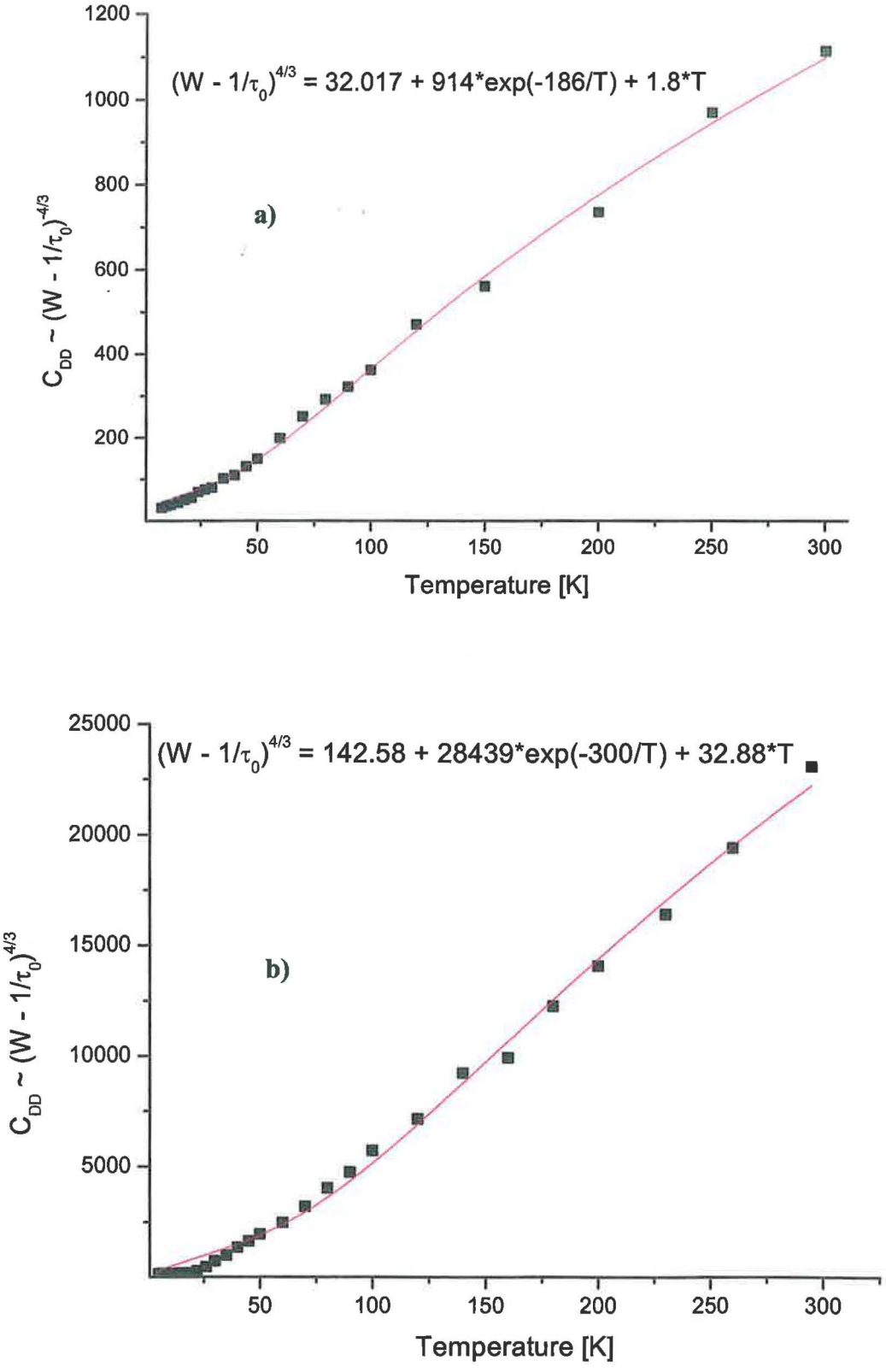

Fig. 31. Temperature dependence of $\tau_D^{-4/3}$. Solid lines show the fitting curves of the experimental results. a) $Na_{69.9}Gd_{30}Ce_{0.1}$; b) $Na_{69}Gd_{30}Ce_1$

temperature at which this begins to happen depends on the details of the one- and two-phonon transfer rates and is difficult to predict theoretically [avgin2002]. The method using two models simultaneously has already been applied [tissue1989].

Also the equation $a \cdot T^b$ was used for fitting. The estimated value of parameter b was less then 2. This fact supports the conclusion that only the two-phonon resonant and one-phonon processes may take place.

The parameter m_2 in the fitting equation is the energy mismatch ΔE_{12} covered by difference of phonons energy [holstein1981]. The value of ΔE_{12} is 129 cm^{-1} for $Na_{69.9}Gd_{30}Ce_{0.1}$ and 208 cm^{-1} for $Na_{69}Gd_{30}Ce_1$. Different kinds of phonons in Gd-enriched phosphate glasses, which have been described [dimartino2004], are presented in the Table 4.

Table 4. Description of phonon peaks in Gd-enriched phosphate glasses [dimartino2004]

Position of the phonon peak, cm^{-1}	Origin of the phonon peak
300-400	Bending and torsion vibrations
700	The symmetric stretching of the bridging oxygens linking neighboring tetrahedra (POP)
800	(POP) asymmetric stretching
1190	The symmetric stretching of a non-bridging oxygen on a Q_2 tetrahedron (PO_2)
1260-1280	(PO_2) asymmetric stretching

To cover the energy mismatch in $Na_{69.9}Gd_{30}Ce_{0.1}$ (129 cm^{-1}) the most suitable are the differences between 700 cm^{-1} and 800 cm^{-1} phonons or between 1190 cm^{-1} and 1260-1280 cm^{-1}. The energy mismatch in $Na_{69}Gd_{30}Ce_1$ has a twice greater value (208 cm^{-1}), which does not correspond to any phonon pair in Table 4. The only reasonable explanation is prevalent influence of the direct energy transfer $Gd^{3+} \rightarrow Ce^{3+}$, which is very probable in this sample with a high concentration of Ce^{3+}.

5.2 Tb^{3+}-doped phosphate glasses

For Tb^{3+} a short distance interaction is typical due to the *4f-4f* forbidden transition. Therefore, in comparison with the Ce^{3+}-doped samples considered in the previous section, effective energy transfer in the Tb^{3+}-doped samples requires higher concentration of the acceptor (Tb^{3+}) ions. The analysis will be mainly focused on the samples with 1 mol% and 10 mol% of Tb^{3+}.

5.2.1 Results

Absorption spectra

The absorption spectra of $Na_xGd_yTb_z$ phosphate glasses are displayed in Fig. 32. The Gd^{3+} line of the absorption spectrum for a Tb^{3+}-free glass is presented in the inset. With an increase of Tb^{3+} content, the intense and broad UV absorption band appears, starting around 230 nm with a weak shoulder about 250 nm. This can be ascribed to the spin-forbidden $4f^8 \rightarrow 4f^8 5d$ transitions of Tb^{3+}, respectively [blasse1982, vries1988b].

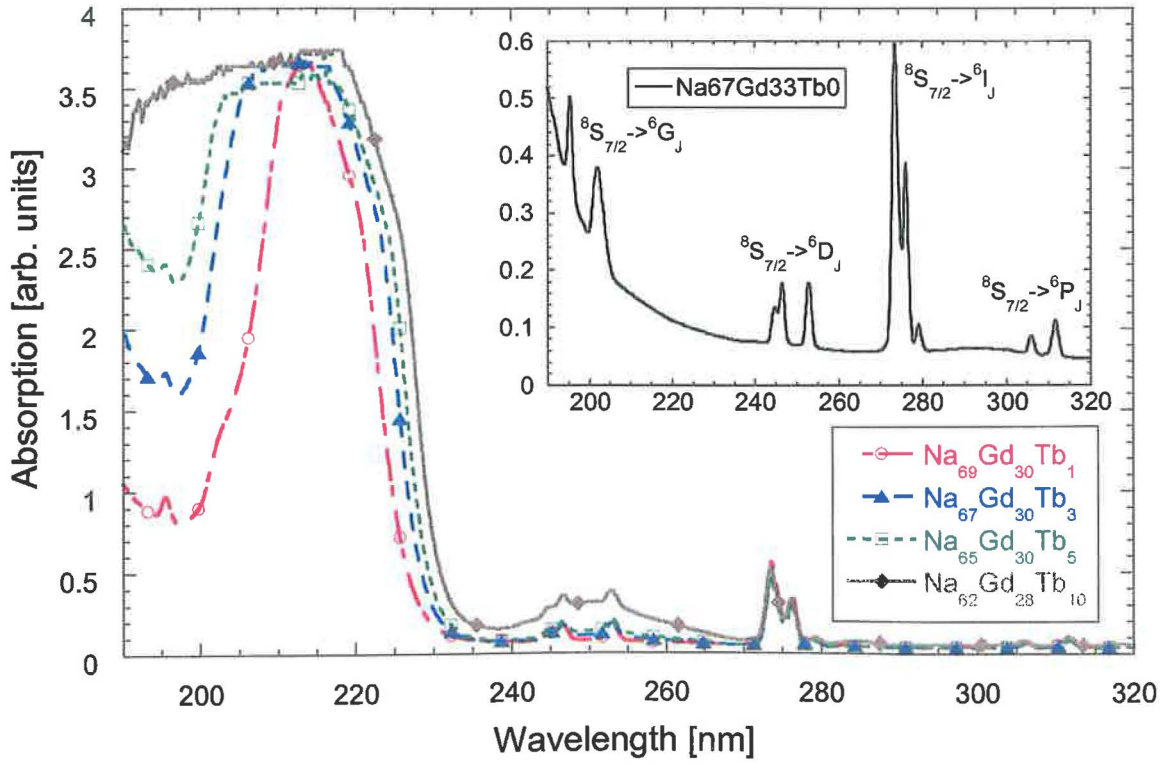

Fig. 32. Absorption spectra of the $Na_xGd_yTb_z$ phosphate glasses at RT. In the inset Gd^{3+} absorption spectrum in Tb-free sample is displayed.

Luminescence spectra

The radioluminescence spectra of the studied Tb^{3+}-doped Gd^{3+}-enriched glasses are presented in Fig. 33. The $^6P_{7/2} \rightarrow {}^8S_{7/2}$ Gd^{3+} line at about 312 nm and four Tb^{3+} $^5D_4 \rightarrow {}^7F_J$ lines (J = 6, 5, 4 and 3) at 488 nm, 542 nm, 581 nm, and 617 nm, respectively, are observed. The peak amplitudes for the Gd^{3+} 312 nm line and the Tb^{3+} 542 nm line are given in Table 5. The same table provides peak amplitudes of the Tb^{3+} 542 nm line for comparable Gd^{3+}-free samples. The inset of Fig. 33 compares excitation spectra corresponding to the Tb^{3+} 542 nm emission line in Gd^{3+}-free and Gd^{3+}-enriched samples. The excitation peak around 275 nm in the Gd^{3+}-enriched sample perfectly matches the absorption peak at 275 nm shown in the inset of Fig. 32.

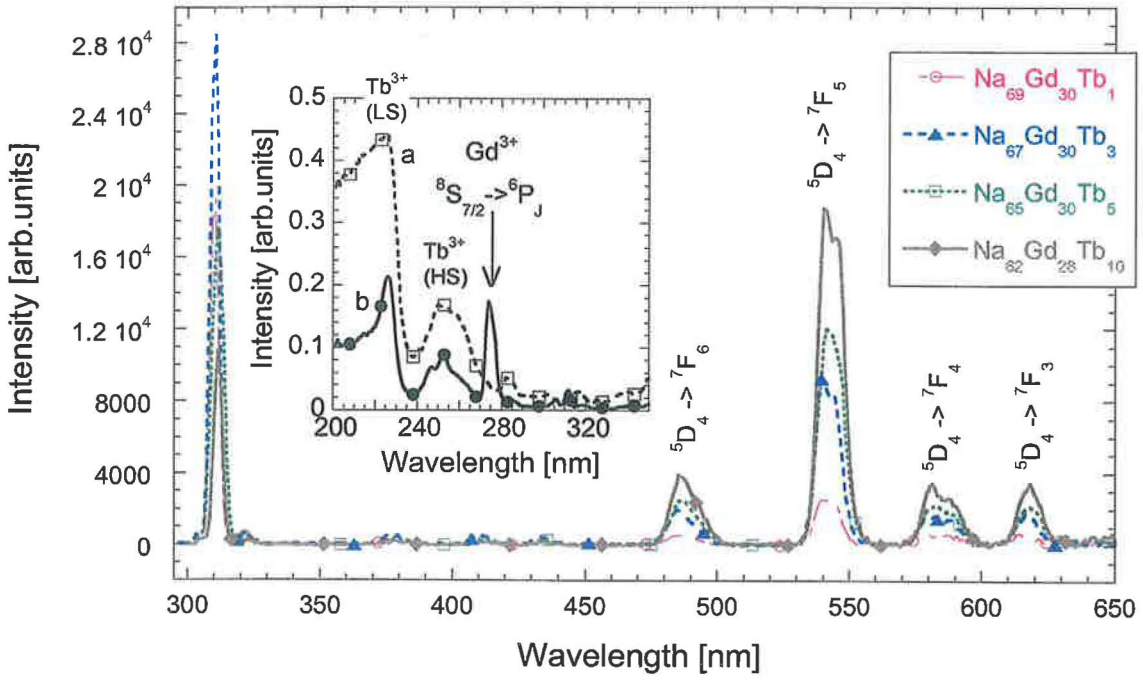

Fig. 33. Radioluminescence spectra the $Na_xGd_yTb_z$ phosphate glasses at RT. In the inset excitation spectra of Tb^{3+} 542 nm emission in $Na_{95}Gd_0Tb_5$ (curve a) and $Na_{67}Gd_{30}Tb_3$ (curve b) are given at RT.

The both excitation spectra in the inset of Fig. 33 show also two excitation bands at 225 and 270 nm corresponding to spin-allowed and spin-forbidden $4f^8 \rightarrow 4f^7 5d$ (*f-d*) transitions on Tb^{3+} [wegh1999]. This assignment is explained with the schematic spin configuration diagrams in Fig. 34. In the ground-state $4f^8$ configuration (GS), the maximum number of unpaired parallel spins is 6, which results in a total spin quantum number $S = 3$ and therefore, a spin multiplicity $2S + 1 = 7$. When one electron is promoted to the $5d$ shell, it can orient its

spin in two ways: either parallel with the 7 remaining $4f$ electrons, giving rise to a high-spin state (HS) with $S = 4$ and $2S + 1 = 9$, or antiparallel, yielding a low-spin state (LS) with $S = 3$ and $2S + 1 = 7$. According to Hund's rule, the high-spin state will be lower in energy. Thus, the transition from the ground state to the lowest $4f^7 5d$ state will be spin forbidden and therefore, relatively weak compared to the higher-energy *f-d* excitations, which are spin allowed.

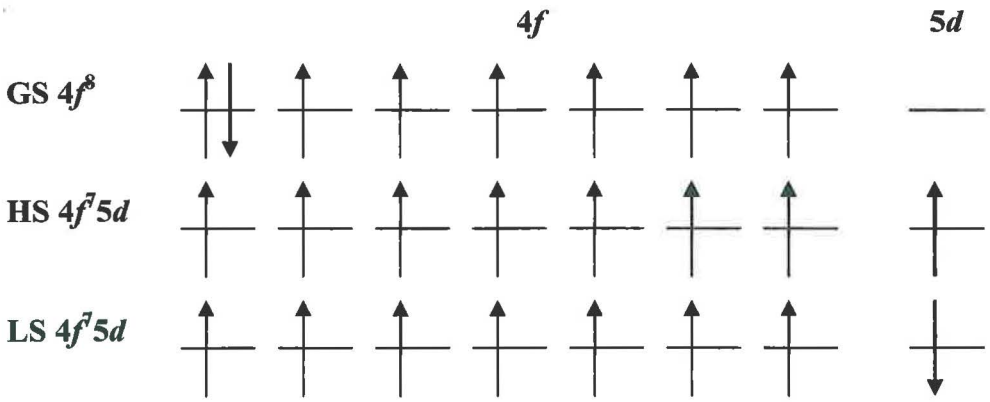

Fig. 34. Schematic electron configurations for the ground state (GS), the lowest-energetic high-spin $4f^7$5d state (HS), and the higher-energetic low-spin $4f^7 5d$ state (LS) for Tb^{3+}.

These data clearly evidence $Gd^{3+} \rightarrow Tb^{3+}$ energy transfer. Specifically,

(i) As the concentration of Tb^{3+} grows, the Gd^{3+} emission intensity decreases, and the Tb^{3+} emission intensity increases (Fig. 33 and Table 5);

(ii) Gd^{3+}-lines ($^8S_{7/2} \rightarrow {}^6P_J$, ^6I_J and higher) appear in the Tb^{3+} excitation spectrum (inset of Fig. 33);

(iii) The Tb^{3+} 542 nm emission intensity is 2–3 times higher for the Gd^{3+}-enriched samples compared to the Gd^{3+}-free samples (Table 5).

Table 5. Composition of the $Na_xGd_yTb_z$ phosphate glasses, Gd^{3+} and Tb^{3+} peak emission intensities for 312 or 542 nm wavelengths, respectively, and Gd^{3+} decay times of 312 nm emission obtained by one-exponential approximation of the decay curves

Sample composition	Intensity of Gd^{3+} 312 nm line [arb. units]	Intensity of Tb^{3+} 542 nm line [arb. units]	Decay time of Gd^{3+} 312 nm line [ms]
$Na_{67}Gd_{33}Tb_0$	4.7×10^4		5.68
$Na_{69}Gd_{30}Tb_1$	1.9×10^4	2.6×10^3	4.83
($Na_{99}Tb_1$)		(9.4×10^2)	
$Na_{67}Gd_{30}Tb_3$	2.8×10^4	9.2×10^3	3.14
($Na_{97}Tb_3$)		(3.7×10^3)	
$Na_{65}Gd_{30}Tb_5$	1.75×10^4	1.2×10^4	2.56
($Na_{95}Tb_5$)		(6.6×10^3)	
$Na_{62}Gd_{28}Tb_{10}$	1.02×10^4	2.1×10^4	1.35

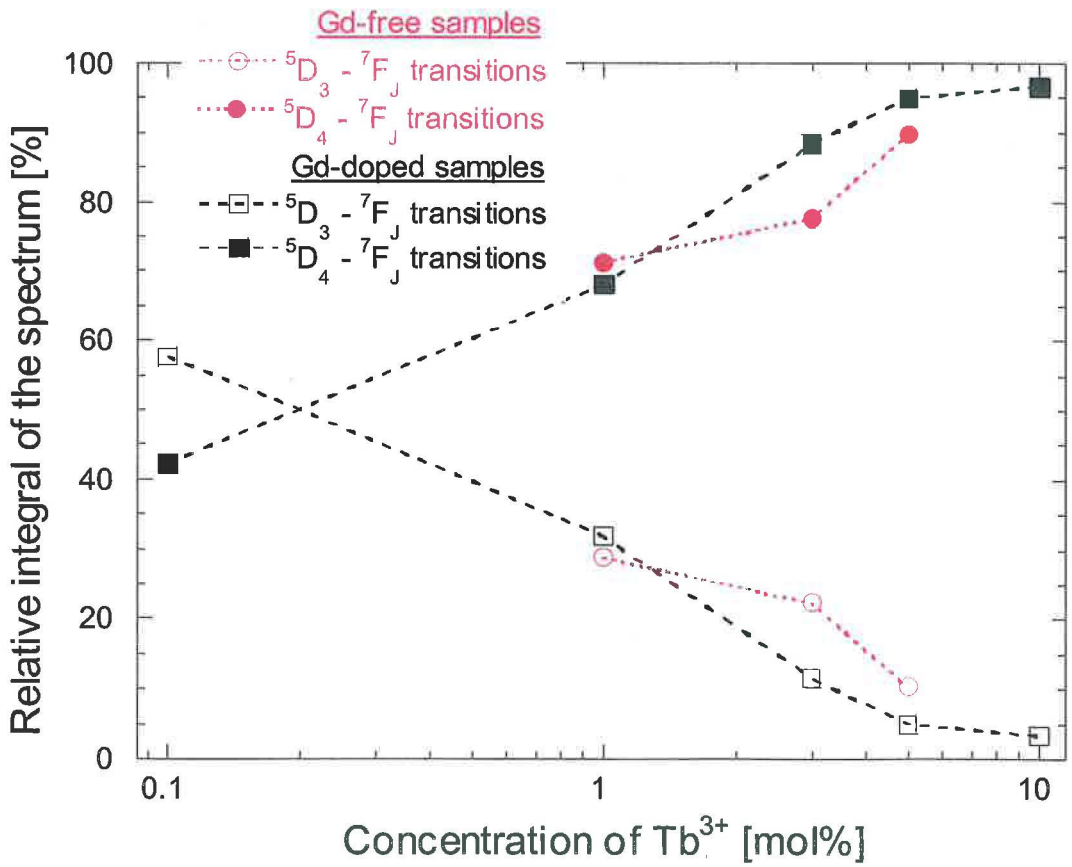

Fig. 35. The comparison of the ratio of integrated luminescence intensities of the $^5D_3 \rightarrow {}^7F_J$ and $^5D_4 \rightarrow {}^7F_J$ transitions of Tb^{3+} ions for evaluation of the cross relaxation process

The radioluminescence spectra allow also to observe the phenomenon of cross relaxation described in Section 3.1. According to the theory, as the concentration of Tb^{3+} ions rises, the probability of the cross relaxation increases and therefore the transitions $^5D_4 \rightarrow {}^7F_J$ occur more frequent than the transitions $^5D_3 \rightarrow {}^7F_J$. Thus the relative area of the peaks of the radioluminescence spectra in the region 462-635 nm ($^5D_4 \rightarrow {}^7F_J$ transitions) should increase as the concentration of the Tb^{3+} grows. Fig. 35 confirms that this is indeed the case.

Position of the Gd^{3+} emission line

The temperature dependence of the peak position of the Gd^{3+} emission band is given in (Fig. 36) [babin2003]. With the increase of the temperature, the position of the Gd^{3+} emission peak moves to higher energies. However, after 150 K the peak position is almost constant.

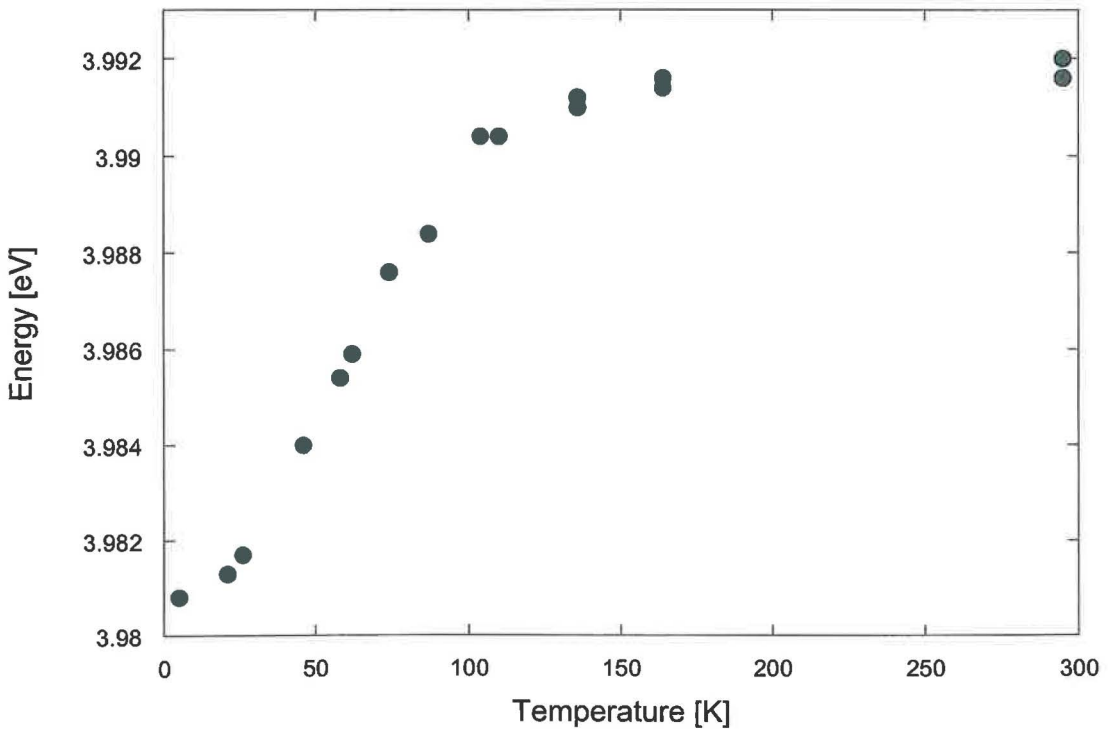

Fig. 36. Temperature dependence of the peak position of the Gd^{3+} emission band for the $Na_{62}Gd_{28}Tb_{10}$ glass under excitation into the Gd^{3+}-related 4.52 eV absorption band.

At 5 K the energy of the Gd^{3+} peak is 3.9808 eV (that corresponds to 32109.2 cm^{-1}), and at room temperature it is about 3.99 eV (is equal to 32183.4 cm^{-1}). To identify these energy levels, the data of crystal field components of Gd^{3+} in $LiYF_4$ were used [vries1988b] (Table 6). According to these data, the observed energy values correspond to various components of $^6P_{7/2}$ level. Therefore, the emission of Gd^{3+} ion is described by the transition

Table 6. Location of the crystal field components of the $^6P_{7/2}$, $^6P_{5/2}$, $^6P_{3/2}$ and $^6I_{7/2}$ levels of Gd^{3+} in $LiYF_4$-1%Gd^{3+} [vries1988b]

Level	Location [cm^{-1}]
$^6P_{7/2}$	32112.7 32153.2 32172.0 32173.7
$^6P_{5/2}$	32709.1 32756.0 32768.1
$^6P_{3/2}$	33309 33338
$^6I_{7/2}$	35844 35865 35892 35945

$^6P_{7/2} \rightarrow {}^8S_{7/2}$. However we have a larger energy range of $^6P_{7/2}$ level (about 90 cm^{-1}) than is calculated in [vries1988b] (about 60 cm^{-1}). This can be explained by inhomogeneous broadening due to crystal field fluctuation in amorphous matrix of glass.

Gd^{3+} decay kinetics

Some of the photoluminescence kinetics and the corresponding decay times for the Gd^{3+} 312 nm emission line are presented in Fig. 37 and Table 5, respectively. The decay time shortens from 5.68 ms for the Tb-free $Na_{67}Gd_{33}Tb_0$ glass down to 1.35 ms for the $Na_{62}Gd_{28}Tb_{10}$ glass, the form of the kinetics being approximately linear. Such a decay character can be explained by the facts that limited Gd^{3+} – Gd^{3+} energy migration takes place, and the rate of Gd^{3+} – Tb^{3+} is much lower than the rate of Gd^{3+} – Gd^{3+} transfer. A detailed analysis of the decay kinetics of the Tb^{3+}-doped samples is presented in the next subsection.

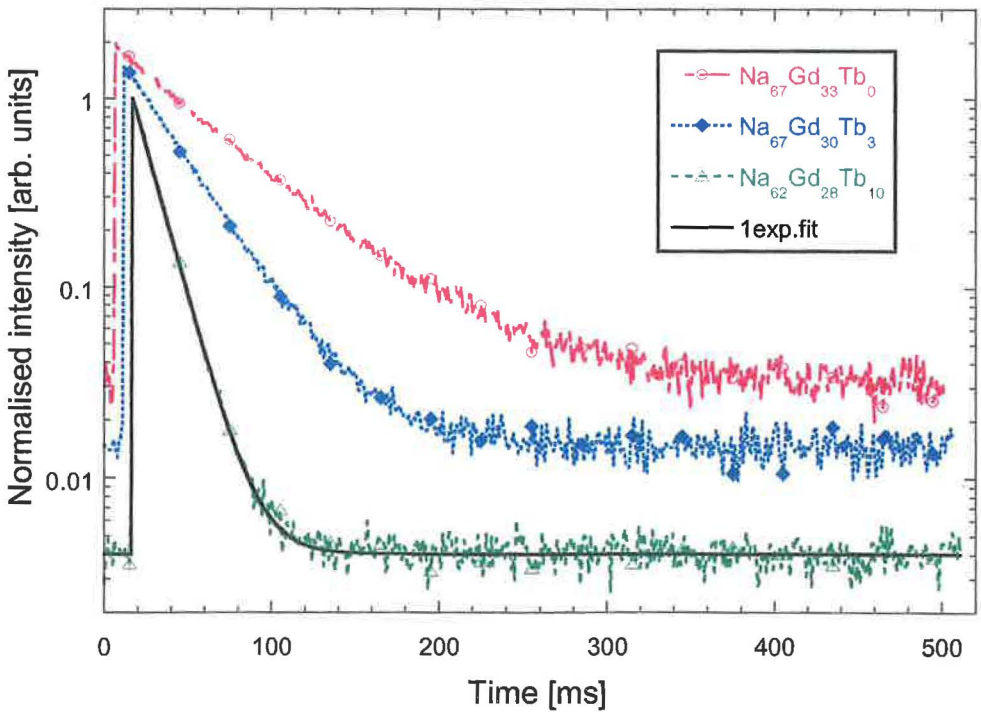

Fig. 37. Gd^{3+} decay kinetics of the $Na_xGd_yTb_z$ phosphate glasses at RT under λ_{exc} = 275 nm and λ_{em} = 312 nm. Solid line is one-exponential fit to the decay kinetics curve

5.2.2 Discussion

5.2.2.1 Type of energy migration

As in Section 5.1 on Ce^{3+}-doped glasses, the analysis of the decay kinetics of the Tb^{3+}-doped glasses presented here has two aims: 1) establish the mechanism of energy migration between the donors (whether it is diffusion-limited or hopping-limited), and 2) identify the role of phonons in the energy transfer process. For this purpose, the decay kinetics of two samples (with 1 mol % and 10 mol % of Tb^{3+}) was measured for the range of temperatures from 5 K through 300 K. Recall that temperature dependences are crucial for the identification of the phonon-assisted transfer.

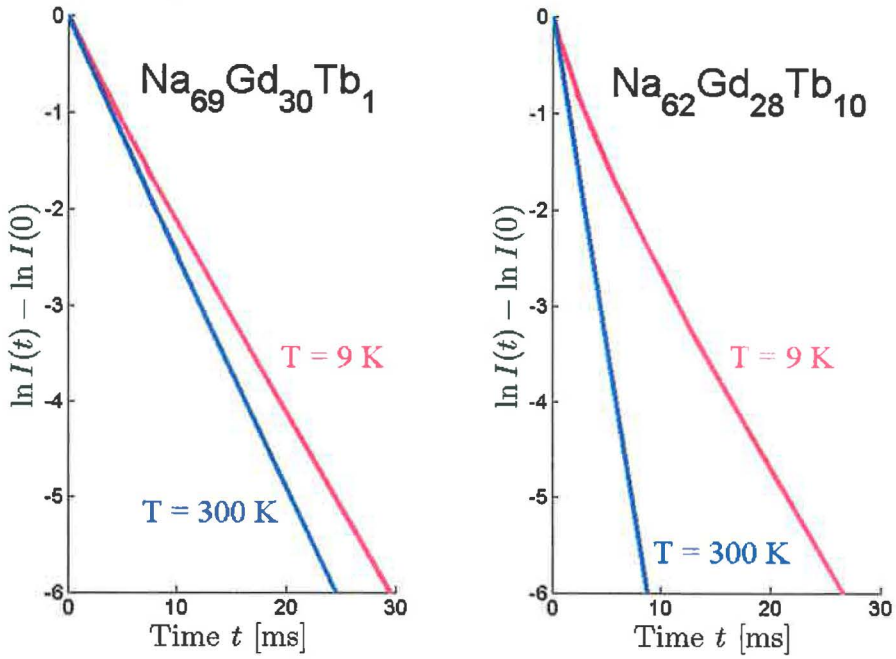

Fig. 38. The initial parts of the decay kinetics curves (log-convex approximation) for the samples $Na_{69}Gd_{30}Tb_1$ (left) and $Na_{62}Gd_{28}Tb_{10}$ (right) an the temperatures 9 K and 300 K

The decay kinetics was measured with the time step of 100 μs/channel. The decay curves were smoothed (filtered) with log-convex approximations (see Appendix A). The examination of the filtered data shows that the observed decay curves are approximately exponential. Specifically, the decay curves in the range 80 – 300 K were classified as purely exponential, while the decay curves at the lower temperatures 5 – 70 K slightly bend (see Fig. 38). In any case, the nonexponential Forster's asymptotic $\ln J(t) = -\gamma\sqrt{t}$ is not detected. This implies that the decay process is close to supermigration (see, e.g. [ursu1989] or [lupei1991] for a similar argument). Since supermigration cannot be observed under

diffusion-limited migration (see Chapter 2), we conclude that the energy migration in the Tb^{3+}-doped samples is hopping-limited. This qualitative argument will be supported by a more rigorous quantitative analysis below.

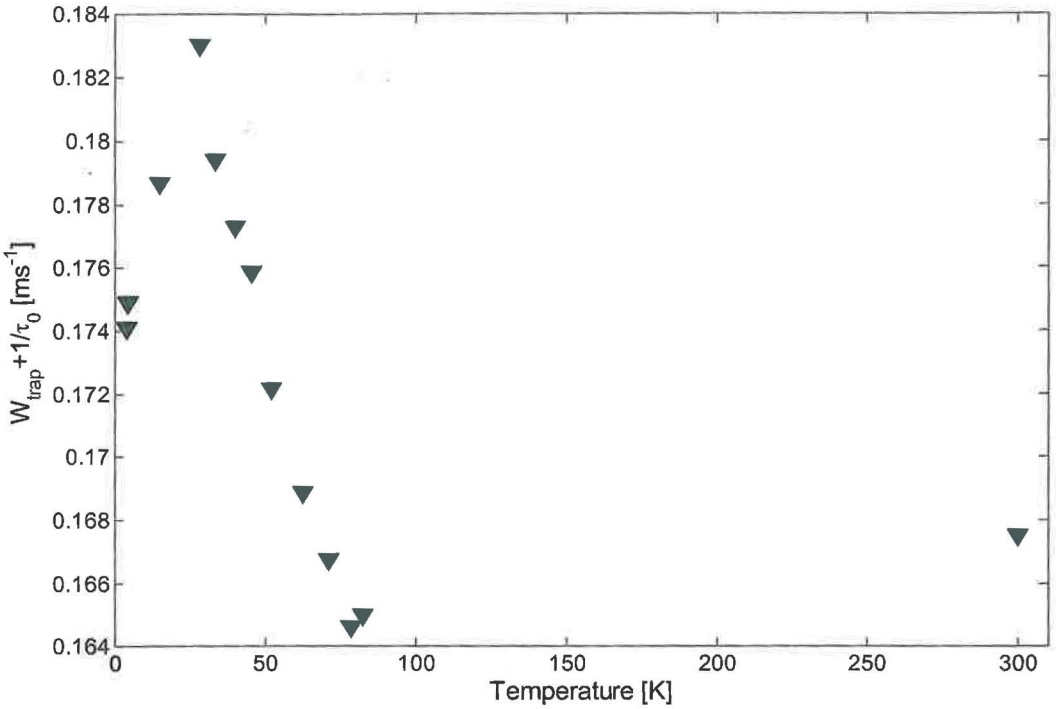

Fig. 39. The temperature dependence of the decay rate in $Na_{69}Gd_{30}$ sample (λ_{exc} = 274 nm, λ_{em} = 311 nm) [babin2003]

The observed nonexponentiality of the decay curves at the temperatures below 80 K can be explained by the presence of shallow energy traps. To be specific, the nonexponentiality may be caused by the differences in the local configurations of these traps around donors (in the same way as different locations of donors around acceptors also tend to make the donor decay nonexponential, see Section 2.5). As the temperature grows, the effect of these traps diminishes, and eventually becomes negligible. This explanation correlates with the observation that the decay rate of the Tb^{3+}-free $Na_{69}Gd_{30}$ sample is approximately constant for all temperatures above 80 K but is not constant for lower temperatures (see Fig. 39). The decay rate of the acceptor-free sample can be represented as the sum $W_{trap}+1/\tau_0$, where W_{trap} is the rate of energy quenching by the traps, and one can see in Fig. 39 can be naturally interpreted as $W_{trap} = 0$ for $T > 80$ K, and $W_{trap} > 0$ for $T < 80$ K. Thus the effect of the traps can be neglected for temperatures higher than 80 K, but it may play an essential role at lower temperatures. The presence of shallow traps is evidenced also by TSL spectra for Ce^{3+}-doped

Table 7. Temperature dependence of the parameters of energy transfer for two Tb^{3+}-doped samples

T [K]	Tb 1 mol %			Tb 10 mol %		
	$\overline{W}$ [ms^{-1}]	C_{DA} [m^6/ms] x10^{-56}	$Z=C_{DA}/C_{DD}$	$\overline{W}$ [ms^{-1}]	C_{DA} [m^6/ms] x10^{-56}	$Z=C_{DA}/C_{DD}$
160	0.0608 ± 0.0039	4.6482 ± 0.4596	2.7504	0.4947 ± 0.1274	4.3523 ± 1.4928	2.5754
180	0.0592 ± 0.0066	4.3750 ± 0.6709	2.2413	0.3859 ± 0.0679	3.1316 ± 0.7067	1.6038
200	0.0664 ± 0.0068	5.0230 ± 0.7041	2.5785	0.3627 ± 0.0349	2.9126 ± 0.3644	1.4952
230	0.0657 ± 0.0065	4.8999 ± 0.7036	2.3844	0.4236 ± 0.0423	3.4619 ± 0.4873	1.6846
260	0.0653 ± 0.0038	4.7564 ± 0.4079	2.0502	0.4765 ± 0.0452	3.8917 ± 0.5038	1.6775
300	0.0702 ± 0.0047	5.0488 ± 0.4887	1.8797	0.5308 ± 0.0562	4.3058 ± 0.6196	1.6031

sample (Fig. 27). If these traps are created by the glass matrix, they must be the same for the Ce^{3+}- and Tb^{3+}-doped samples.

Since Forster's asymptotic is not observable, the parameter γ cannot be estimated, and the only available information about the microparameters C_{DA} and C_{DD} is contained in the parameter $\overline{W}$ that describes the tail of the decay curve. Its values were retrieved in the same way as it was done for the Ce^{3+}-dopped glasses (see Subsection 5.1.2). The values of $\overline{W}$ for the six highest temperatures are gathered in Table 7.

Assuming hopping-limited energy migration as the initial hypothesis for the Tb^{3+}-doped samples, let us relate $\overline{W}$ to the parameters C_{DA} and C_{DD} by Huber's formula (50), where $R_0 = 6 \cdot 10^{-10}$ m (see Section 3.5), and, as before, use the estimates of the ion concentrations n_A and n_D obtained under the assumption that there is no matter loss during the glass preparation. Note that using only equation (50) alone, it is impossible to estimate C_{DA} and C_{DD} simultaneously. Therefore the values of C_{DD} are taken as estimated for the Ce^{3+}-doped sample (see Table 3 in Section 5.1), and substituted together with $\overline{W}$ into (50) to estimate C_{DA} for the Tb^{3+}-doped samples. Then the ratio $Z = C_{DA} / C_{DD}$ was computed. The results are given in Table 7. All values of Z in this table are of the order of 1. This clearly indicates that the energy migration mechanism in the considered Tb^{3+}-doped samples is close to being hopping-limited.

5.2.2.2 Role of phonons in energy transfer

The observed (almost) exponentiality of the decay curves means that the rate of decay at time $t = 0$ is approximately the same as the decay rate at large times t, i.e. $-\frac{d \ln J}{dt}(0) \approx \overline{W}$. Therefore using formula (44), one can state that $\overline{W}$ is approximately proportional to C_{DA}. Recall from Section 5.1 that the temperature variation of $\overline{W}$ for the Ce^{3+}-doped glasses was mainly determined by the corresponding variation of C_{DD}, which allowed to identify the type of phonon assistance in the $Gd^{3+} - Gd^{3+}$ energy transfer. The situation with the Tb^{3+}-doped glasses is different: the value of $\overline{W}$ is almost exclusively determined by C_{DA}, which results in the analysis of the role of phonons in the $Gd^{3+} - Tb^{3+}$ energy transfer. The graphs of the temperature dependences of $\overline{W}$ in the whole temperature range from 5 K to 300 K are shown in Fig. 40.

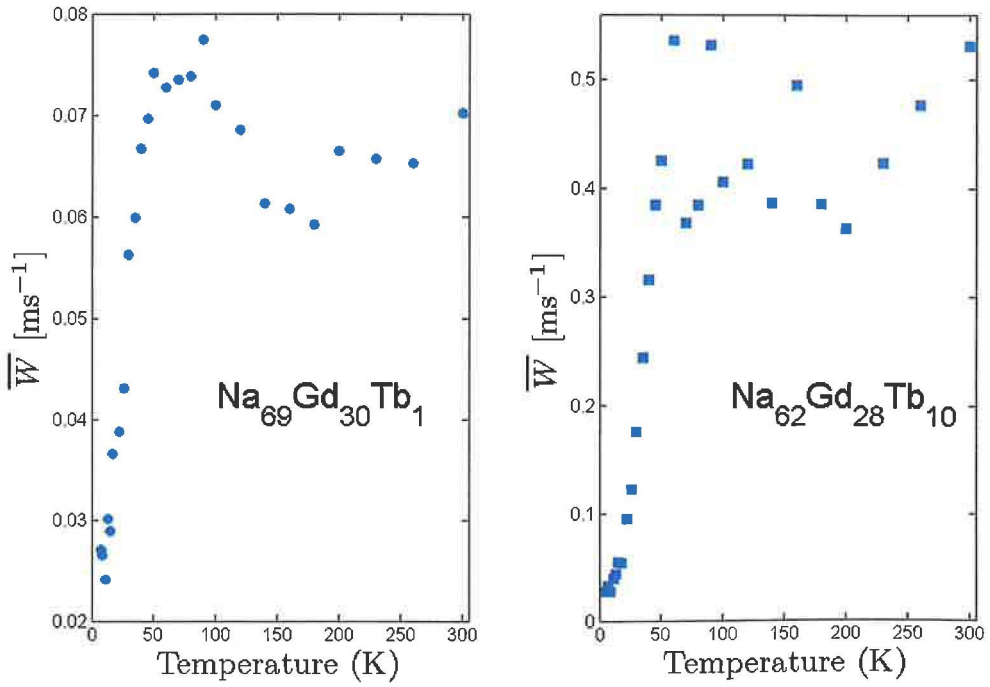

Fig. 40. The temperature dependence of $\overline{W}$ for the samples $Na_{69}Gd_{30}Tb_1$ and $Na_{62}Gd_{28}Tb_{10}$

Consider first the sample with 10 mol % of Tb^{3+}. The curve $\overline{W}(T)$ can be apparently separated into three zones. First $\overline{W}$ smoothly and nonlinearly grows. This lasts until the temperature reaches 60 K, when $\overline{W}$ begins to fluctuate around a constant value. Then, about the temperature of 200 K, $\overline{W}$ begins to grow again. Now let us analyse the first zone (5 –

60 K) in more detail (Fig. 41). To identify the type of phonon assistance, the same technique as that applied in Section 5.1 was used. Like in Section 5.1, following the ideas of [tissue1989], the temperature dependence of $\overline{W}$ was fitted with equation

$$\overline{W}(T) = m_0 + m_1 \exp(-m_2/T) + m_3 T + m_4 T^3 + m_5 T^7, \qquad (60)$$

where the exponential, linear, and cubic terms of the regression function represent the effects of the two-phonon resonant, the one-phonon, and the two-phonon two-site non-resonant energy transfer, respectively, and the last term describes the joint effect of the (two-phonon) Raman and the two-phonon one-site non-resonant energy transfers (see Section 2.7). The intercept (term m_0) is included to partially eliminate measurements errors.

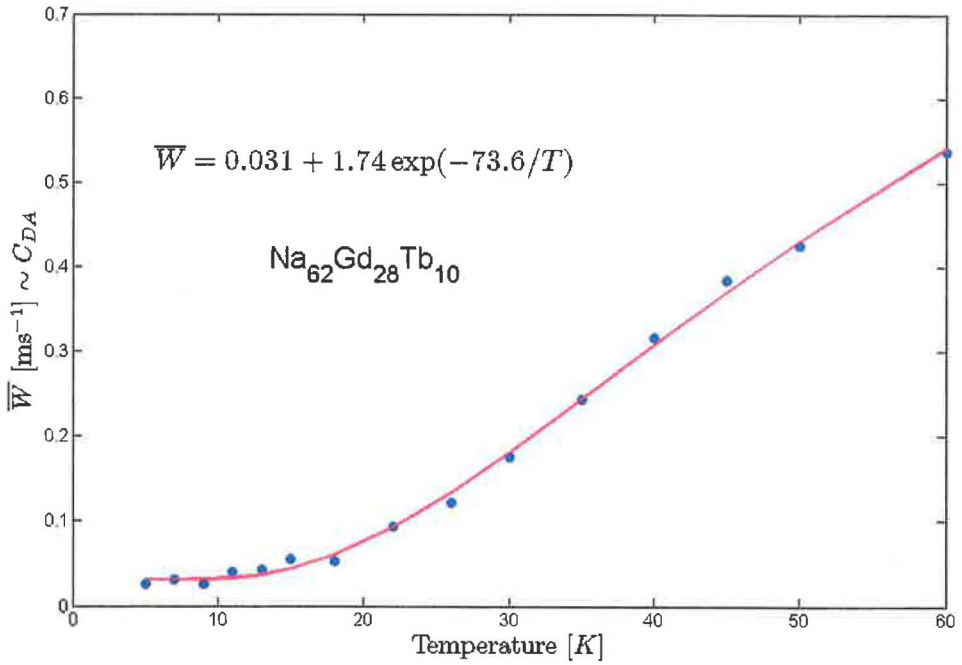

Fig. 41. The fitting curve of the temperature dependence of $\overline{W}$ for the sample $Na_{62}Gd_{28}Tb_{10}$.

a) It was found that the goodness of fit by the most general linear combination $m_0 + m_1 \exp(-m_2/T) + m_3 T + m_4 T^3 + m_5 T^7$ with arbitrary fitting parameters $m_0 - m_5$ does not much differ from the goodness of fit by linear combination $m_0 + m_1 \exp(-m_2/T)$, which is restricted to include only the exponential term (apart from the intercept, which will be present in every considered combination). This implies that the data can be explained by the two-phonon resonant phonon-assisted processes.

b) To check for alternative explanations of the data (say, can we successfully substitute the exponential component with the linear or cubic one?), the temperature dependence was also fitted by combination $m_0 + m_3 T + m_4 T^3 + m_5 T^7$. The goodness of fit was satisfactory, but at the expense a negative coefficient in front of T^7. The presence of negative coefficients implies that one or more components in the combination are redundant. Therefore the data was fitted by the simpler combinations $m_0 + m_3 T + m_4 T^3$, $m_0 + m_3 T + m_5 T^7$, and $m_0 + m_4 T^3 + m_5 T^7$. These combinations were found to approximate the data significantly worse than the combination $m_0 + m_1 \exp(-m_2/T)$. Thus no new candidates for the explanation of the data were found.

We conclude that the $Gd^{3+} - Tb^{3+}$ energy transfer in the $Na_{62}Gd_{28}Tb_{10}$ sample in the low temperature range 5 – 60 K is due to the two-phonon resonant process. The behavior of $\overline{W}$ in the opposite range of the high temperatures 200 – 300 K is obviously linear, which implies that the phonon-assisted process at these high temperatures is one-phonon. Finally, the middle temperature range 60 – 200 K is likely to be a transition zone between the two-phonon resonant and one-phonon processes.

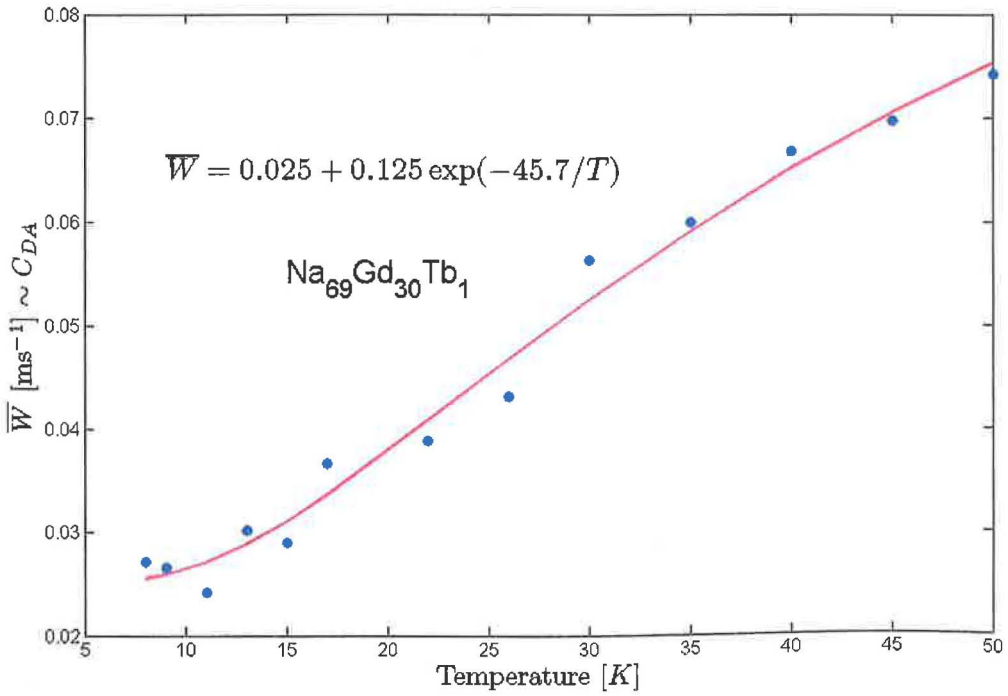

Fig. 42. The fitting curve of the temperature dependence of $\overline{W}$ for the sample $Na_{69}Gd_{30}Tb_1$.

The temperature dependence of $\overline{W}$ for the $Na_{69}Gd_{30}Tb_1$ sample with 10 mol % of $Tb^{3+}$and its analysis are very similar to those for the $Na_{62}Gd_{28}Tb_{10}$ sample, and therefore only the results and some special features will be pointed out. First, like for the $Na_{62}Gd_{28}Tb_{10}$ sample, the $Gd^{3+} - Tb^{3+}$ energy transfer in the $Na_{69}Gd_{30}Tb_1$ sample in the low temperature range 5 – 50 K is two-phonon resonant (see Fig. 42). Second, the fluctuations in the middle temperature range are not as strong as for the $Na_{62}Gd_{28}Tb_{10}$ sample, and one can see that after reaching a local maximum at 50 K, $\overline{W}$ begins to fall. This fall seems to be a stable pattern. Third, the growth of $\overline{W}$ starting at about 200 K cannot be clearly identified. Maybe, the transition period ends at temperatures higher than the room temperature.

The energy difference ΔE_{12} (the parameter m_2 in the fit formula) is equal 32 cm^{-1} for the sample $Na_{69}Gd_{30}Tb_1$ and 51 cm^{-1} for the sample $Na_{62}Gd_{28}Tb_{10}$. Such the phonons energies belongs to acoustic phonons and consequently cannot be measured by Raman spectroscopy and identified with the energies from Table 4.

5.3. Summary

- Two groups of samples of Na-Gd phosphate glasses are considered, which represent Ce^{3+}-doped glasses (Section 5.1) and Tb^{3+}-doped glasses (Section 5.2). The experimental results provide a comprehensive description of optical properties of the studied samples (absorption, excitation, and emission spectra, and decay kinetics).
- The increase of the Ce^{3+} and Tb^{3+} radioluminescence intensities after enriching the glasses with Gd^{3+} ions clearly indicates energy transfer from Gd^{3+} ions to Ce^{3+} and Tb^{3+} ions. The presence of the energy transfer phenomenon is also supported by the shortening of the Gd^{3+} luminescence decay times with the increase of the temperature or the increase of the Gd^{3+} concentration.
- The type of the energy transfer mechanism was established through the investigation of the Gd^{3+} decay kinetics, which involved the analysis of the shape of the decay curves and the estimation of the microparameters C_{DA} and C_{DD} describing the rates of the ion-ion interactions. It was found that the energy transfer in the Ce^{3+}-doped samples is diffusion-limited, and the energy transfer in the Tb^{3+}-doped samples is hopping-limited. In addition, the energy transfer in the Tb^{3+}-doped samples is close to the kinetic limit (supermigration).
- The analysis of the temperature dependences of the rates of energy transfer reveals the role of phonons in the energy transfer process. In particular, it was established that the dominating role in the $Gd^{3+} - Gd^{3+}$ and $Gd^{3+} - Tb^{3+}$ energy transfer is played by two-phonon resonant and one-phonon processes.
- It was found that the position of the Gd^{3+} emission line in the $Na_{62}Gd_{28}Tb_{10}$ sample changes with the temperature, which is apparently influenced by the participation of different sublevels of the $^6P_{7/2}$ level in the $^6P_{7/2} \rightarrow S$ transition.
- For Ce^{3+}-doped samples, back energy transfer is found. It is explained by the overlap of the absorption and emission spectra, and is also supported by the observed decay kinetics after laser excitation.
- For Tb^{3+}-doped samples, the phenomenon of cross-relaxation was studied. Fig. 35 proves its existence.

Chapter 6

Improved Ce^{3+}-doped phosphate glasses: influence of high concentration of Gd^{3+}

In this chapter we consider the optical and scintillation properties of a new set of Ce^{3+}-doped phosphate glasses, obtained by a new improved technology [rodova2004]. These glasses can be thought of as the second generation of the glasses considered in the previous chapters (therefore the samples a denoted as $Na_xGd_yCe_z$-II). The new technology allows to prepare a more homogeneous mixture of matrix and doping components, which makes possible to produce samples with a very high concentration of Gd^{3+}. Using the new technology, two sets of samples were obtained. The sets differ from each other by the concentration of the acceptor (1 mol% and 4 mol% of Ce^{3+}), and in each group the samples vary in the concentration of the donor (10 mol% - 90 mol% of Gd^{3+}). Such the variety gives us an opportunity to investigate concentrational dependencies of various parameters and characteristics. Their key characteristics are discussed to provide a rough estimate of their quality compared to the glasses of "the first generation".

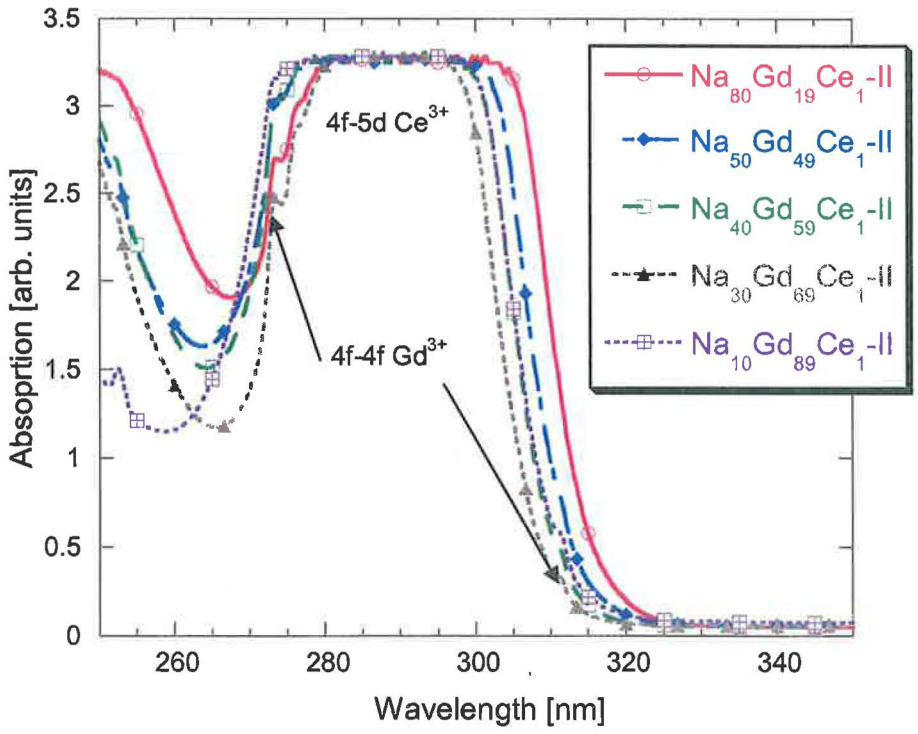

Fig. 43. The absorption spectra of some of the new Ce^{3+}-doped phosphate glasses. The composition of glasses is marked in the legend.

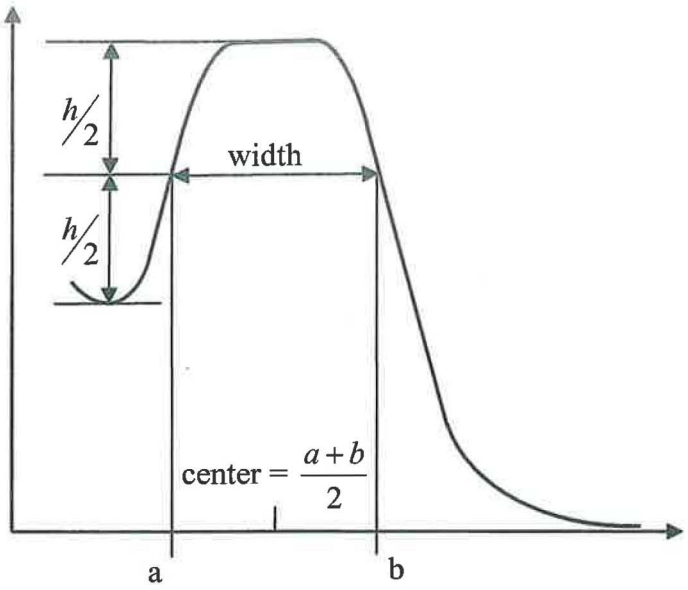

Fig. 44. Scheme of calculation the width and the position of the centre of the absorption band

Absorption spectra

The absorption spectra of some of the new glasses are presented in Fig. 43. The wide band corresponding to the 4f-5d Ce^{3+} transition and small narrow peaks (at 275 nm and 310 nm) of the 4f-4f Gd^{3+} transition are shown by arrows. Due to the overlap of the absorption and emission peaks of both Ce^{3+} and Gd^{3+} the bidirectional transfer is possible. The positions of the Gd^{3+} peaks are completely identical, but the Ce^{3+} peaks differ by both the width and the position of the centre.

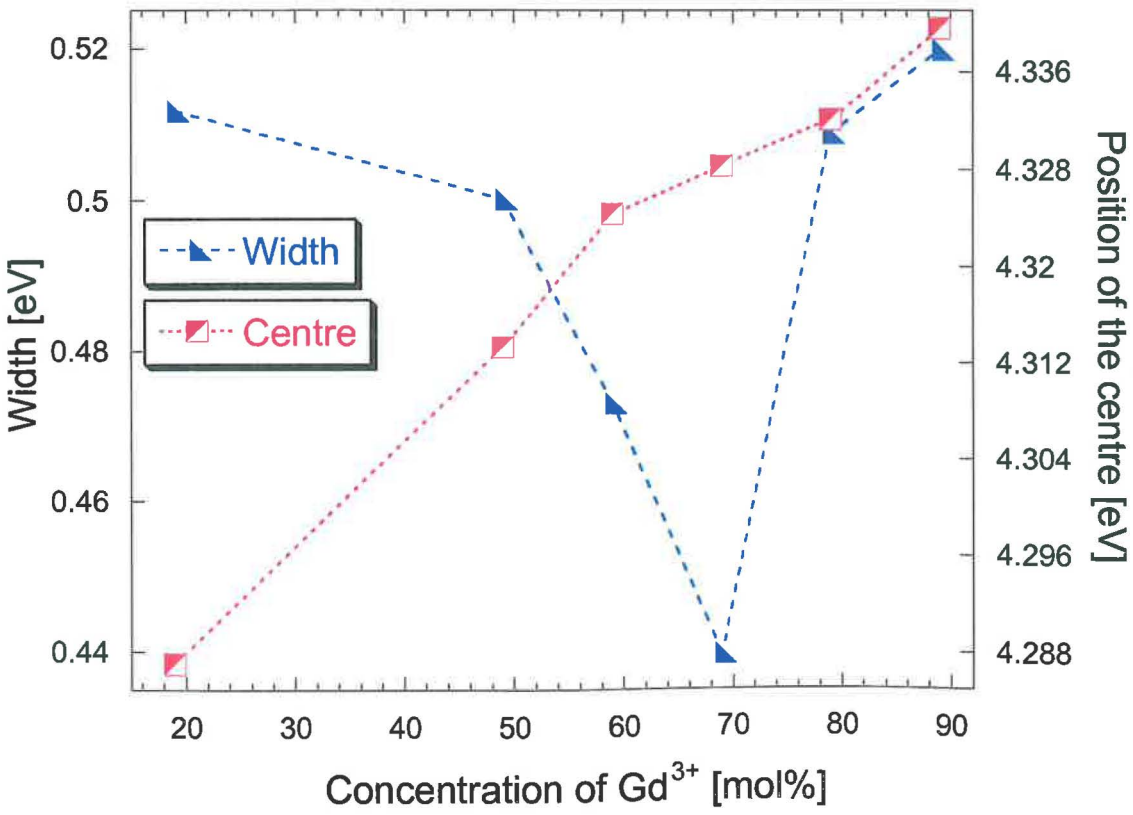

Fig. 45. The dependence of the width and the position of the centre of the 4*f*-5*d* Ce^{3+} absorption band for the samples with 1 mol% of Ce^{3+} on the concentration of Gd^{3+}

The width and the center of the absorption band of the *4f–5d* Ce^{3+} transition was found analogously to the similar quantities commonly used in spectroscopy. See Fig. 44. Both parameters were converted to eV units, and their dependence on the concentration of Ce^{3+} is shown in Fig 45. As the concentration of the donor grows, the width of the band changes very little with the exception of two samples, $Na_{40}Gd_{59}Ce_1$-II and $Na_{30}Gd_{69}Ce_1$-II. The reasons for this exception will be explained later in this chapter. At the same time, the center of the band steadily moves to the right, i.e. to the high energy region. The observed variance in the location of the center of the band is apparently due to the differences in the glass structure, which affects the symmetry of the local configuration of ions around acceptors and the strength of the crystalline field.

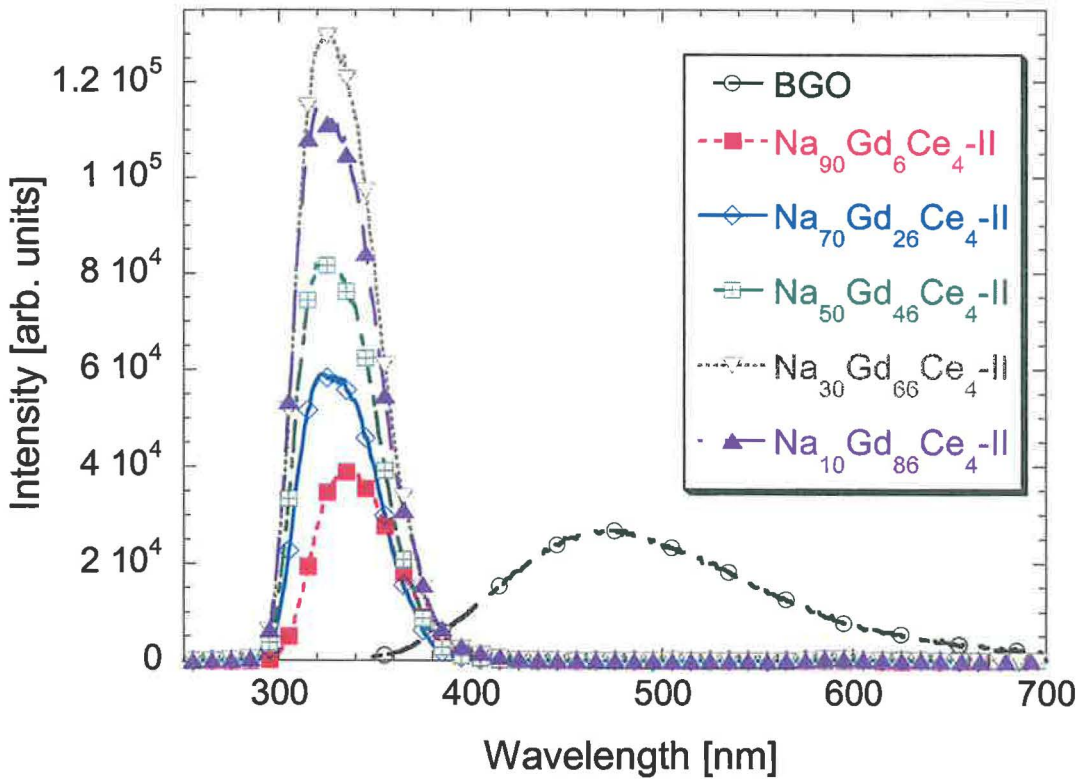

Fig. 46. The X-ray excited luminescence spectra of NaGdCe-II (concentration of Ce^{3+} is 4mol% and the concentration of Gd^{3+} is noted in the legend) and BGO (for comparison). The spectra are compared in an absolute scale.

Radioluminescence spectra

Fig. 46 presents the radioluminescence spectra of Ce^{3+}-doped phosphate glasses with various concentrations of Gd^{3+}. The spectrum of $Bi_4Ge_3O_{12}$ (BGO), which is a well-known and widely applied single crystal scintillator, is also shown to provide a benchmark. Let us

explore how the intensity of the spectra changes as the concentration of Gd^{3+} grows. As it can be seen in the figure, the intensity first grows along with the concentration, but then, reaching the maximum at the sample $Na_{30}Gd_{66}Ce_4$-II, decreases at the sample $Na_{10}Gd_{86}Ce_4$-II. The increase in the intensity proves the positive effect of Gd^{3+} ions in the host-to-activator energy transfer process and light output enhancement. The observed drop of intensity for the highest concentration of Gd^{3+} can be explained by the back energy transfer $Ce^{3+} \rightarrow Gd^{3+}$ and loss at defects, the role of which extremely increases at high donor concentrations. Remarkably, even small concentrations of the doping result in a substantially higher intensity, and the intensity of all samples from the considered set is higher than the intensity of BGO. The intensity of the best sample of the set, $Na_{30}Gd_{66}Ce_4$-II, exceeds the BGO intensity by six times, which is a very good result for a glass scintillator.

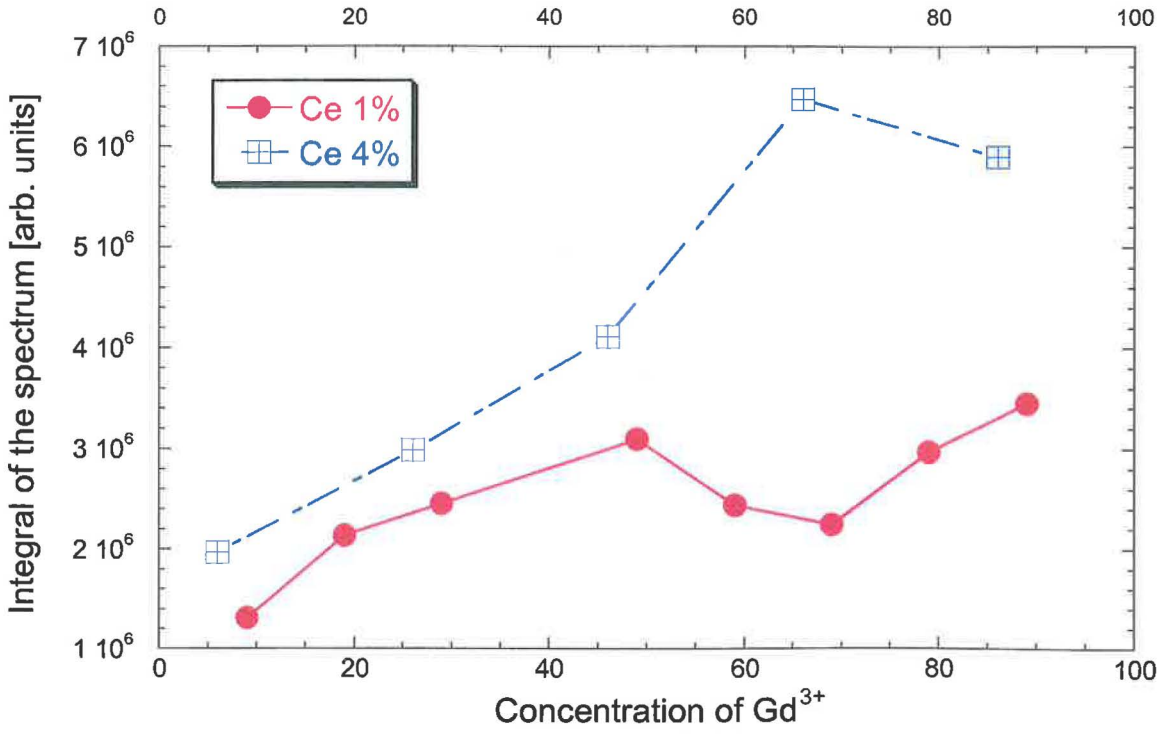

Fig. 47. The dependence of the integral of the absolute radioluminescence spectra on the concentration of Gd^{3+} for the samples with 1% of Ce and 4% of Ce.

Fig. 47 shows the dependence of the integral of the absolute radioluminescence spectra on the concentration of Gd^{3+} for two sets of samples: with 1 mol% and 4 mol% of Ce^{3+}. The integrals of the spectrum of the samples with concentration of 4 mol% of Ce^{3+} are bigger than the integrals of the samples with 1 mol% of Ce^{3+} for all the pairs with the same concentration of Gd^{3+}. For the set of samples with 1 mol% of Ce^{3+}, the highest integral value is obtained for the sample with the highest concentration of Gd^{3+} ($Na_{10}Gd_{89}Ce_1$-II). However,

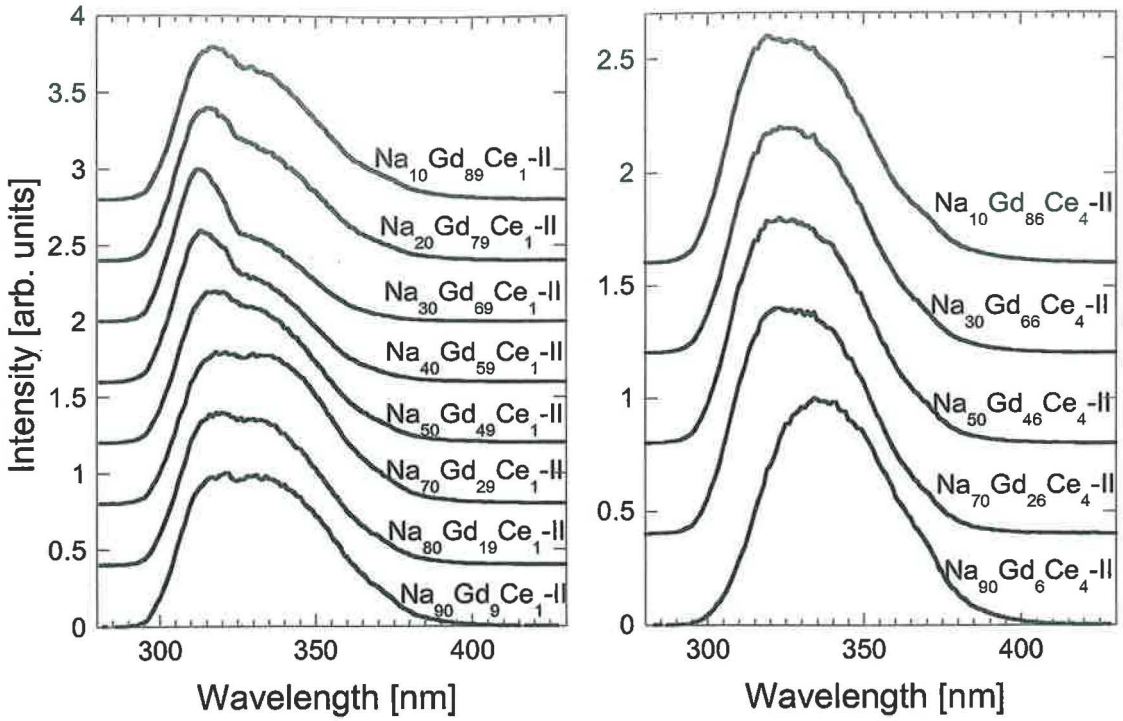

Fig. 48. Comparison of the shape of the X-ray excited spectra in a relative scale for all the samples a) with 1 mol% of Ce^{3+}; b) with 4 mol% of Ce^{3+}.

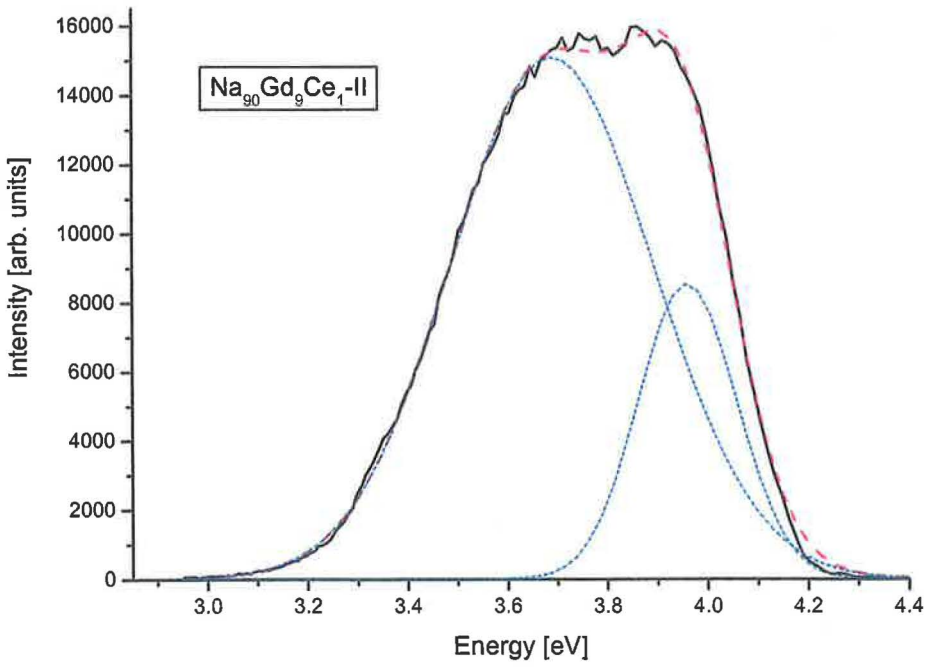

Fig. 49. Double-Gaussian fit of the X-ray excited spectrum of the sample $Na_{90}Gd_9Ce_1$-II

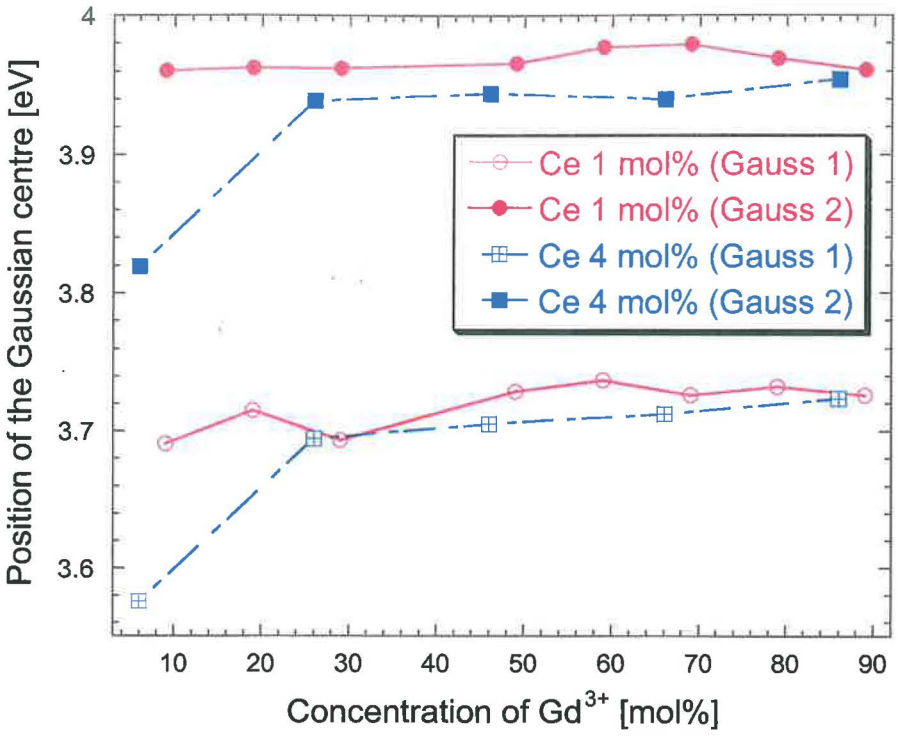

Fig. 50. The dependence of the position of the Gaussian centre on the concentration of Gd^{3+}

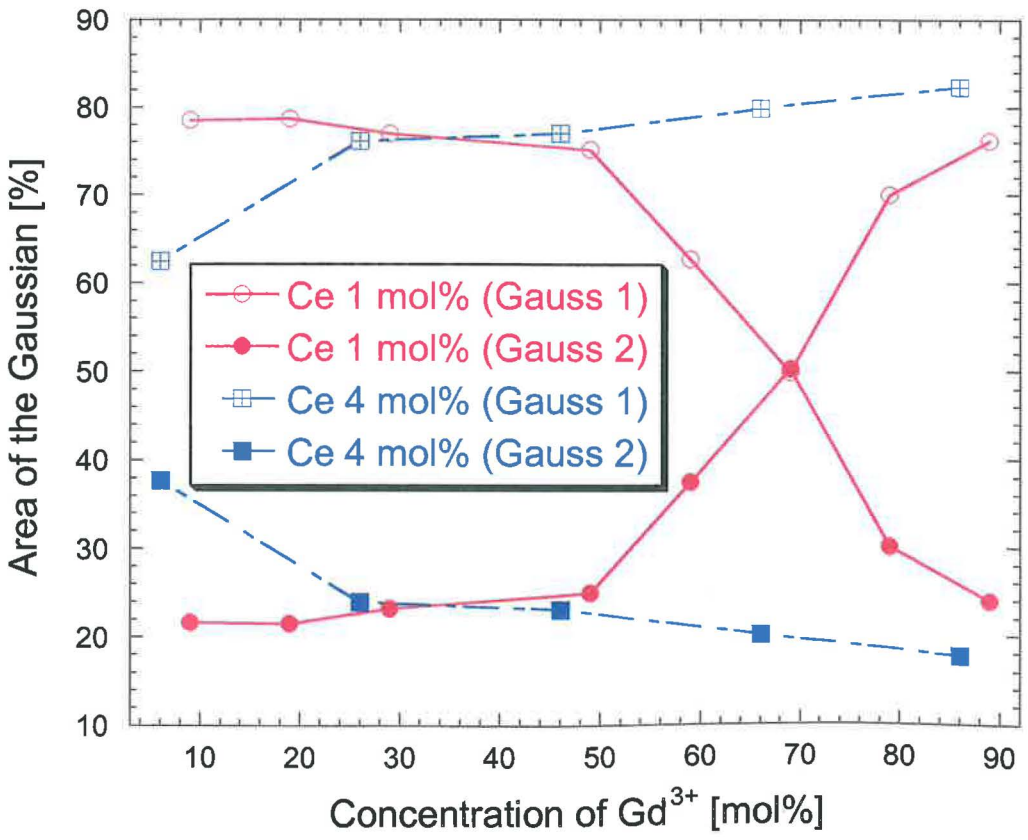

Fig. 51. The dependence of the area of the Gaussian centre on the concentration of Gd^{3+}

a very good result, which is comparable with that of the sample $Na_{10}Gd_{89}Ce_1$-II, is also obtained for the sample $Na_{50}Gd_{49}Ce_1$-II. The concentration of Gd^{3+} about 50 mol% in this sample is optimal with respect to the structure of matrix: the two components of glass ($NaPO_3$ and $GdPO_4$) are present in equal quantities, which results in the most homogeneous mix of the constituents. This fact is also confirmed by the density of the sample $Na_{50}Gd_{49}Ce_1$-II (see Table 2), which is higher than the density of the sample $Na_{30}Gd_{69}Ce_1$-II. Higher density indicates a more compact packing of particles. At a little bit higher concentration of Gd^{3+} (59 mol% and 69 mol%), the constituents of glass matrix are badly mixed and the material homogeneity decreases , which results in lower density and intensity of the radioluminescence spectrum compared to the sample $Na_{50}Gd_{49}Ce_1$-II (Fig. 47).

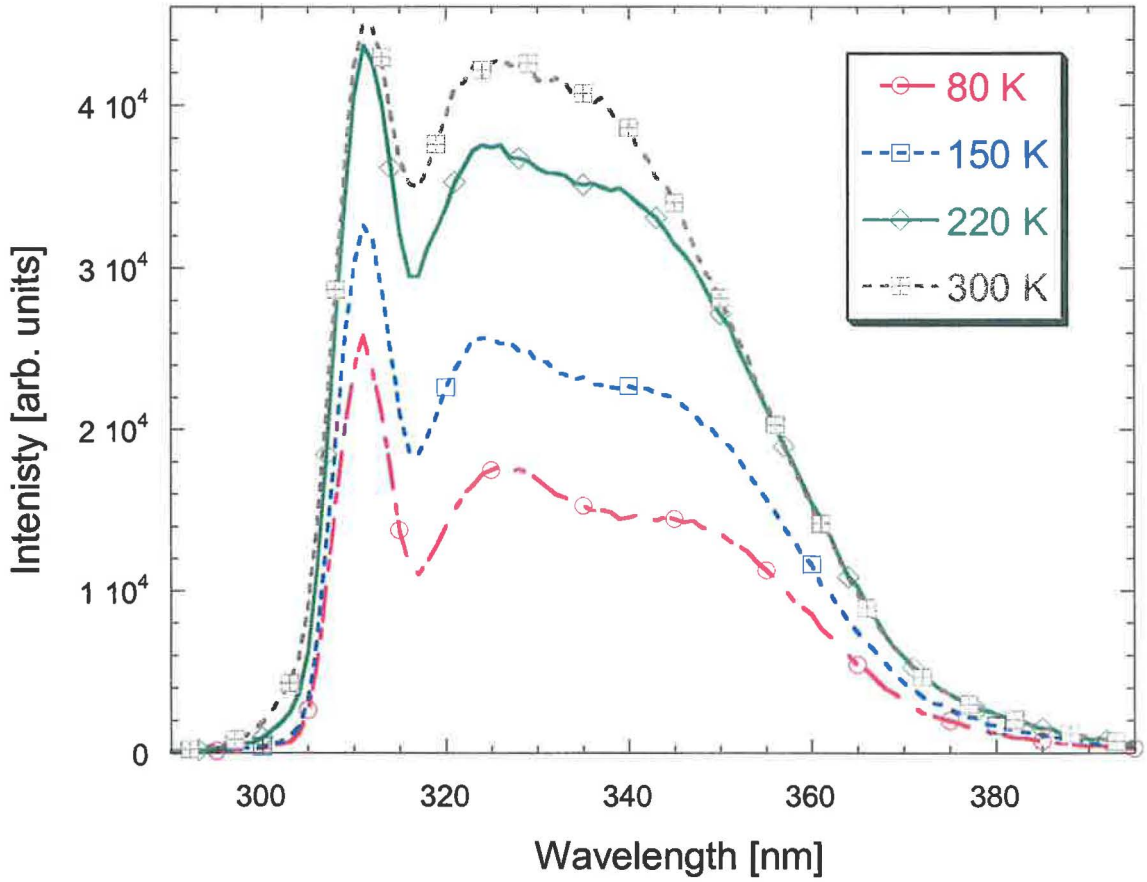

Fig. 52. The temperature dependence of the X-ray emission spectra for the sample $Na_{70}Gd_{29}Ce_1$-II

Let us consider now the set of the samples with 4 mol% of Ce^{3+} (Fig. 47). The sample $Na_{30}Gd_{66}Ce_4$-II has the highest integral of the radioluminescence spectrum, however the sample with the highest concentration of Gd^{3+} ($Na_{10}Gd_{86}Ce_4$-II) has a somewhat lower intensity, most likely due to the back energy transfer $Ce^{3+} \rightarrow Gd^{3+}$. This character of the

Table 8. The parameters of double-gaussian fitting of the radioluminescence spectra of the sample $Na_{70}Gd_{29}Ce_1$-II at four temperatures

T, K	80	150	220	300
Area	4700	8000	13000	16000
	3600	4500	5800	5700
Width, eV	0.28	0.30	0.32	0.34
	0.200	0.195	0.202	0.212
Position of the center, eV	3.58	3.61	3.64	3.67
	3.83	3.86	3.88	3.90
ΔE, eV	0.252	0.245	0.238	0.225
ΔE, cm^{-1}	2034	1979	1921	1813

dependence of the integral of the spectra on the concentration resembles the behavior of the radioluminescence spectra considered above (Fig. 46).

A closer inspection of Fig. 46 reveals that the radioluminiscence bands differ not only by the height, but also by the shape and the horizontal location. Fig 48 presents these bands after normalization. Now one can clearly distinguish two peaks in each band. The attempt to decompose the bands into two Gaussian functions was successful for all the samples (see Fig. 49 as an example). Such a successful decomposition is rather surprising because luminescence bands for glasses often have a strong broadening, and the attempt to fit them by Gaussian functions usually fails. The high goodness of fit in our case is the evidence that despite the amorphous structure of the glass matrix, there is a certain regularity in the ion configuration in the vicinities of luminescence centers.

The concentration dependences of the locations of the maximum points (centers) of both Gaussian functions are presented in Fig. 50. These locations for the samples with Ce^{3+} 1 mol % vary insignificantly; as the concentration of Gd^{3+} grows, the centre of each of the Gaussian components slowly moves to the high energy region, reaches the maximum at $Na_{30}Gd_{69}Ce_1$-II, and then slowly moves back. For the samples with Ce^{3+} 4 mol %, both centers persistently move to the high energy region, with a notably large jump between the two samples with the lowest concentration of Gd^{3+}. Thus one can clearly see that the Ce^{3+} emission shifts to the higher energies as the Gd^{3+} concentration rises due to change of the symmetry of the crystalline field. The concentration of Gd^{3+} in the sample $Na_{90}Gd_6Ce_4$-II is too small to influence the crystalline field. It is also clearly seen that the difference between the centers of the first and the second Gaussian components is constant over all the samples; it equals approximately 2000 cm^{-1}, which coincides with the difference between the two components of the 4*f*-level of Ce^{3+} (see Fig. 15).

Fig. 51 shows the concentration dependence of the percentage of each of the Gaussian components in the total area of the radioluminiscence band. For the samples with Ce^{3+}

4 mol %, the dependence of the share of the first Gaussian component resembles that of the location of the centre of this component shown in Fig. 50: the same monotonic increase with a high jump at the lowest concentration of Gd^{3+}. The dependence of first Gaussian component share for the samples with Ce^{3+} 1 mol % is different; the share of the first component first decreases, reaching the minimum at $Na_{30}Gd_{69}Ce_1$-II, and then steeply increases; this resembles the concentration dependence of the width of the absorption bands for the same samples shown in Fig. 45.

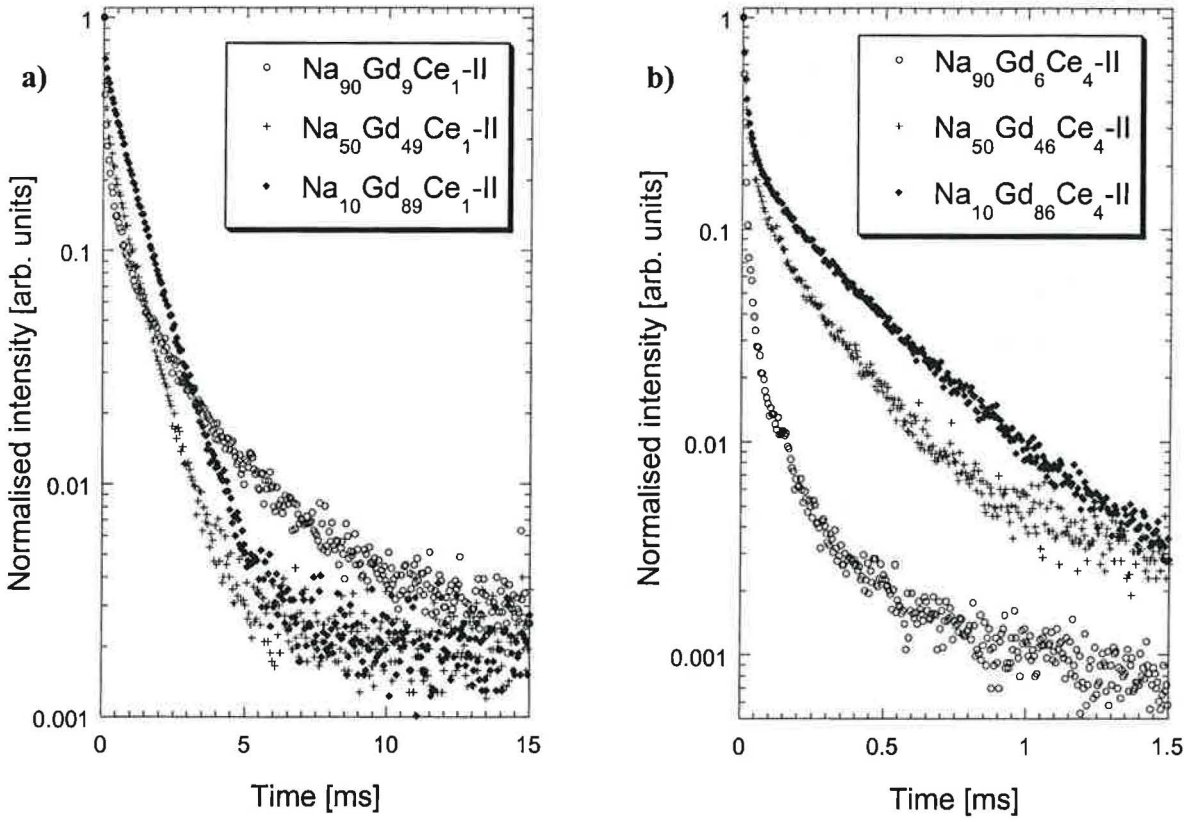

Fig. 53. Decay kinetics of Gd^{3+} line (λ_{em} = 275 nm, λ_{exc} = 312 nm) at room temperature of a) Ce 1mol% b) Ce 4mol% samples. The concentration of Gd is noted in the legend.

Fig. 52 presents the radioluminescence spectra of the sample $Na_{70}Gd_{29}Ce_1$-II measured at four temperatures within 80-300 K. All the spectra were fitted by the double-gaussian function. The fitting parameters are presented in Table 8. As the temperature increases, the intensity of the radioluminescence spectra rises also due to thermalisation of electrons captured by shallow traps (their presence was shown by TSL spectra, see Fig. 27). For the same reason the areas of the gaussian bands increases. The width of gaussian bands icnreases as the temperature rises because of temperature broadening. The centers of the both

gaussian components shift to the high energy region with the increasing temperature due to thermalization of charge carriers. The distance between the bands is 1800-2000 cm^{-1} that corresponds to the distance between levels of spin-orbital coupling of the 4*f* level (Fig. 15).

Gd^{3+} decay kinetics

The decay kinetics of Gd^{3+} line (λ_{em} = 275 nm, λ_{exc} = 312 nm) for all the samples was measured at room temperature. Some of the normalized decay curves are shown in Fig. 53. Looking at this figure, one can make two observations. First, the decay for Ce^{3+} 4 mol% is almost ten times faster than that for Ce^{3+} 1 mol%, which is seen from the scale of the time axes. Second, at the first glance, the relative location of the decay curves exhibits no regularity. In particular, these curves are not located one above another, as one can often see in other decay kinetics. The reason for this seemingly irregular behavior is rooted in the complex shape of the decay curves. Note that each curve can be divided into two parts (Section 2.5, Fig. 11): a non-exponential initial segment (corresponding to the single-step donor-acceptor transfer, Stage 2) and a long exponential tail (when donor-donor energy migration prevails, Stage 3). The shape of such curves can be described by three characteristics: $\tau_{0,short}$, t_b, and $\tau_{0,long}$ (see Fig. 54). The parameter t_b is the border time between the non-exponential and exponential parts, $\tau_{0,short}$ characterizes the slope of the decay curve in the non-exponential part, and, $\tau_{0,long}$ is the decay parameter of the exponential tail. These parameters can be more precisely defined as follows. First, introduce function $\tau_{1/e}^*(t)$ as the solution to the equation

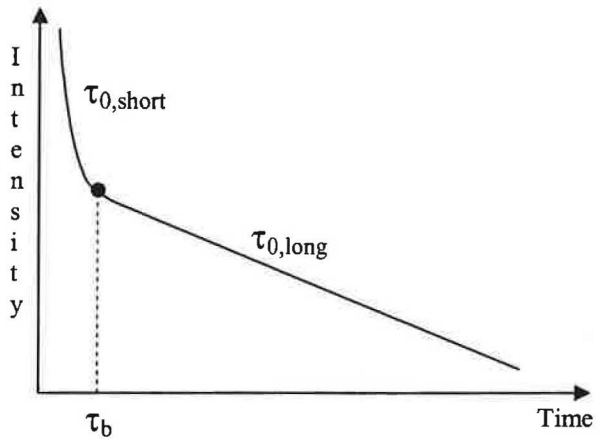

Fig. 54. Three characteristics of a non-exponential decay curve

$$I(t)/\, I(t+\tau_{1/e}^*(t)) = e.$$

This function generalizes parameter $\tau_{1/e}$ introduced earlier by equation (6). Now define

$$\tau_{0,short} = \tau_{1/e}^*(0),$$

$$\tau_{0,long} = \lim_{t\to\infty} \tau_{1/e}^*(t),$$

$$\text{and } t_b = \min\{t : |\tau_{1/e}^*(t) - \tau_{0,long}| \le \varepsilon\},$$

where ε is an accuracy parameter, $\varepsilon > 0$. The accuracy parameter ε is necessary because there is no exact border between the non-exponential and exponential parts. The decay process transits from one part to another smoothly, the transition is not momentary. The parameter $\tau_{0,short}$ defined as $\tau_{1/e}^{*}(0)$ (or, equivalently, $\tau_{1/e}$) is certainly only a rough proxy for the slope of the initial part of the curve, since $\tau_{1/e}^{*}(t)$ rapidly changes at small t, as we will see in Fig. 60 and Fig. 61. Of course, other numerical parameters, such as the commonly used τ_{mean} (see equation (5)) may also be useful. We proceed with estimating τ_{mean}, $\tau_{1/e}$, and two ways of estimating t_b and $\tau_{0,long}$, and analyze their dependencies on the concentration of the Gd^{3+} and Ce^{3+} ions.

All the decay kinetics curves were fitted by functions that are sums of exponentials (see equation (4)). Due to a complex form of the decay curves, these sums contained more than one nontrivial exponential term. Thus, to achieve a satisfactory fit, sums of 2 or 3 exponents were used for fitting the decay curves of Ce^{3+} 1 mol%, and a sum of 4 exponential functions were used to fit the decay curves of Ce^{3+} 4 mol%. A commonly used quantitative characteristic of such a "multiexponential" fit is the mean decay time τ_{mean} (see formula (5)). However, this parameter is distorted in the considered case by exponential terms with very large decay parameters (long decay times), which makes the parameter τ_{mean} useless.

Let us consider now parameter $\tau_{1/e}$, which characterizes the steepness of the initial part of the curve (see equation (6)). Recall that the initial part of the decay kinetics is mostly due to the single-step donor-acceptor transfer, which corresponds to the non-exponential part of the decay curve. The dependence of $\tau_{1/e}$ on the concentration of Gd^{3+} for the two sets of samples (one set corresponding to Ce^{3+} 1 mol% and the other to Ce^{3+} 4 mol%) is graphically shown on Fig. 55. Consider first the set of samples with Ce^{3+} 4 mol%. Note that the value of $\tau_{1/e}$ almost does not change as the concentration of Gd^{3+} grows. The probable reason is the following. The number of acceptors is so large that the most part of the energy absorbed by the donors is immediately transferred to the acceptors, even if the concentration of donors is high. This fact is also illustrated by Fig. 53, where the initial non-exponential part of the decay curves for Ce^{3+} 4 mol% is clearly distinguishable even for samples with high content of Gd^{3+}. The behavior of $\tau_{1/e}$ for the set of samples with Ce^{3+} 1 mol% is more complicated. However, one can see and explain the following three regularities. First, the increase in $\tau_{1/e}$ with the concentration of Gd^{3+} is probably due to the increasing role of the donor-donor transfer, which is not suppressed by a too high concentration of the acceptors. Also the back

energy transfer $Ce^{3+} \rightarrow Gd^{3+}$ can have an influence. In fact, this indicates that $\tau_{1/e}$ characterizes here not only the initial, non-exponential segment of the decay curve but also part of the

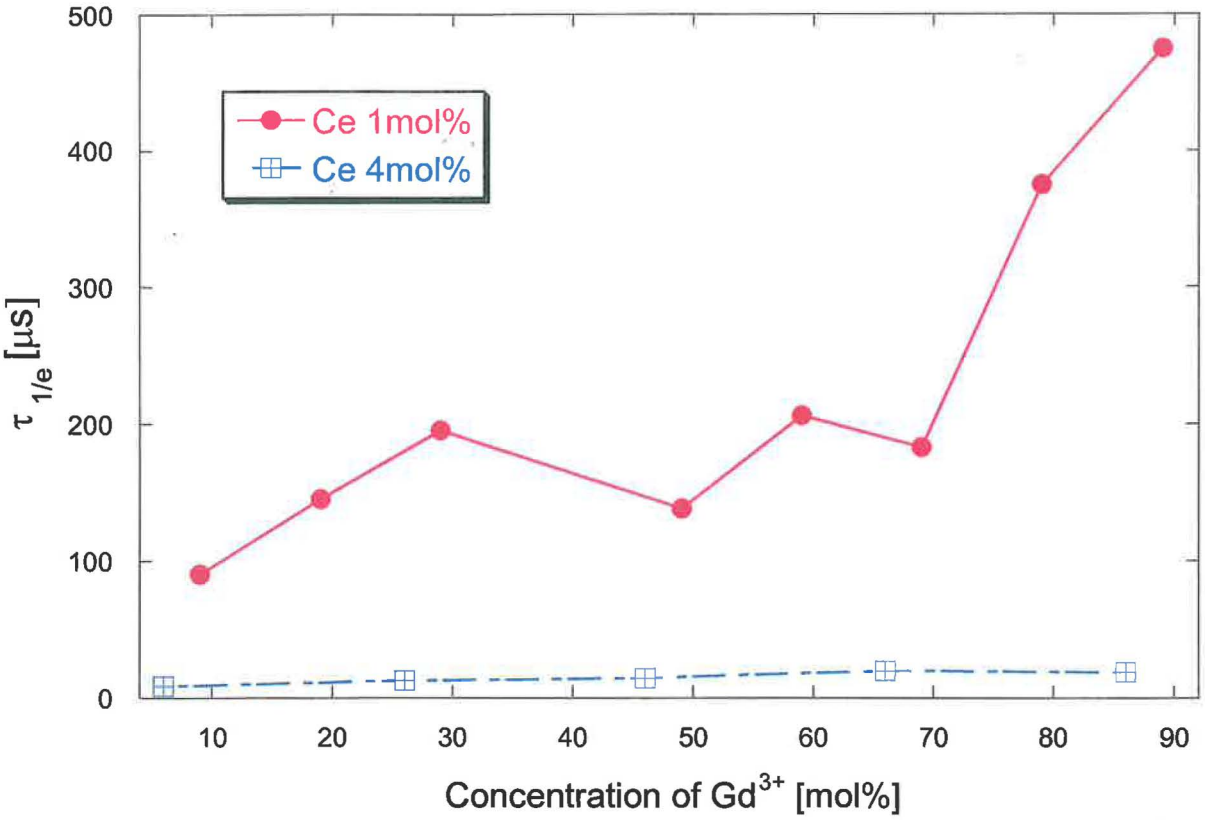

Fig. 55. The dependence of the parameter $\tau_{1/e}$ on the concentration of Gd^{3+} for the samples with 1 mol% and 4 mol% of Ce^{3+}.

exponential tail. Second, a drop in $\tau_{1/e}$ at 50 mol% of Gd^{3+} is likely due to the "homogeneous mixture" effect described above. Finally, the surprisingly very high values of $\tau_{1/e}$ for high concentrations of Gd^{3+} can be explained by the fact the transfer Gd^{3+}– Gd^{3+} begins to play the decisive role due to $Ce^{3+} \rightarrow Gd^{3+}$ back transfer. In this case $\tau_{1/e}$ actually characterizes the exponential tail of the decay curve. Summarizing, in the sample set with 1mol% of Ce^{3+}, the observed behavior of $\tau_{1/e}$ can be reasonably explained by the relative concentration of the donors and acceptors. However, one should also take into account the "homogeneous mixture" effect and a non-smooth behavior of $\tau_{1/e}$ due to a complex shape of the decay curve.

To characterize the decay kinetics at longer times, the tails of the decay curves were fitted with exponential functions. The left bound of the tail was first chosen as the time by

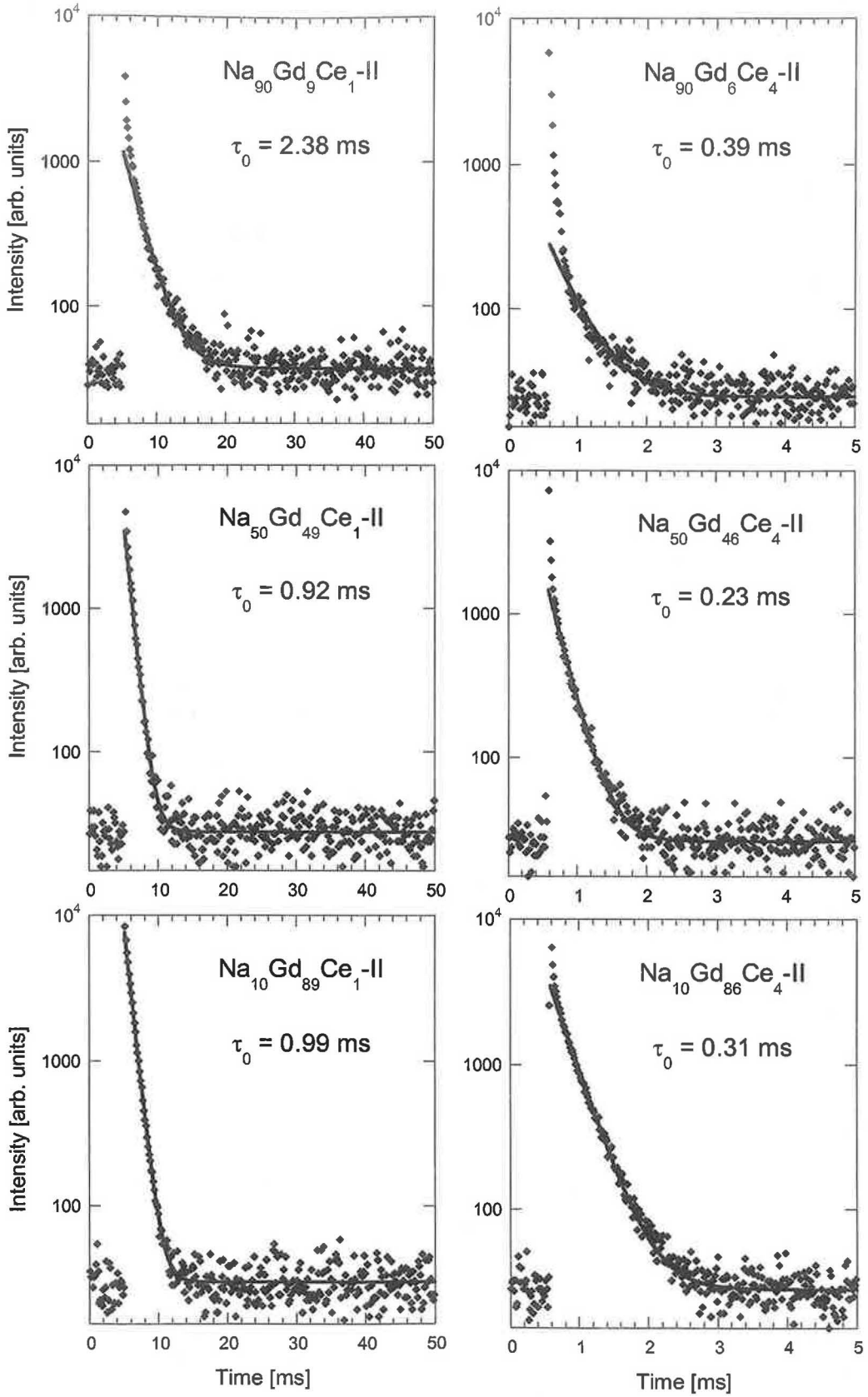

Fig. 56. Semilogarithmic decay curves of the Gd^{3+} emission (λ_{exc} = 275 nm, λ_{em} = 312 nm) in the new Ce-doped glasses (the concentration of Ce and Gd is noted in the legend), recorded at room temperature. Solid lines: fit to $I(t) = I_0 \exp(-t/\tau_{0,long})$.

which the intensity drops to 10% of the initial level, which can be denoted as $\tau_{1/10}$. Then, if necessary, the left bound was slightly moved to the right until a satisfactory goodness of fit was obtained. This approach of estimating $\tau_{0,long}$ is based on the assumption that $t_b > \tau_{1/10}$. The results can be seen on Fig. 56. Using this figure, one can visually estimate t_b as the point at which the exponential fit and the measured data diverge. The graphs clearly show that the share of the exponential part increases with the concentration of Gd^{3+} and decreases with the concentration of Ce^{3+}. This again supports the statement that the donor-donor transfer is more active in samples with higher concentration of donor ions, and at the same time this transfer is less important in samples with high content of acceptors.

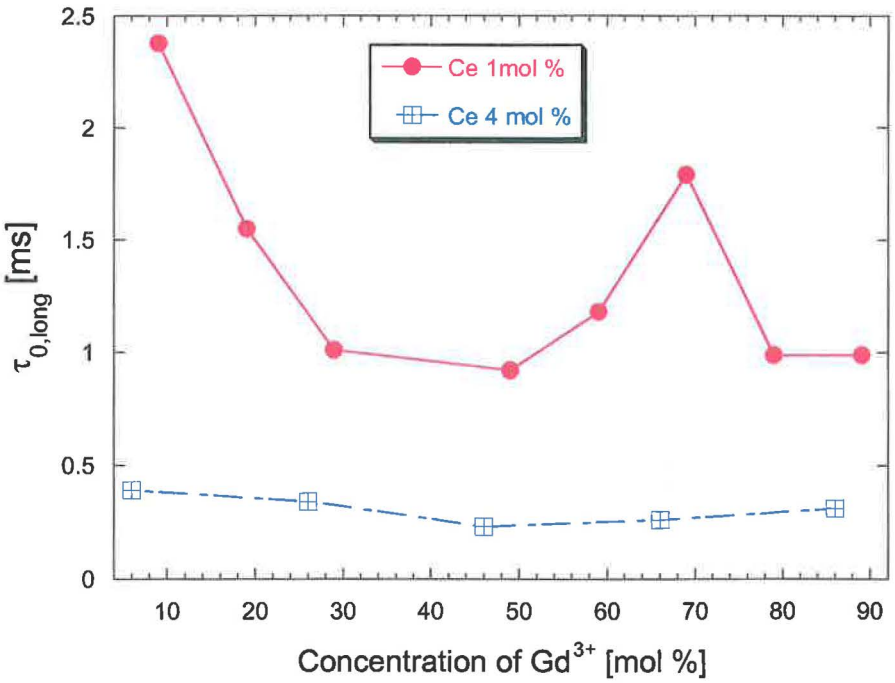

Fig. 57. The dependence of parameter $\tau_{0,\,long}$ on the concentration of Gd^{3+} ions

The dependence of $\tau_{0,long}$ on the concentration of the ions for all the samples is plotted on Fig. 57. The general trend of $\tau_{0,long}$ is the *decrease* with the growth of the concentration of the Gd^{3+}. This is in sharp contrast to the behavior of $\tau_{1/e}$, which generally *increases* with the donor concentration. The drop of the decay time at 50 mol% of Gd^{3+} can be again explained with the more homogeneous mixture of the constituents resulting in faster energy migration over Gd^{3+} subsystem. This effect is the same for both $\tau_{0,long}$ and $\tau_{1/e}$. A small increase in $\tau_{0,long}$ for high concentrations of Gd^{3+} can be explained by the increasing role of back energy transfer. The only surprise is the value of $\tau_{0,long}$ at Gd^{3+} 70 mol% in the set with Ce^{3+} 1 mol%.

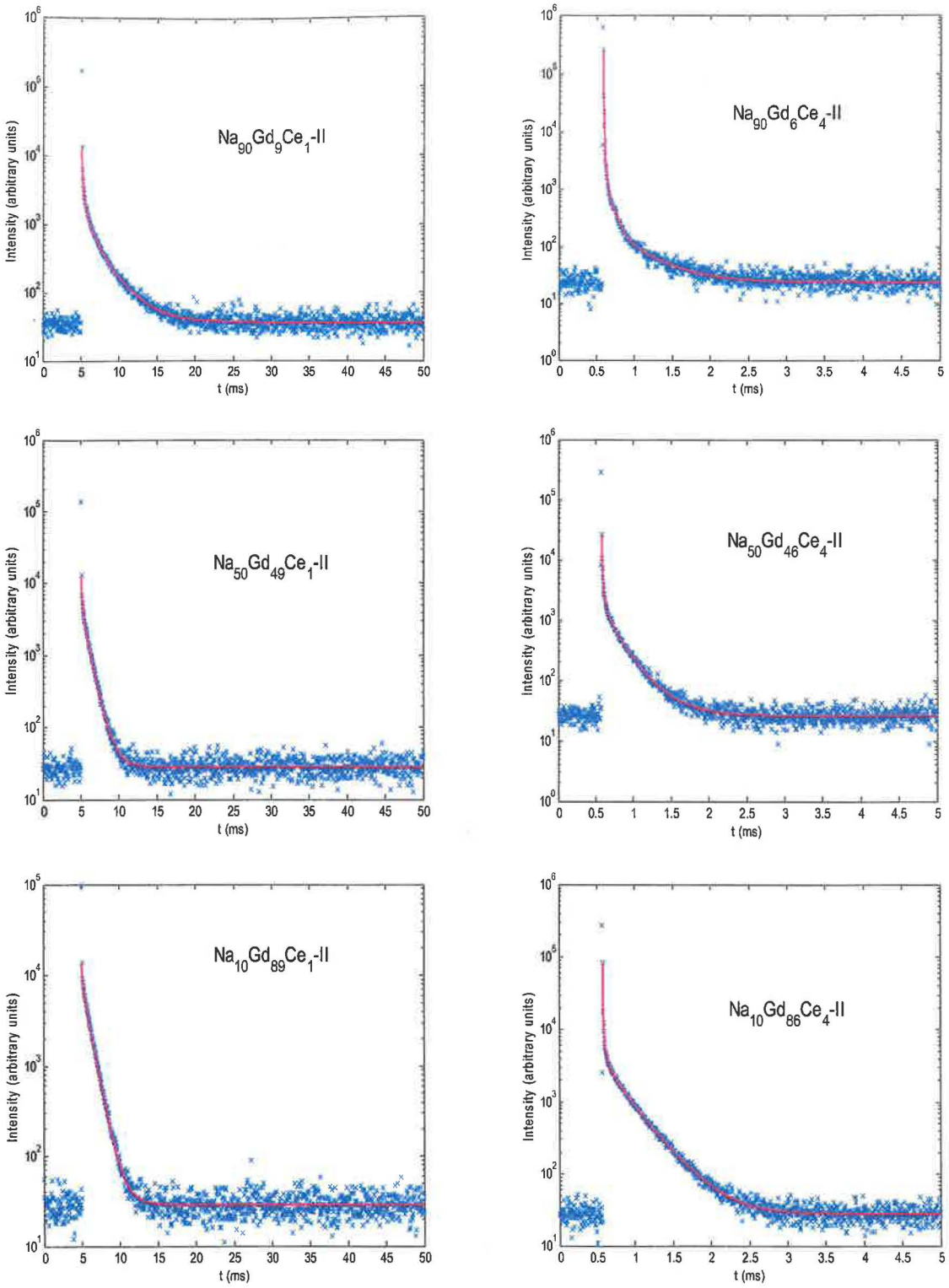

Fig. 58. Original (x) and smoothed (solid lines) semilogarithmic decay curves of the Gd^{3+} emission for the new Ce-doped glasses.

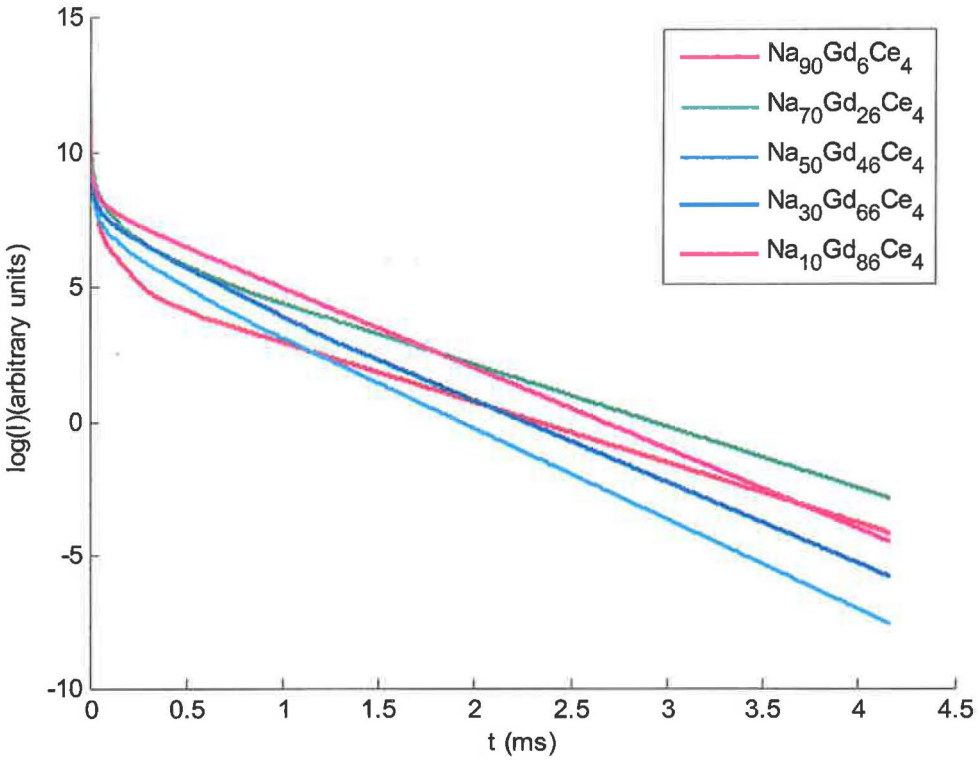

Fig. 59. The smoothed semilogarithmic decay curves (with substructed background) of the Gd^{3+} emission for the new glasses with the concentration of Ce^{3+} 4 mol% in the melt

A possible explanation is that the deviation from the optimal structure of the glass still has a strong effect even at this concentration.

Another way to estimate the parameters $\tau_{0,long}$ and t_b would be through a direct estimation of the function $\tau_{1/e}^*(t)$ for all t. The horizontal asymptote would give an estimate of $\tau_{0,long}$, and the time at which the graph becomes virtually indistinguishable from this asymptote could be thought of as the border time τ_b. The estimation of $\tau_{1/e}^*(t)$, like estimation of any characteristic related to the slope of the curve, requires smoothing of the data. As an appropriate smoothing procedure, the least squares approximation by a log-convex nonincreasing function was used. That is, the measured data were approximated by a function from the class K = {exp(h(t)) : h is nonincreasing and convex}, using the least squares as the approximation criterion. This smoothing method exploits only two *shape restrictions* on the true decay curve: the monotonicity (nonincreasingness) and convexity of the logarithm of the light intensity as a function of time (see Appendix A for details). The goodness of fit is demonstrated in Fig. 58. See also Fig. 59 for the logarithm of the approximating curves after subtracting the background: the exponential tails are very clearly seen here. Having derived

the smoothed curve, one can then easily compute and draw the graph of $\tau_{1/e}^{*}(t)$. These graphs for some of the samples are given on Fig. 60 and 61. They clearly show how $\tau_{1/e}^{*}(t)$ gradually grows till it reaches a certain constant level. Except providing alternative estimates of $\tau_{0,long}$ and t_b, these graphs also prove that the decay kinetics eventually becomes exponential indeed.

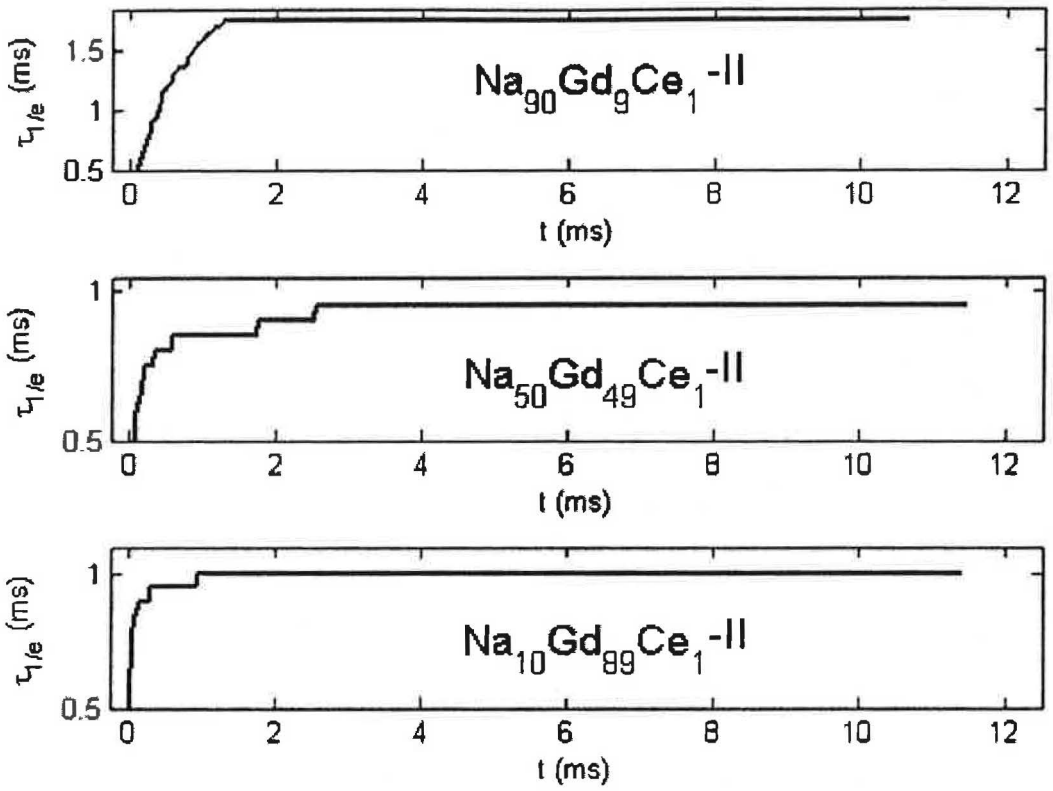

Fig. 60. Change of the slope of the initial part of the decay curve of the Gd^{3+} emission (see the text) for the samples with the concentration of Gd^{3+} 1 mol% in the melt

Bidirectional energy transfer

To verify the fact of the back transfer $Ce^{3+} \rightarrow Gd^{3+}$, let us use the method described in Section 5.1. Recall that the decay kinetics of Ce^{3+} ions (λ_{exc} = 319 nm, λ_{em} = 340 nm) in the Gd^{3+}-free sample has an exponential shape with the decay time 28.2 ns (see Section 5.1). When the sample is doped with Gd^{3+} donor ions, the shape of the decay kinetics curve changes. First, an initial shortening of the decay is observed due to nonradiative energy transfer back to the donor ions. (The transfer to another acceptor ion is excluded because of small concentrations of acceptor ions.) Second, a slow non-exponential tail appeares due to the later return of the excitation energy to Ce^{3+} ions after its migration through the donor subsystem with subsequent radiative emission (see Fig. 28 and the comments to it).

The decay kinetics of the Ce^{3+} emission (λ_{em} = 340 nm) with excitation through Gd^{3+} ions (λ_{exc} = 275 nm) or with the direct excitation of Ce^{3+} ions (λ_{exc} = 319 nm) have been measured for all the samples. As in the case of the glasses of the first generation (Fig. 28), a slow decay component was observed, and therefore the measurement were carried out both in the nanosecond and microsecond regimes.

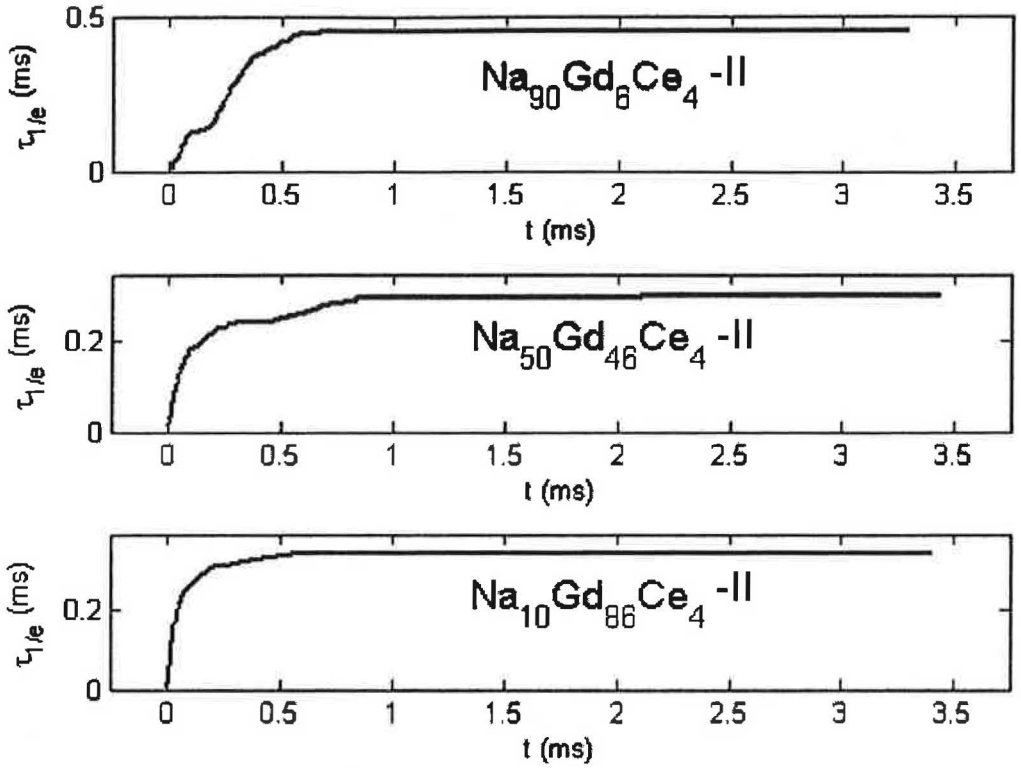

Fig. 61. Change of the slope of the initial part of the decay curve of the Gd^{3+} emission (see the text) for the samples with the concentration of Gd^{3+} 4 mol% in the melt

Consider first the decay kinetics in the nanosecond time interval. Fig. 62 and 63 shows the decay kinetics curves for two sets of samples corresponding to two concentration of Ce^{3+} (1 mol% and 4 mol% in the melt). Each set contained samples with three concentrations of Gd^{3+} (around 10 mol%, 50 mol% and 90 mol% in the melt). One can see from Fig. 62 and 63 that the decay kinetics curves have very little difference in the shape with the exception of the decay curve for the sample $Na_{50}Gd_{49}Ce_1$-II. The decay curve (λ_{exc} = 275 nm, λ_{em} = 340 nm) for this sample has a noticeable shortening compared to the two other samples.

All the curves were fitted by one- or two-exponential functions. In the case of fitting by the sum of two exponents, the second of them describes the slow μs component (for this μs component the separate measurement in the microsecond scale was conducted).

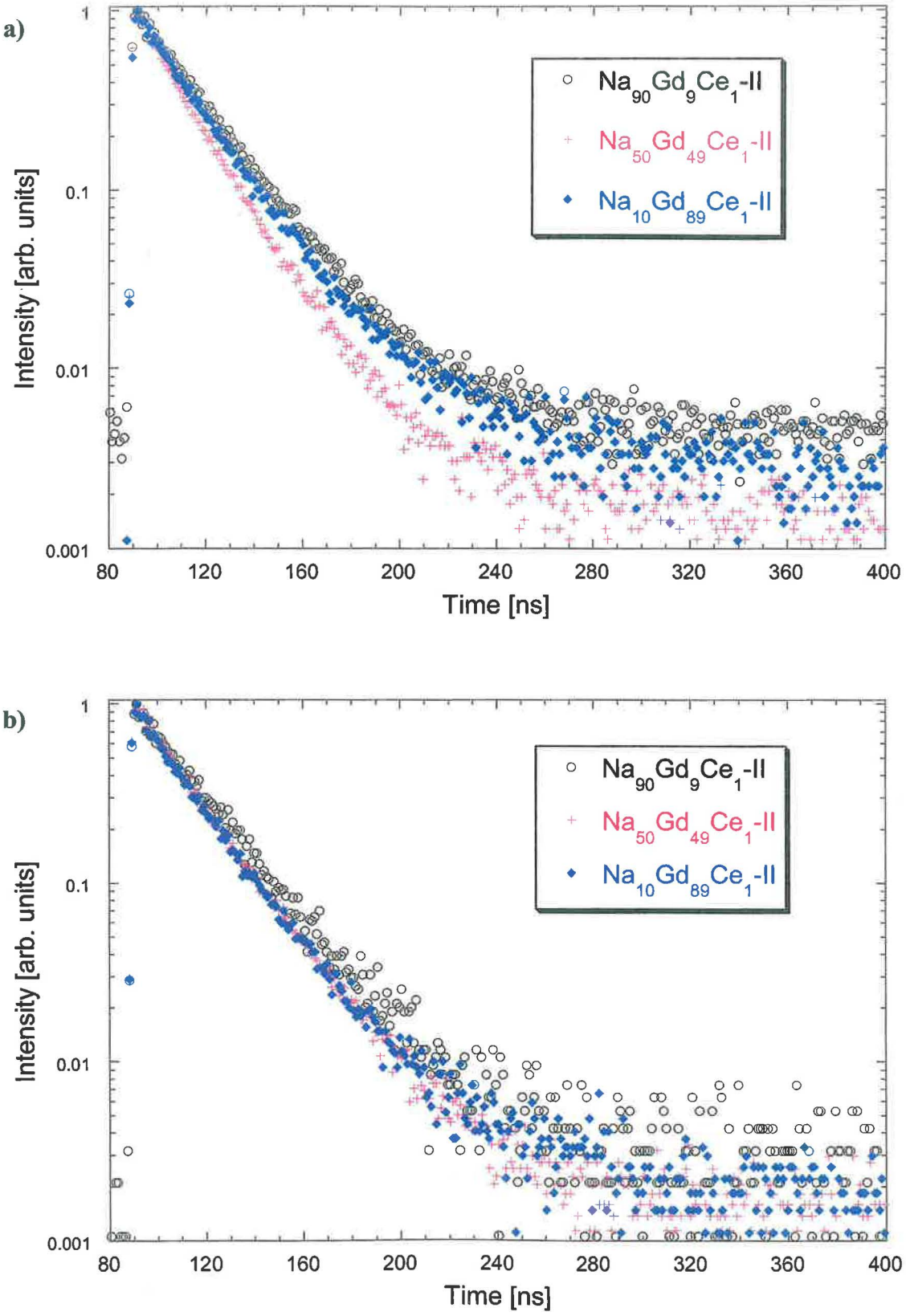

Fig. 62. Fast component of the decay kinetics of the Ce^{3+} emission (λ_{em} = 340 nm) with the excitation a) through the Gd^{3+} ions (λ_{exc} = 275 nm); b) directly through the Ce^{3+} ions (λ_{exc} = 319 nm) new glasses with the concentration of Ce^{3+} 1 mol% in the melt

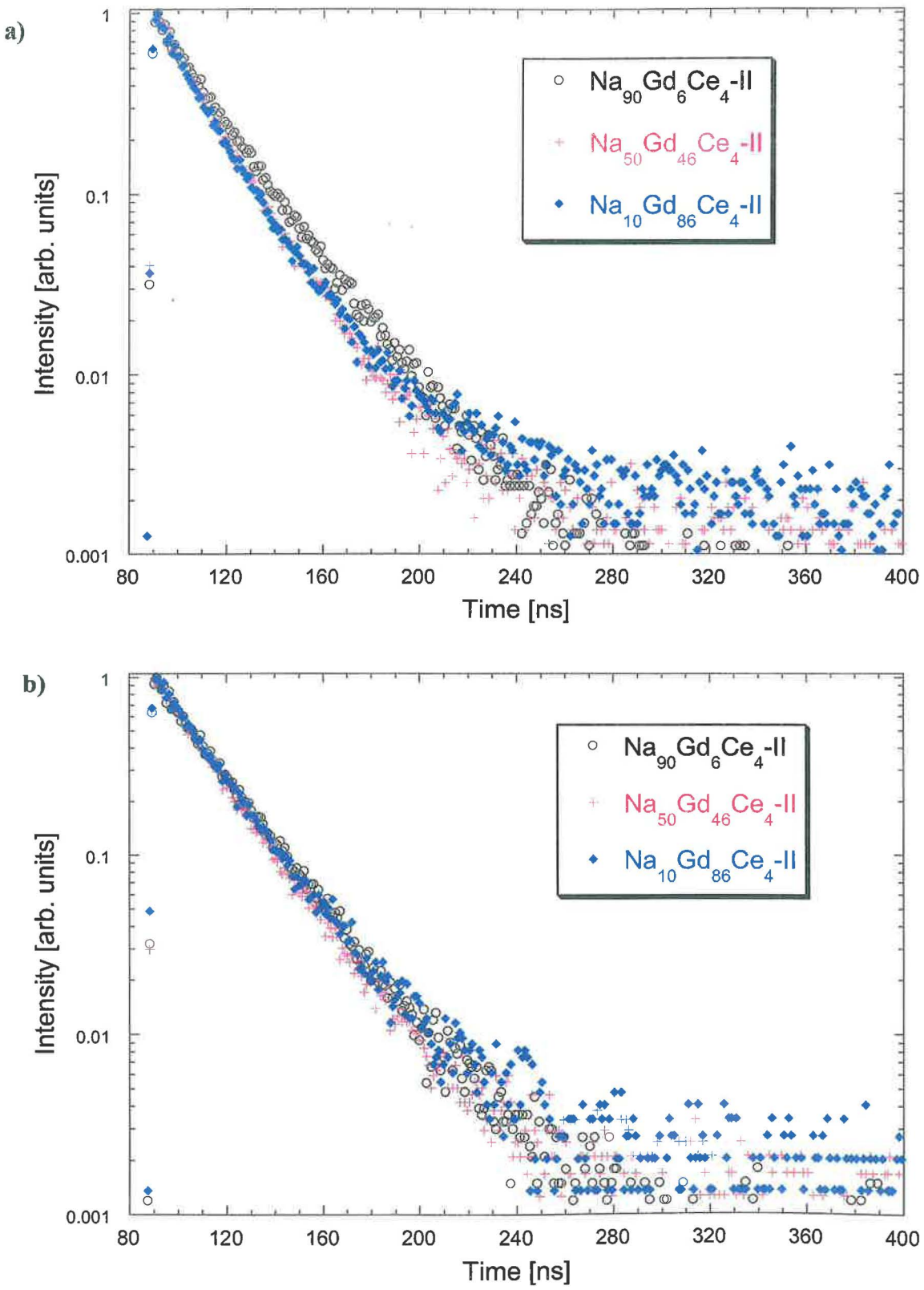

Fig. 63. Fast component of the decay kinetics of the Ce^{3+} emission (λ_{em} = 340 nm) with the excitation a) through the Gd^{3+} ions (λ_{exc} = 275 nm); b) directly through the Ce^{3+} ions (λ_{exc} = 319 nm) new glasses with the concentration of Ce^{3+} 4 mol% in the melt

The dependence of the decay time τ_0 of the fast components on the concentration of Gd^{3+} is shown in Fig. 64 for the excitation and the emission of Ce^{3+} levels (λ_{exc} = 319 nm, λ_{em} = 340 nm). The decay times for all the samples vary from 13.6 ns up to 25.4 ns, which is less than the decay time of 28.2 ns for Ce^{3+} ions in the Gd-free sample (see Section 5.1). Thus, the back transfer process $Ce^{3+} \rightarrow Gd^{3+}$ takes place in every considered sample.

Also we can see at Fig. 64 that shortening of decay kinetics in the samples with 4 mol% of Ce^{3+} is more than that of the samples with 1 mol% of Ce^{3+}. Thus, the back transfer is more probable in the samples with higher concentration of acceptor. It is logical because in the case of hiher concentration the interaction between donor and acceptor is much more. Every atom of Ce^{3+} is surrounded by a few atoms of Gd^{3+}, therefore the transfer $Ce^{3+} \rightarrow Gd^{3+}$ can easy take place.

These facts that the back transfer $Ce^{3+} \rightarrow Gd^{3+}$ takes place indeed and becomes stronger as the concentration of Gd^{3+} or the concentration of Ce^{3+} grows. However, the estimation of the decay time of the fast component for the samples with high concentrations of Gd^{3+} might be distorted by the beginning of the slow μs component, because for the samples with high concentrations both of Ce^{3+} and Gd^{3+} the third exponential component appeares.

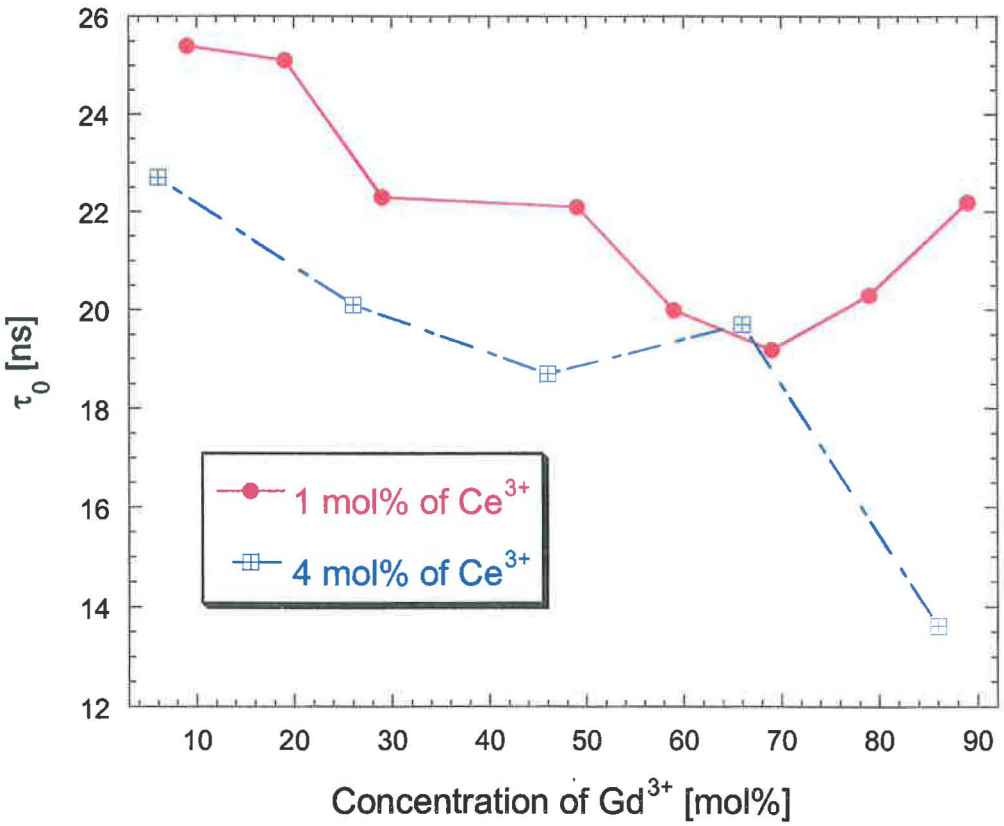

Fig. 64. The dependence of the decay time τ_0 on the Gd^{3+} concentration for Ce^{3+} line (λ_{exc} = 319nm, λ_{em} = 340 nm)

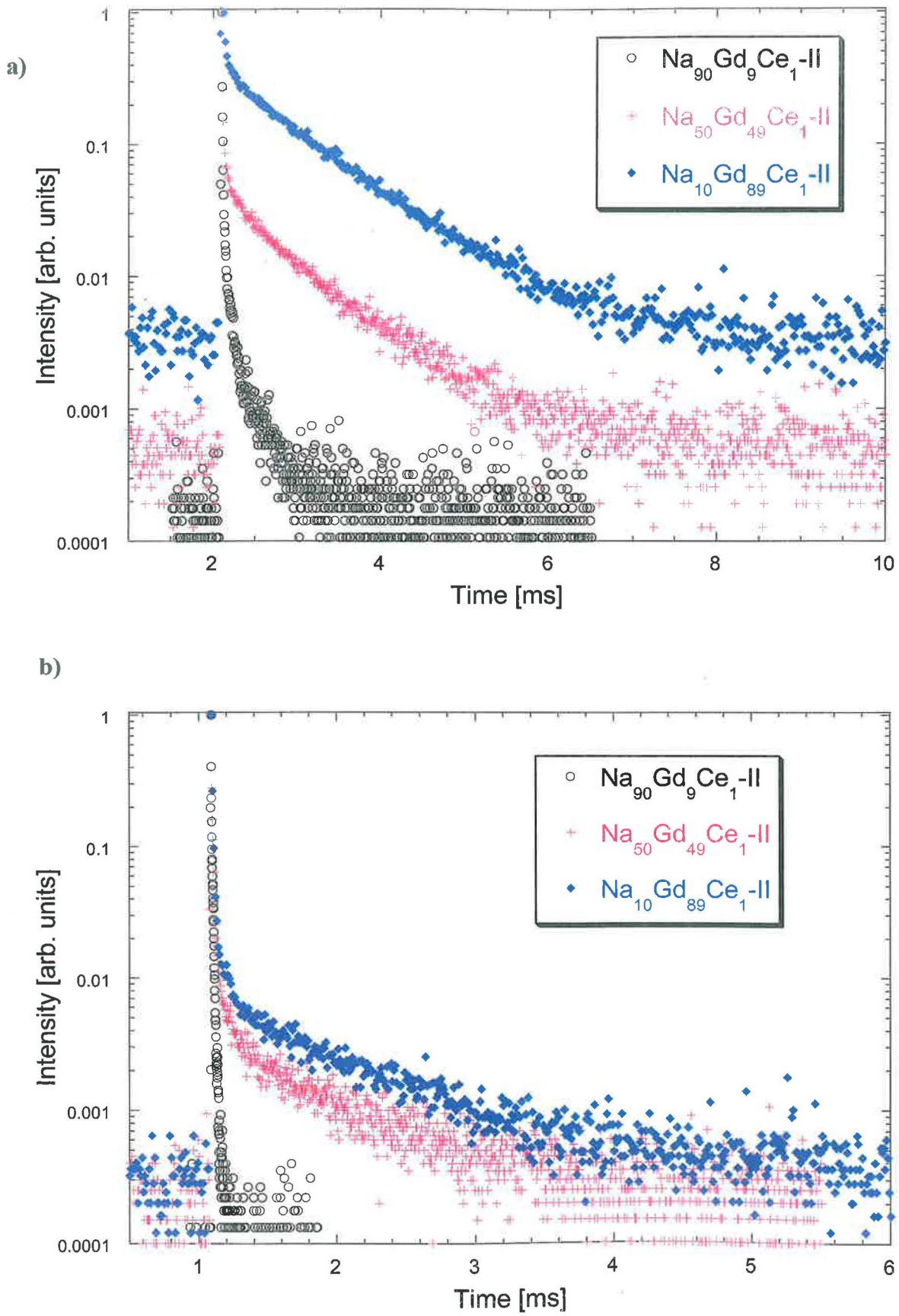

Fig. 65. Slow component of the decay kinetics of the Ce^{3+} emission (λ_{em} = 340 nm) with the excitation a) through the Gd^{3+} ions (λ_{exc} = 275 nm); b) directly through the Ce^{3+} ions (λ_{exc} = 319 nm) new glasses with the concentration of Ce^{3+} 1 mol% in the melt

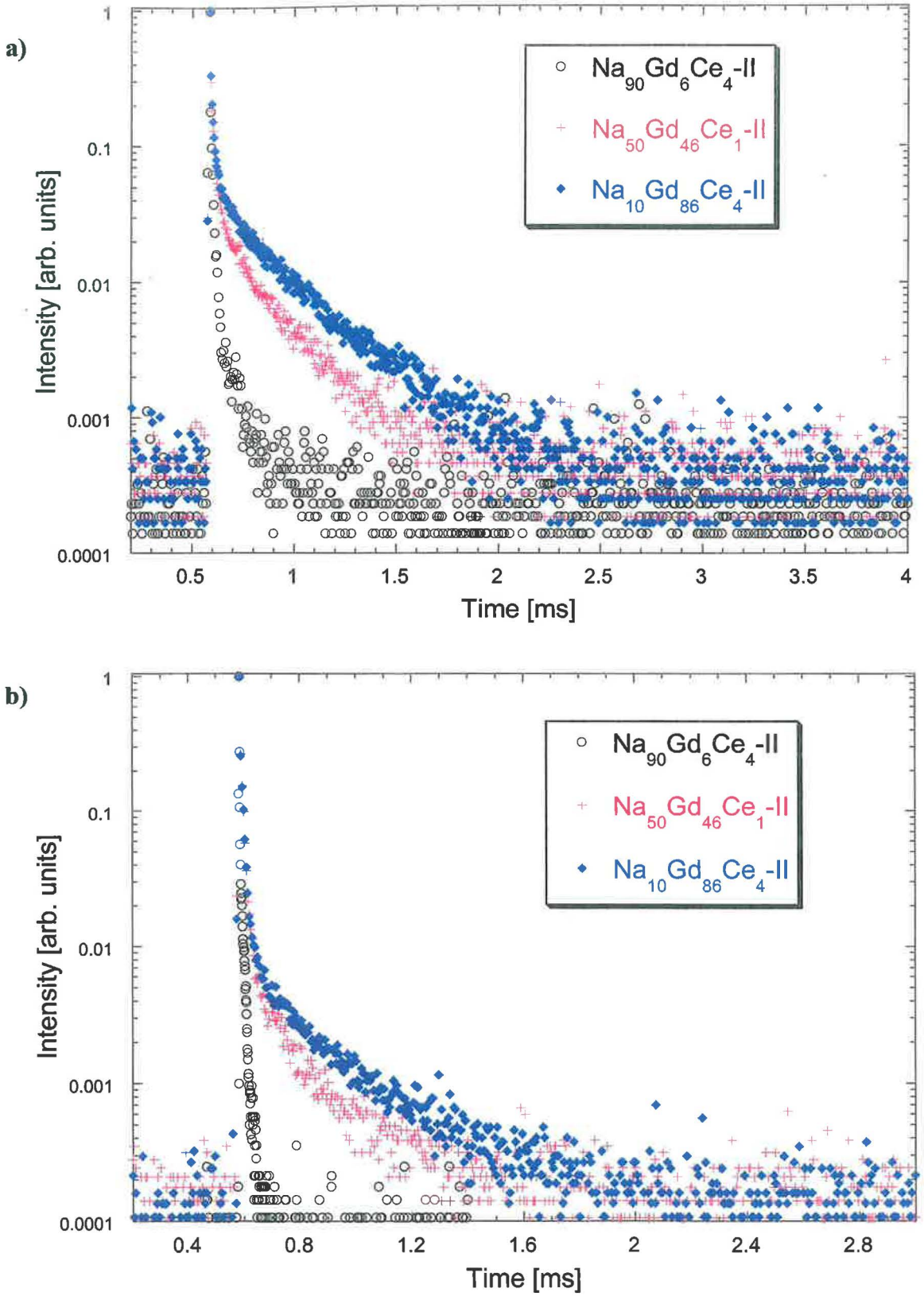

Fig. 66. Slow component of the decay kinetics of the Ce^{3+} emission (λ_{em} = 340 nm) with the excitation a) through the Gd^{3+} ions (λ_{exc} = 275 nm); b) directly through the Ce^{3+} ions (λ_{exc} = 319 nm) new glasses with the concentration of Ce^{3+} 4 mol% in the melt

The decay kinetics curves of the μs range are depicted in Fig. 65 and 66. On every graph one can see that the contribution of the slow component increases with the increase of the concentration of Gd^{3+}. The slow component appeares for the following reason. After the back transfer $Ce^{3+} \rightarrow Gd^{3+}$ the excitation migrates in the Gd^{3+} subarray. Then part of this excitation returns to the same or another Ce^{3+} ion, but with a significant time lag. This argument implies a relationship with the shortening of the nanosecond part of the decay curve must exist. The more intensive back transfer $Ce^{3+} \rightarrow Gd^{3+}$ (i.e. the shorter decay time τ_0 of the nanosecond component), the more energy must be emitted in the microsecond region (i.e. the bigger mean decay time τ_{mean} of the microsecond component).

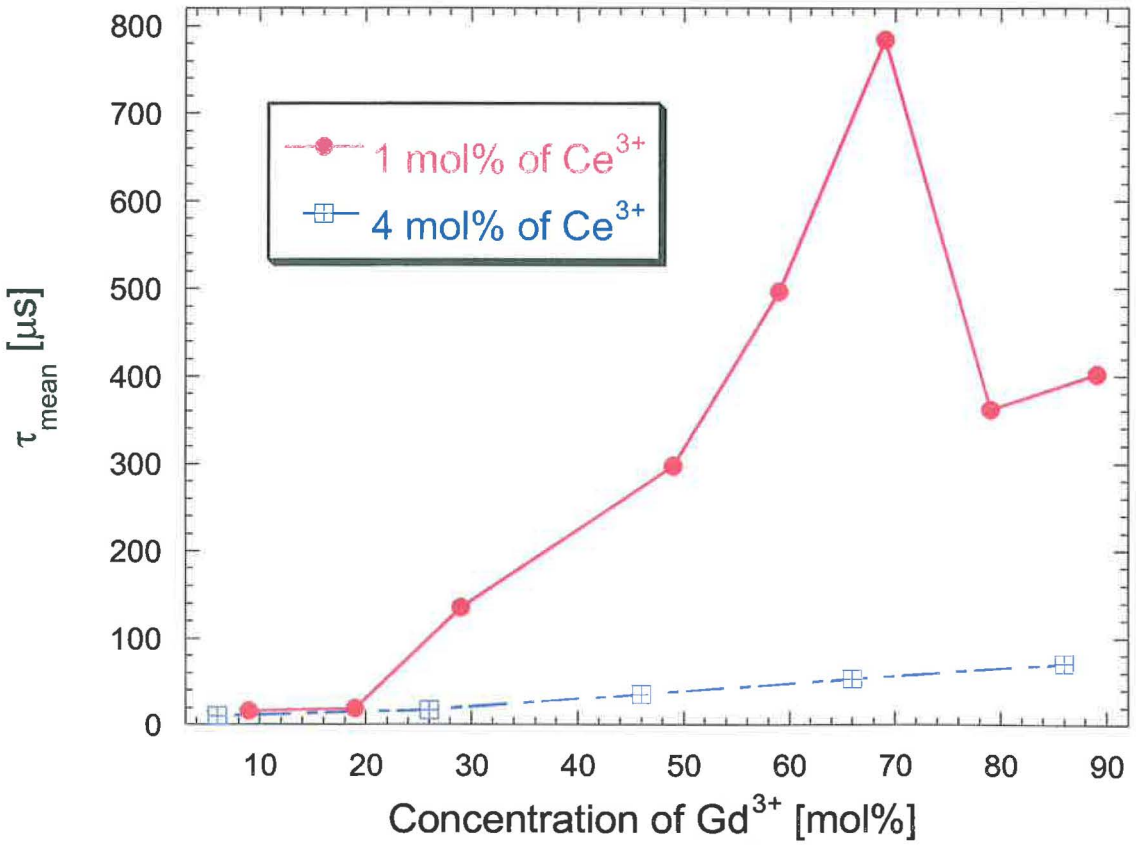

Fig. 67. Dependence of the mean decay time τ_{mean} of the Ce^{3+} decay (λ_{exc} = 319 nm, λ_{em} = 340 nm) on the Gd^{3+} concentration

To check this relationship the fitting procedure with the sum of three or four exponential functions was applied to all the decay kinetics curves in the microsecond region. The mean decay time τ_{mean} was calculated by equation (5). The graph of the dependence of this parameter τ_{mean} on the concentration of Gd^{3+} is given in Fig. 67 for both sets of the samples. For the set of samples with the concentration of Ce^{3+} 1 mol%, the interval of values of τ_{mean} is

much wider (from 16.6 μs for the sample with the lowest concentration of Gd^{3+} $Na_{90}Gd_9Ce_1$-II to 785 μs for the sample $Na_{30}Gd_{69}Ce_1$-II) than for the samples with the concentration of Ce^{3+} 4 mol% (from 10.4 μs for the sample with the lowest concentration of Gd^{3+} $Na_{90}Gd_6Ce_4$-II to 71.5 μs for the sample with the highest concentration of Gd^{3+} $Na_{10}Gd_{86}Ce_4$-II). Thus, for the samples with 1 mol% of Ce^{3+}, the presence of the slow component is stronger than for the samples with 4 mol% of Ce^{3+}. In could be explained by the fact that between the back transfer $Ce^{3+} \rightarrow Gd^{3+}$ and the return to Ce^{3+} ions, the energy migrates through the Gd^{3+} subsystem much longer in the samples with a lower concentration of acceptors.

Within each set of samples, the relationship between τ_{mean} of the microsecond decay component (Fig. 67) and τ_0 of the nanosecond decay component (Fig. 64) can be clearly traced. In the set of samples with 1 mol% of Ce^{3+}, the samples that have larger shortening of the nanosecond component, also have a larger contribution to the microsecond component (the samples $Na_{40}Gd_{59}Ce_1$-II and $Na_{30}Gd_{69}Ce_1$-II). For the sample with very small shortening of the decay in the nanosecond range, the influence of the microsecond component is very small (these are the samples with the small concentration of Gd^{3+} ions $Na_{90}Gd_9Ce_1$-II and $Na_{80}Gd_{19}Ce_1$-II).

In the case of the samples with 4 mol% of Ce^{3+}, one can see an almost linear decrease of the nanosecond component decay time and a steady increase of the microsecond components decay time as the concentration of Gd^{3+} grows. The only exception is the sample $Na_{30}Gd_{66}Ce_4$-II, than drops out of the general trend for the dependence of τ_0 [ns] on the concentration of Gd^{3+}. However, in this case, as it was already mentioned above, the estimate of τ_0 can be significantly distorted by the slow component.

Scintillation decay

The scintillation decay has been measured for all the samples with the concentration of Ce^{3+} 4 mol% at the room temperature. An example of the scintillation decay curve with the fitting curve for the sample $Na_{50}Gd_{46}Ce_4$-II is shown at Fig. 68. The fitting equation with the obtained parameters and the coefficient α calculated by the equation (7) are written in the legend of the figure. The scintillation decay times of all the measured samples are presented in Table 9. The scintillation decay time τ_1 corresponds to the distortion by the instrumental response. The scintillation decay time τ_2 has the values from 13.9 ns to 24.1 ns. The coefficient α grows as the concentration of Gd^{3+} increases. The exception is only for the

Table 9. Parameters of fit of scintillation decay of Ce-doped phosphate glasses

Sample	τ_1, ns	τ_2, ns	α, %
$Na_{86}Gd_{10}Ce_4$	1.97	13.9	16.23
$Na_{66}Gd_{30}Ce_4$	2.50	18.1	2.10
$Na_{46}Gd_{50}Ce_4$	1.46	24.1	4.26
$Na_{26}Gd_{70}Ce_4$	1.69	17.6	5.50
$Na_6Gd_{90}Ce_4$	0.78	16.9	7.50

sample $Na_{90}Gd_6Ce_4$-II, which has a very big value (16.23%) in comparison to other samples. It can be explained not only by long decay times of the components of the scintillation decay curve, but also by high amplitude of these long components.

If we compare the scintillation and Ce^{3+} photoluminescence decay times, the short components lie in the range 13.5 - 24 ns, but the detail dependence on the concentration of Gd^{3+} differs. The coefficient α rises as the concentration of Gd^{3+} grows, what is a result of the back transfer $Ce^{3+} \rightarrow Gd^{3+}$. However, the concentration dependence of the long component of photoluminescence decay is more complicated (Fig. 67).

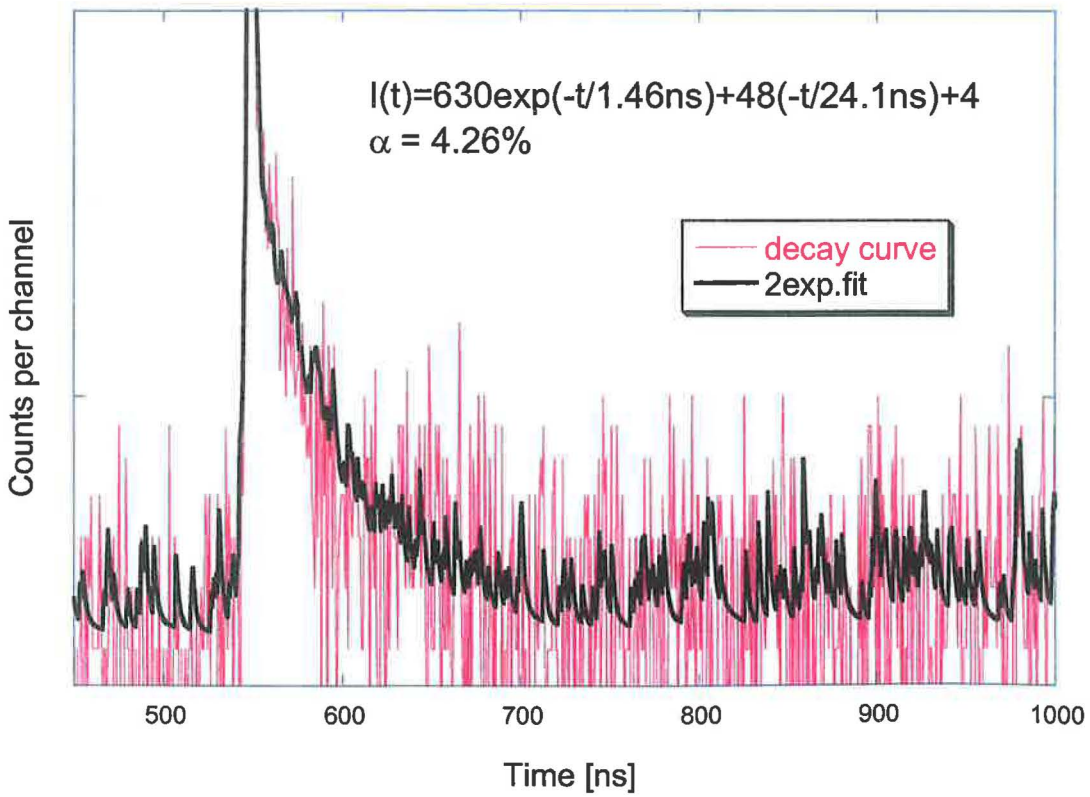

Fig. 68. Scintillation decay (excited by the radioisotope ^{22}Na) of $Na_{46}Gd_{50}Ce_4$-II with fitting curves. The equation of the fit is also presented. The coefficient α is calculated by the equation (7).

Table 10. The parameters of double-gaussian function fit of the normalised radioluminescence spectra of $Na_{74}Gd_{25}Ce_1$ and $Na_{70}Gd_{29}Ce_1$-II samples

	$Na_{74}Gd_{25}Ce_1$		$Na_{70}Gd_{29}Ce_1$-II	
	Gaussian component 1	Gaussian component 2	Gaussian component 1	Gaussian component 2
Area	0.40	0.10	0.38	0.12
Width	0.34	0.18	0.35	0.21
Position of the center, eV	3.63	3.83	3.66	3.88
ΔE, eV	0.214		0.226	
ΔE, cm^{-1}	1726		1820	

Comparison of the glasses of the first and second generation

As it has already been mentioned, the preparation technique of the new improved glasses is different from the old one, therefore it is interesting to compare two samples with the same chemical composition and dopand concentration prepared by these two methods. Fig. 69

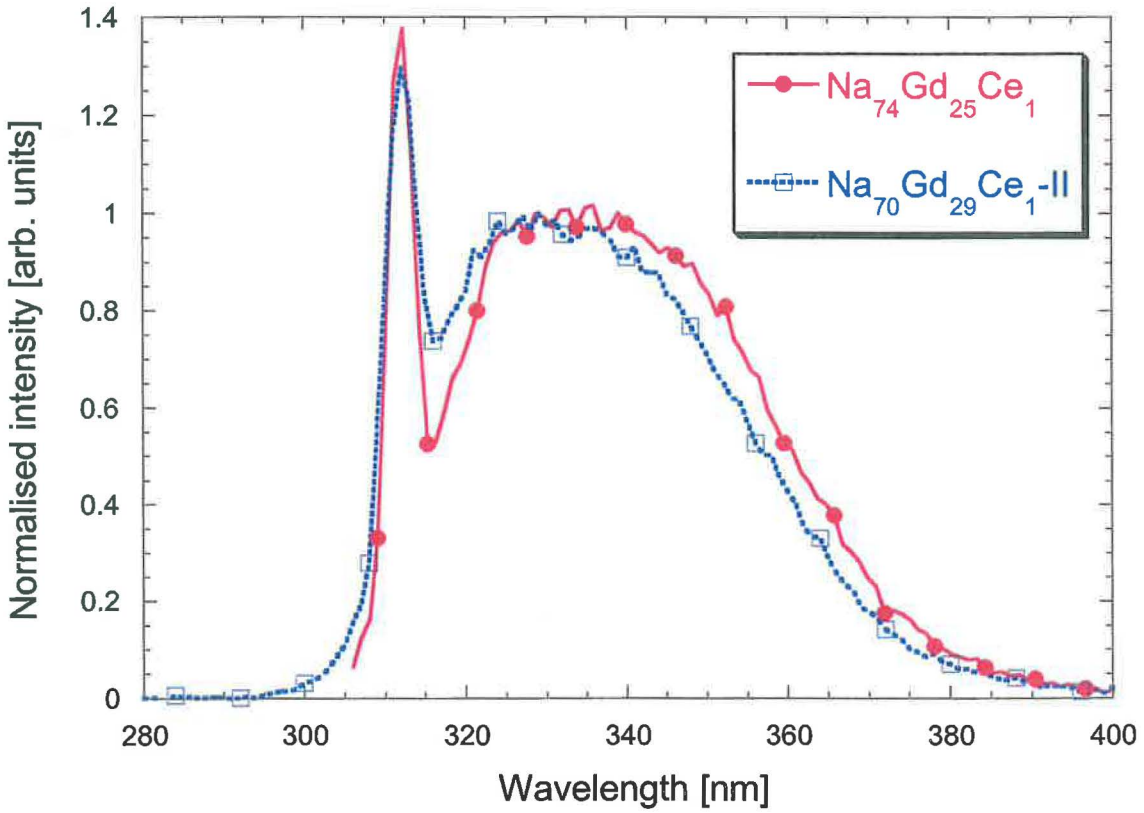

Fig. 69. Normalised radioluminescence spectra of $Na_{74}Gd_{25}Ce_1$ and $Na_{70}Gd_{29}Ce_1$-II samples at room temperature

presents the radioluminescence spectra of two samples with 1 mol% of Ce^{3+} both and 25 mol% and 29 mol% of Gd^{3+}. The spectra are given with the normalised intensity, so it is possible to compare them in a proper way. The difference is in both the position and the shape of the spectra. The both radioluminescence spectra were fitted by the double-gaussian function. The good result of such the fit evidences once more the presence of the short range order in the glass matrix. The parameters of the fit are presented in Table 10. The ratio of the gaussian areas is almost the same for the both samples. However, the width of the gaussians is bigger for the sample $Na_{70}Gd_{29}Ce_1$-II. The positions of the center of the both gaussians are shifted to the high energy region for the sample $Na_{70}Gd_{29}Ce_1$-II. The distance between the centers of the band is about 1700-1800 cm^{-1}, that corresponds to the distance between two 4*f* levels of spin-orbit coupling (Fig. 15).

Summary

- A new set of Ce^{3+}-doped Na, Gd-phosphate glasses was prepared using a new improved technology. The modification of the technology allows to make glasses with very high concentration of the donor (Gd^{3+}). The radioluminescence spectra, the decay kinetics and the scintillation decay kinetics were measured, and their main parameters were calculated.
- For the samples with 4 mol% of Ce^{3+} the direct donor-acceptor energy transfer plays the main role due to a high concentration of Ce^{3+}. The increase of the concentration of Gd^{3+} has a least impact on the enhancement of energy transfer compared to the set with 1 mol% of Ce^{3+}, and at high concentration of Gd^{3+} the back energy transfer $Ce^{3+} \rightarrow Gd^{3+}$ is increasing.
- The doping of the Gd^{3+} ions to the glasses with 1 mol% of Ce^{3+} essentially helps to deliver energy to the activator ions, which increases the efficiency of the glasses.
- The unique characteristics of the samples with the concentration of Gd^{3+} about 50 mol% for both the sets with 1 mol% and 4 mol% of Ce^{3+} deserve special attention. This concentration of Gd^{3+} is optimal from the point of view of the homogeneity of the mixture of the constituents. The luminescent properties of these samples are comparable to those of the samples with a very high concentration of Gd^{3+} (about 90 mol%).
- The intensity of radioluminescence spectra of the glasses with small concentration of Gd^{3+} is comparable to that of crystal scintillator BGO, and the intensity of the glasses with very high concentration of Gd^{3+} is four times more than the intensity of BGO.

- Thus the method of enhancement of integral scintillation efficiency of phosphate glasses by the delivery of energy to the activator through the sublattice of Gd^{3+} again proves very efficient for glasses.

Conclusions

The dissertation presents an experimental study of energy transfer in Ce^{3+}-doped and Tb^{3+}-doped Gd^{3+}-enriched Na-phosphate glasses. It was recently shown that the integral scintillation efficiency of Ce^{3+}-doped or Tb^{3+}-doped phosphate glasses can be substantially increased by enriching them with Gd^{3+} ions [nikl2000a, nikl2001b]. This scintillation efficiency enhancement technique, known in the literature as "sensitization", makes use of energy transfer phenomena taking place inside the scintillator. An investigation of these phenomena can help to optimize the further search for better scintillation materials.

Two series of samples of the glasses are investigated, which are referred to as the glasses of the first and second generations, respectively. The measured characteristics include absorption, photo- and radioluminescence spectra, and photo- and scintillation decay kinetics. The collected experimental data provide a complex picture of the scintillation and optical properties of the investigated samples.

The main focus in the dissertation is made on the samples of the first generation, which includes both Ce^{3+}-doped and Tb^{3+}-doped glasses. The measurements for the glasses of the first generation were conducted at various temperatures in the range from 5 K through 300 K. The glasses of the second generation were obtained with an improved technology, which allowed to prepare samples with high concentrations of Gd^{3+} up to 90 mol%, and to study the influence of the Gd^{3+} concentration on the considered optical and scintillation characteristics. However, the second generation is represented by Ce^{3+}-doped glasses only, and all their characteristics were measured at the room temperature.

The analysis of the experimental data begins with the comparison of the absorption, excitation, and emission spectra, which implies that energy transfer from the host matrix to the Ce^{3+} and Tb^{3+} luminescence centers ("acceptors") through a subsystem of Gd^{3+} ions ("donors") really takes place in all considered samples. The presence of the energy transfer phenomenon is also supported by the shortening of the luminescence decay times with the increase of the temperature or the increase of the Gd^{3+} concentration. Moreover, the presence of exponential tails in the decay curves indicates that the energy transfer from the donors to the acceptors is not direct but is accompanied with a multi-step energy migration between the donors.

The further investigation of the decay kinetics determines the type of the energy migration in the donor subsystem. For this purpose, the parameters of the initial parts and the

tails of the Gd^{3+} decay curves were numerically estimated to derive the microparameters C_{DA} and C_{DD}. These parameters characterize the rates of the D → A and D → D ion-ion energy transfer respectively (A = Ce^{3+} in the Ce^{3+}-doped glasses, A = Tb^{3+} in the Tb^{3+}-doped glasses, and D = Gd^{3+}). The evaluation of the ratio C_{DA} / C_{DD} implies that the energy migration in the Ce^{3+}-doped samples is diffusion-limited, and the energy migration in the Tb^{3+}-doped samples is hopping-limited. In addition, the energy transfer in the Tb^{3+}-doped samples is close to the kinetic limit ("supermigration").

The estimation of the microparameters C_{DA} and C_{DD} from the experimental data is a non-trivial task. The dissertation outlines a general methodology of its solution. This includes both the systematization of the known methods and the exploration of new ones. In particular, a new method of preliminary smoothing of the measured decay kinetics with so-called log-convex approximations is proposed; this procedure makes the successive estimation of the parameters more precise and reliable.

The analysis of the temperature dependences of the microparameters C_{DA} and C_{DD} reveals the role of phonons in the energy transfer process. It is established that the dominating role in the Gd^{3+} → Gd^{3+} energy transfer is played by two-phonon resonant and one-phonon processes, while Gd^{3+} → Tb^{3+} energy transfer is most likely to be a two-phonon resonant processes.

The examination of the improved Ce^{3+}-doped glasses (i.e. glasses of the second generation) shows that the increase of the concentration of Gd^{3+} generally results in the increase of the intensity of radioluminescence spectra. This intensity for the glasses with small concentration of Gd^{3+} (6-10 mol%) is comparable to that of crystal scintillator BGO, and the radioluminescence intensity for the glasses with very high concentration of Gd^{3+} (about 90 mol%) is six times larger than the corresponding intensity of BGO. However, higher concentration of donors does not always imply better scintillation and luminescence properties. It was found that while these properties for the samples with the concentration of Gd^{3+} about 50 mol% are comparable to those of the samples with the 80-90 mol% of Gd^{3+}, the corresponding characteristics of the samples with the Gd^{3+} concentration of 60-70 mol% are essentially worse. This phenomenon is explained by the fact that the 50% proportion of the donor ions ensures a homogeneous mixture of the glass constituents, which is distorted at higher donor concentrations.

Other results include the following. For the Ce^{3+}-doped samples, bidirectional energy transfer is found. It is explained by the overlap of the absorption and emission spectra, and is

also supported by the observed Ce^{3+} decay kinetics. It was also established that the position of the Gd^{3+} emission line in the $Na_{62}Gd_{28}Tb_{10}$ sample changes with the temperature, which is apparently influenced by the participation of different sublevels of the $^6P_{7/2}$ level in the $^6P_{7/2} \rightarrow S$ transition. For the Tb^{3+}-doped samples, the phenomenon of cross-relaxation is detected. It is argued that the considered glasses have the short-range order, which is evidenced by a successful decomposition of the radioluminescence spectra into Gaussian functions.

Appendix A

Log-convex approximations

A.1 Basic idea

It is a common practice to fit the experimental decay curve with a parametric functional form, e.g. by the sum of exponentials (see formula (4)). Unfortunately, the existing theory provides no exact analytical expression for the general process of donor luminescence decay with energy migration (see Section 2.5). In this situation one can try a few candidate forms and choose the one that results in the best fit to the data. But the success of this trial-and-error method is questionable. There is no obvious way to guess a particular functional form that would simultaneously provide a good fit to the data and have a reasonable theoretical justification.

Log-convex approximation represents an alternative approach. Instead of guessing a specific functional form, one postulates general assumptions that must hold for *every* candidate functional form. The assumptions made in this dissertation are the following.

Assumption 1. *The decay curve is a positive nonincreasing function.*

Assumption 2. *The logarithm of the decay curve is a convex function.*

Assumption 1 is obvious and hardly raises any questions. As for Assumption 2, there is no evidence that would contradict it. First, this assumption is suggested by the visual form of the data. Second, the known theoretical expressions for particular stages of the decay (see Section 2.5) all satisfy Assumption 2. To see the generality of the proposed assumptions, notice also that if functions f and g satisfy Assumptions 1 and 2 then $f \cdot g$, $f + g$, and $\max\{f, g\}$ also satisfy Assumptions 1 and 2. In particular, the sum of exponentials with nonnegative coefficients meets these assumptions.

The idea of log-convex approximation is to find the best approximation to the data among *all* functions that satisfy Assumptions 1 and 2. The precise formulation of the method is given in Section A.2. Applications of the method are discussed in Section A.3, where log-convex approximation is treated as a method of data smoothing.

A.2 Detailed mathematical description

For every convex subset S of $\mathbf{R}$, let $K(S)$ denote the set of real-valued functions defined on S and satisfying Assumptions 1 and 2, that is

$$K(S) = \{ x \in S \to g(x) \in \mathbf{R} : \\ g \text{ is positive and nonincreasing, } \log g \text{ is convex} \}. \tag{A1}$$

Consider now an arbitrary real-valued function f defined on a bounded closed real interval $[a,b]$:

$$f : [a,b] \to \mathbf{R}. \tag{A2}$$

Suppose that we are given the values of f at a finite number of points $\{x_i\}_{i=0}^{n+1}$ such that $a = x_0 < x_1 < \ldots < x_n < x_{n+1} = b$, and we want to approximate the function f by a function $g \in K([a,b])$. We can construct the function g as follows.

1) Use the least squares method to derive the values $g(x_i)$ from $f(x_i)$ for $i = 0,1,\ldots,n+1$. This means solving the following constrained minimization problem:

$$\begin{aligned} &\min_{g(x_0),g(x_1),\ldots,g(x_{n+1})} \sum_{i=0}^{n+1} \left(g(x_i) - f(x_i)\right)^2 \quad \text{subject to} \\ &g(x_i) > 0 \quad \text{for all } i = 0,1,\ldots,n+1 \\ &g(x_i) \geq g(x_{i+1}) \quad \text{for all } i = 0,1,\ldots,n \\ &\log g(x_i) \leq \frac{x_{i+1} - x_i}{x_{i+1} - x_{i-1}} \log g(x_{i-1}) + \frac{x_i - x_{i-1}}{x_{i+1} - x_{i-1}} \log g(x_{i+1}) \quad \text{for all } i = 1,\ldots n. \end{aligned} \tag{A3}$$

2) Extend the values $g(x_i)$ to the values $g(x)$ for all $x \in [a,b]$ by log-linear interpolation. That is, define

$$\log g(x) = \frac{x_{i+1} - x}{x_{i+1} - x_i} \log g(x_i) + \frac{x - x_i}{x_{i+1} - x_i} \log g(x_{i+1}) \\ \text{for all } i = 1,\ldots,n \text{ and } x \in [x_i, x_{i+1}]. \tag{A4}$$

The function g defined in this way is referred to as the *log-convex approximation* of f.

How can problem (A3) be solved in practice? Assume that $x_{i+1} - x_i = const$ for all $i = 0,1,\ldots,n$, i.e. the net $\{x_i\}_{i=0}^{n+1}$ has a finite step. In this case problem (A3) can be written as

$$\begin{aligned} &\min t \quad \text{subject to} \\ &t \geq \sqrt{\sum_{i=0}^{n+1} \left(g(x_i) - f(x_i)\right)^2} \\ &g(x_i) > 0 \quad \text{for all } i = 0,1,\ldots,n+1 \\ &g(x_i) \geq g(x_{i+1}) \quad \text{for all } i = 0,1,\ldots,n \\ &g(x_i)^2 \leq g(x_{i-1})g(x_{i+1}) \quad \text{for all } i = 1,\ldots,n. \end{aligned} \tag{A5}$$

This is a second-order conic convex optimization problem. Such problems have the merit that highly efficient methods of their numerical solution are available.[1] Within the presented dissertation research, optimization problems of this type were solved with the SeDuMi optimization toolbox (http://sedumi.mcmaster.ca).

A.3 Discussion

Log-convex approximation can be treated as a method of data smoothing. The basic idea of smoothing is that function values at close points must be close. Smoothed data can be used for estimating the slope of the data curve. In particular, log-convex approximations are used in this dissertation to demonstrate the existence of the exponential tail of the decay curve and estimate the decay parameter of the tail.

Like other methods of smoothing, log-convex approximation can serve as a preliminary step before parametric fitting. In this respect, the following trick has proven especially useful. Instead of fitting the data curve $f(t)$ with a parametric dependence $\varphi(t,\alpha)$, one constructs the log-convex approximation $g(t)$ of $f(t)$, and then fits $\log g(t)$ with $\log\varphi(t,\alpha)$. The point here is that fitting the logarithm of the curve is often computationally simpler than fitting the original curve, and at the same time it is impossible to take logarithm of the unsmoothed data because of negative values (which inevitably appear after the subtraction of the background).

However, there is an essential difference between log-convex approximation and the standard smoothing procedures. The latter make only *local* corrections to the shape of the curve. The corrections made to two different pieces of the curve are almost independent, provided the two pieces are sufficiently far from each other. Relations between distant data points are ignored. The method of log-convex approximation accounts for the *global* shape of the curve. This results in a more efficient smoothing procedure, which takes into account the specificity of decay data.

[1] These methods were discovered in the 1990s.

References

andryushchenko2003 — A.Yu. Andryushchenko, A.B. Blank, S.V. Budakovsky, N.Z. Galunov, N.I. Shevtsov, O.A. Tarasenko: *Scintillation material for determination of radionuclides in water*. Nucl. Instr. Meth. A **511** (2003) 425-430

arbuzov1992 — В.И. Арбузов, М.А. Элертс: *Фотоперенос электрона между редкоземельными соактиваторами в щелочносиликатных стеклах*. Физ. Хим. Стекла **18** (1992) 49-65

arbuzov1992a — В.И. Арбузов, В.Я. Грабовскис, Я.Я. Дзенис: *Особенности возбуждения рентгенолюминесценции ионов Ce^{3+} и Tb^{3+} в силикатном стекле*. Физ.Хим. Стекла **18** (1992) 96-106

artamonova1972 — М.В. Артамонова, Ч.М. Брискина, А.И. Бурштейн, Л.Д. Зусман, А.Г. Склезнев: *Изучение временного хода люминесценции ионов Nd^{3+} и оценка миграции электронного возбуждения по этим ионам в стекле*. ЖЭТФ **62** (1972) 863-871

atkinson1987 — M. Atkinson, J. Fent, C. Fisher, P. Freund, P. Hughes, J. Kirkby, A. Osthoff, K. Pretzl: *Initial tests of a high resolution scintillating fibre (SCIFI) tracker*. Nucl. Instr. Meth. A **254** (1987) 500-514

avgin2002 — I.Avgin, D.L.Huber: *One-phonon assisted energy transfer in periodic arrays of optically active ions*. J. Lumin. **96** (2002) 149-154

babin2003 — V.Babin, A.Krasnikov, J.A.Mares, M.Nikl, K.Nitsch, N.Solovieva, and S.Zazubovich: *Luminescent spectroscopy of the Gd-rich Ce^{3+}-, Tb^{3+}- and Mn^{2+}-doped phosphate glasses*. Phys. Stat. Sol. (a) **196**, No. 2 (2003) 484-495

baccaro2000 — S.Baccaro, R.Dall'Igna, P.Fabeni, M.Martini, J.A.Mares, F.Meinardi, M.Nikl, K.Nitsch, G.P.Pazzi, P.Polato, C.Sussini, A.Vedda, G.Zanella, R.Zannoni: *Ce^{3+} or Tb^{3+}-doped phopshate and silicate scintillating glasses*. J. Lumin. **87-89** (2000) 673-375

barbon1996 — F. Barbon, V. Colombrino, R. Dall'Igna, P. Polato, B. Profilo, G. Zanella, R. Zannoni: *Workability problems in lithium scintillating glasses for neutron detection*. Rivista della Staz. Sper. del Vetro **5** (1996) 223-238

bettinelli1989 — M. Bettinelli, G. Ingletto: *Energy transfer between Tb^{3+} and Tm^{3+} in a lead silicate glass*. J. Lumin. **43** (1989) 115-119

bettinelli1996 M. Bettinelli, G. Ingletto, P. Polato, G. Pozza, G. Zanella, R. Zannoni: *Optical spectroscopy of Ce^{3+}, Tb^{3+} and Eu^{3+} in new scintillating glasses*. Phys. Chem. Glasses **37** (1996) 4-8

birks1970 J.B.Birks: *Energy transfer in organic systems X. Pure and mixed crystals*. J. Phys. B: Atom. Molec. Phys. **3** (1970) 1704-1714

blasse1982 G.Blasse: *Energy Transfer Phenomena in the System (Y, Ce, Gd, Tb)F_3*. Phys. Stat. Sol. (a) **73** (1982) 205-208

blasse1986 G.Blasse, H.S.Kiliaan, A.J.de Vries: *A study of the energy transfer processes in sensitized gadolinium phosphors*. J. Less Common Metals **126** (1986) 139-146

blasse1994 G. Blasse, B.C. Grabmaier: *Luminescent Materials*. Springer (1994)

bollinger1962 L.M. Bollinger, G.E. Thomas: *Neutron detection with glass scintillators*. Nucl. Instr. Meth. **17** (1962) 97-116

bondar1981 И.А. Бондарь, А.И. Бурштейн, А.В. Крутиков, Л.П. Мезенцева, В.В. Осико, В.П. Сакун, В.А. Смирнов, И.А. Щербаков: *Исследование процессов релаксации электронного возбуждения в кристаллах при произвольных соотношениях микропараметров взаимодействия и концентраций доноров и акцепторов энергии*. ЖЭТФ **81** (1981) 96-114

bondar1983 И.А. Бондарь, А.В. Крутиков, Л.П. Мезенцева, С.Н. Перепечко, В.А. Смирнов, И.А.Щербаков: *Исследование процессов переноса энергии в кристаллах редкоземельных пентафосфатов*. ФТТ **25** (1983) 1983-1988

buijs1988 M. Buijs, G. Blasse: *One- and three-dimensional energy migration in domorphic EuP_3O_9*. J. Lumin. **39** (1988) 323-334

burshtein1972 А.И. Бурштейн: *Прыжковый механизм передачи энергии*. ЖЭТФ **62** (1972) 1695-1701

burshtein1984 А.И. Бурштейн: *Концентрационное тушение некогерентных возбуждений в растворах*. Усп. Физ. Наук **143** (1984) 553-600

burshtein1985 A.I. Burshtein: *Energy transfer kinetics in disordered systems*. J. Lumin. **34** (1985) 167-188

courrol2001 L.C. Courrol, L.V.G. Tarelho, L. Gomes, N.D. Vierra Jr., F.C. Cassanjes, Y. Messaddeq, S.J.L. Ribeiro: *Time dependence and energy-transfer mechanisms in Tm^{3+}, Ho^{3+} and Tm^{3+}-Ho^{3+} co-doped alkali niobium tellurite glasses sensitized by Yb^{3+}*. J. Non-Cryst. Sol. **284** (2001) 217-222

dalligna1997 R. Dall'Igna, P. Polato, G. Zanella, R. Zannoni, P. Ottonello, G.A. Rottigni: *Scintillating glass fiber optic plates for neutron imaging.* Proc. Fundament. of Glass Scien. and Technol. (1997) 101-108

dalton1987a A.W. Dalton: *Light conversion efficiency of small lithium scintillators for electrons, protons, deutrons and alpha particles.* Nucl. Instr. Meth. A **254** (1987) 361-366

devitsin1998 E.G. Devitsin, N.Yu. Kirikova, V.A. Kozlov, V.N. Makhov, S.Yu. Potashov, L.N. Dmitruk, M.A. Terekhin, I.H. Munro, C. Mythen, D.A. Shaw, K.W. Bell, R.M. Brown, P.S. Flower, P.W. Jeffreys, J.M. Parker: *Time-resolved studies of emission properties of cerium-doped fluoro-hafnate glasses under VUV synchrotron radiation excitation.* Nucl. Instr. Meth. A **405** (1998) 418-422

dexter1953 D.L. Dexter: *A Theory of Sensitized Luminescence in Solids.* J. Chem. Phys. **21** (1953) 836-850

dexter1954 D.L. Dexter, J.H. Schulman: *Theory of Concentration Quenching in Inorganic Phosphors.* J. Chem. Phys. **22** (1954) 1063-1070

dexter1969 D.L. Dexter, Th. Forster, R.S. Knox: *The Radiationless Transfer of Energy of Electronic Excitation between Impurity Molecules in Crystals.* Phys. Stat. Sol. **34** (1969) K159

dimartino2004 D.Di Martino, A.Krasnikov, M.Nikl, K.Nitsch, A.Vedda, S.Zazubovich: *The 3.83 eV luminescence of Gd-enriched phosphate glasses.* Phys. Stat. Sol. (a) **201** (2004) 38-40

dorenbos1997 P. Dorenbos, J.C. Spijker, C.W.E. van Eijk: *Luminescence and scintillation mechanisms in Ce^{3+} activated Gd-compounds.* In: Proc. Int. Conf. on Inorg. Scint. And Their Appl. SCINT97 (Ed. Y.Zhiwen, L.Peijun, F.Xiqi, X.Zhilin), Shanghai (1997) 307-310

dorenbos2003 P. Dorenbos: *Systematic behaviour in trivalent lantanide charge transfer energies.* J. Phys.: Condens. Matter **15** (2003) 8417

ebendorff1996a H. Ebendorff-Heidepriem, D. Ehrt: *UV radiation effects in fluoride phosphate glasses.* J. Non-Cryst. Sol. 196 (1996) 113-117

ebendorff1996b H. Ebendorff-Heidepriem, D. Ehrt: *Spectroscopic properties of Eu^{3+} and Tb^{3+} ions for local structure investigations of fluoride phosphate and phosphate glasses.* J. Non-Cryst. Sol. **208** (1996) 205-216

ebendorff1999a H. Ebendorff-Heidepriem, D. Ehrt: *Tb^{3+} f-d absorption as indicator of the effect of covalency on the Judd-Ofelt Ω_2 parameter in glasses.* J. Non-Cryst. Sol. **248** (1999) 247-252

ebendorff1999b H. Ebendorff-Heidepriem, D. Ehrt: *Electron spin resonance spectra of Eu^{2+} and Tb^{4+} ions in glasses*. J. Phys.: Condens. Matter **11** (1999) 7627-7634

ebendorff2000 H. Ebendorff-Heidepriem, D. Ehrt: *Formation and UV absorption of cerium, europium and terbium ions in different valencies in glasses*. Opt. Mat. **15** (2000) 7-25

ebendorff2002 H. Ebendorff-Heidepriem, D. Ehrt: *Effect of Tb^{3+} ions on X-ray-induced defect formation in phosphate containing glasses*. Opt. Mat. **18** (2002) 419-430

edgar1999 A. Edgar, J.-M. Spaeth, S. Schweizer, S. Assmann, P.J. Newman, and D.R. MacFarlane: *Photostimulated luminescence in a rare earth-doped fluorobromozirconate glass ceramic*. Appl. Phys. Lett. **75** (1999) 2386-2388

ehrt1992 D. Ehrt, W. Vogel: *Radiation effects in glasses*. Nucl. Instr. Meth. B **65** (1992) 1-8

eijk1994 C.W.E. van Eijk, J. Andriessen, P. Dorenbos, R. Visser: *Ce^{3+} doped inorganic scintillators*. Nucl. Instr. Meth. A **348** (1994) 546-550

eijk1997a C.W.E. van Eijk: *New scintillators, new light sensors, new aplications*. In: Proc. Int. Conf. on Inorg. Scint. And Their Appl. SCINT97 (Ed. Y.Zhiwen, L.Peijun, F.Xiqi, X.Zhilin), Shanghai (1997) 3-12

eijk2001 C.W.E. van Eijk: *Inorganic-scintillator development*. Nucl. Instr. Meth. A **460** (1987) 1-14

fairley1978 E.J. Fairley, A.R. Spowart: *Neutron scintillating glasses part III Pulse decay time measurements at room temperature*. Nucl. Instr. Meth. **150** (1978) 159-163

flach1975 R. Flach, D.S. Hamilton, P.M. Selzer, and W.M. Yen: *Time-resolved fluorescence line-narrowing studies in $LaF_3:Pr^{3+}$*. Phys. Rev. Lett. **35** (1975) 1034-1037

forster1948 Von Th. Forster: *Zwischenmolekulare Energiewanderung und Fluoreszenz*. Annalen der Physik, **6**, 2 (1948) 55-75

forster1949 Von Th. Forster: *Experimentelle und theoretische Untersuchung des zwischenmolekularen Ubergangs von Electronenanregungsenergie*. Z. Natruforschg. **4a** (1949) 321-327

fouassier1997 C.Fouassier: *Luminescent materials*. Current Opinion in Solid State & Material Science **2** (1997) 231-235

francini1997 R. Francini, U.M. Grassano, L. Landi, A. Scacco, M. D'Elena, M. Nikl, N. Cechova, and N. Zema: *Ce^{3+} luminescent centers of different symmetries in $KMgF_3$ single crystals*. Phys. Rev. B **56** (1997) 15109

garcia1999 A.J. Garcia, R. Balda, J. Fernandez: *Energy transfer assisted by localized excitations in amorpohous solids*. J. Lumin. **83-84** (1999) 177-181

gorin2002 A. Gorin, K. Kuroda, I. Manuilov, K. Morimoto, T. Oku, A. Ryazantsev, H.M. Shimizu, J. Suzuki, F. Tokanai: *Development of scintillation imaging device for cold neutrons*. Nucl. Instr. Meth. **A 479** (2002) 456-460

graaf2003 D.de Graaf, H.T. Hintzen, G.de With: *The influence of the composition on the luminescence of Ce(III)-Ln-Si-Al-O-N glasses (Ln = Sc, Y, La, Gd)*. J. Lumin. **104** (2003) 131-136

grabmaier1993 B.C.Grabmaier, W.Rossner: *New scintillators for X-ray computed tomography*. Nucl. Tracks Radiat. Meas. **21** (1993) 43-45

grabmaier1994 B.C.Grabmaier: *Luminescent materials for medical application*. J. Lumin. **60&61** (1994) 967-970

hayakawa1996 T. Hayakawa, N. Kamata, K. Yamada: *Visible emission characteristics in Tb^{3+}-doped fluorescent glasses under selective excitation*. J. Lumin. **68** (1996) 179-186

hayakawa1997 T. Hayakawa, N. Kamata, Y. Koike, K. Yamada: *Direct observation of optically controlled energy transfer in Tb^{3+}-doped glasses*. J. Lumin. **72-74** (1997) 925-926

heber1970 J.Heber: *Energy transfer and Rate Equations - Application to Ruby*. Phys. Stat. Sol. **42** (1970) 497-506

holstein1977 T.Holstein, S.K.Lyo, R.Orbach: *Phonon-assisted radiative transfer*. Phys. Rev. B **16** (1977) 934

holstein1981 T. Holstein, S.K. Lyo, R. Orbach: *Excitation Transfer in Disordered Systems*. In: W.M.Yen, P.M.Selzer (Eds.), Laser Spectroscopy of Solids, Topics in Applied Physics, Vol. **49**, Springer, Berlin (1981) 47-82

hong1974 H. Y-P. Hong: *The crystal structure of ytterbium metaphosphate, YbP_3O_9*. Acta Cryst. B **30** (1974) 1857

hosono1998 H. Hosono, T. Kinoshita, H. Kawazoe, M. Yamazaki, Y. Yamamoto, and A. Sawanobori: *Long lasting phosphorescence properties of Tb^{3+}-activated reduced calcium aluminate glasses*. J. Phys.: Condens. Matter **10** (1998) 9541-9547

huber1979 D.L. Huber: *Fluorescence in the presence of traps*. Phys. Rev. B **20** (1979) 2307

huber1981a D.L. Huber: *Dynamics of incoherent transfer*. In: Topics in Applied Physics; Ed. W.M. Yen, P.M. Selzer; Springer-Verlag, Berlin, Heidelberg, New York (1981) 83-111

ilieva2001 D. Ilieva, B. Jivov, D. Kovacheva, Ts. Tsacheva, Y. Dimitriev, G. Bogachev, Ch. Petkov: *FT-IR and Raman spectra of Gd phosphate crystals and glasses*. J. Non-Cryst. Sol. **293-295** (2001) 562-568

imbush1981 G.F. Imbusch, R. Kopelman: *Optical Spectroscopy of Electronic Centers in Solids*. In: Laser Spectroscopy of Solids; Ed. by W.M.Yen, P.M.Selzer; Springer-Verlag (1981) 1-38

inokuti1965 M. Inokuti, F. Hirayama: *Influence of Energy Transfer by the Exchange Mechanism on Donor Luminescence*. J. Chem. Phys. **43**, 6 (1965) 1978-1989

ishii1991 M.Ishii, M.Kobayashi: *Single crystals for radiation detectors*. Prog. Crystal Growth and Charact. **23** (1991) 245-311

iwai1998 S. Iwai, S. Murata, M. Tachiya: *Ultrafast fluorescence quenching by electron transfer and fluorescence from the second excited state of a charge transfer complex as studied by femtosecond up-conversion spectroscopy*. J. Chem. Phys. **109** (1998) 5963-5970

jia2001 D. Jia, J. Zhu, B. Wu, S. E: *Luminescence and energy transfer in $CaAl_4O_7:Tb^{3+}$, Ce^{3+}*. J. Lumin. **93** (2001) 107-114

jouhari1996 N.E. Jouhari, C. Parent, G. Le Flem: *Photoluminescence of Ce^{3+}, Tb^{3+}, and Mn^{2+} in Glasses of Base Composition $LaMgB_5O_{10}$*. J. Sol. Stat. Chem. **123** (1996) 398-407

kellendonk1982 F. Kellendonk, G. Blasse: *Luminescence and energy transfer in $TbAl_3B_4O_{12}$*. J. Phys. Chem. Sol. **43** (1982) 481-490

lacha2004 L.M. Lacha, R. Balda, J. Fernandez, J.L. Adam: *Time-resolved fluorescence line narrowing spectroscopy and fluorescence quenching in Nd^{3+}-doped flouroarsenate glasses*. Opt. Mat. **25** (2004) 193-200

lin2002 H. Lin, X.R. Liu, E.Y.B. Pun: *Sensitized luminescence and energy transfer in Ce^{3+} and Eu^{3+} codoped calcium magnesium chlorosilicate*. Opt. Mat. **18** (2002) 397-401

lupei1991 V.Lupei: *Laser processes and energy transfer*. J. Lumin. **48&49** (1991) 157-165

mares1995 J.A. Mares, M. Nikl, C. Pedrini, D. Bouttet, C. Dujardin, B. Moine, J.W.M. Verweij, J. Kvapil: *Further results on $GdAlO_3$:Ce scintillator*. Rad. Eff. Def. Sol. **135** (1995) 369-373

mares1996 J.A. Mares, M. Nikl: *Energy transfer, fluorescence and scintillation processes in Cerium-doped $RE^{3+}AlO_3$ fast scintillators*. Acta Physica Polonica A **90** (1996) 45-54

mares1997 J.A. Mares, M. Nikl, E. Mihokova, J. Kvapil, J. Gilba, K. Blazek: *Spectroscopy and transfer processes in $Lu_xGd_{1-x}AlO_3$:Ce scintillators*. J. Lumin. **72-74** (1997) 737-739

martin2004 I.R. Martin, F. Lahoz, V. Lavin, M. Hernandez-Molina: *Optical properties of Eu^{3+} ions in malonate crystals to monitor a structural phase transition*. Opt. Mat. **25** (2004) 223-229

maruyama1997 F. Maruyama, K. Yamada: *The parity conservation model for the energy cross relaxation among Tb^{3+} ions in glasses*. J. Lumin. **72-74** (1997) 956-958

melcher1991 C.L. Melcher, J.S. Schweitzer, R.A. Manente, C.A. Peterson: *Applications of single crystals in oil well logging*. J. Cryst. Growth **109** (1991) 37-42

murata1995 S. Murata, S.Y. Matsuzaki, M. Tachiya: *Transient Effect in Fluorescence Quenching by Electron Transfer. 2. Determintation of the Rate Parameters Involved in the Marcus Equation*. J. Phys. Chem. **99** (1995) 5354-5358

nikl2000 M. Nikl: *Wide Band Gap Scintillation Materials: Progress in the Technology and Material Understanding*. Phys. Stat. Sol. (a) **178** (2000) 595-620

nikl2000a M. Nikl, K. Nitsch, E. Mihokova, N. Solovieva, J.A. Mares, P. Fabeni, G.P. Pazzi, M. Martini, A. Vedda, S. Baccaro: *Efficient radioluminescence of the Ce^{3+}-doped Na-Gd phosphate glasses*. Appl. Phys. Lett. **77** (2000) 2159-2161

nikl2001b M. Nikl, J.A. Mares, E. Mihokova, K. Nitsch, N. Solovieva, V. Babin, A. Krasnikov, S. Zazubovich, M. Martini, A. Vedda, P. Fabeni, G.P. Pazzi, S. Baccaro: *Radio- and thermoluminescence and energy transfer processes in $Ce^{3+}(Tb^{3+})$-doped phosphate scintillating glasses*. Rad. Meas. **33** (2001) 593-596

nikl2006 M. Nikl: *Scintillation detectors for x-rays*. Meas. Sci. Technol. **17** (2006) R37-R54

nitsch2005 K. Nitsch, A. Cihlář, D. Klimm, M. Nikl and M. Rodová: Na-Gd phosphate glasses. Preparation, thermal and scintillating properties. J. Thermal Anal. Calorim. **80** (2005) 735-738

novotny2001 R. Novotny, R. Beck, W. Doring, V. Hejny, A. Hofstaetter, M. Korzhik, V. Metag, K. Romer, H. Stroher: *Electromagnetic calorimetry with $PbWO_4$ in the energy regime below 1 GeV*. Rad. Meas. **33** (2001) 615-618

pedrini1993 C. Pedrini, B. Moine, D. Bouttet, A.N. Belsky, V.V. Mikhailin, A.N. Vasilev, and E.I. Zinin: *Time-resolved liminescence of CeF_3 crystals excited by X-ray sychrotron radiation*. Chem. Phys. Lett. **26** (1993) 470-474

plastino2002 W. Plastino, P. De Felice, F. de Notaristefani: *Radon gamma-ray spectrometry with YAP:Ce scintillator*. Nucl. Instr. Meth. A **486** (2002) 146-149

porras2002 E. Porras, B. Escat, J.M. Benlloch, D. Kadi-Hanifi, S. Lopez, N. Pavon, J.A. Ruiz, F. Sanchez, A. Sebastia: *Portable mini gamma camera for medical applications*. Nucl. Instr. Meth. A **486** (2002) 186-190

rodnyi1997 P.A. Rodnyi: *Physical Processes in Inorganic Scintillators*. CRC Press (1997)

rodova2004 M. Rodova, A. Cihlar, K. Knizek, K. Nitsch, N. Solovieva: *Preparation and properties of Ce-doped Na-Gd phosphate glasses*. Rad. Meas. **38** (2004) 489-492

rotman1989 S.R. Rotman: *Nonradiative energy transfer in Nd:YAG - evidence for the correlated placement of ions*. Appl. Phys. Lett. **54**, 21 (1989) 2053-2055

sakun1972 В.П. Сакун: *Кинетика переноса энергии в кристаллах*. ФТТ **14** (1972) 2199-2210

salley2002 G.M. Salley, R. Valiente, H.U. Gudel: *Phonon-assisted cooperative sensitization of Tb^{3+} in $SrCl_2$:Yb,Tb*. J. Phys.: Condens. Matter **14** (2002) 5461-5475

schippers2002 J.M. Schippers, S.N. Boon, P. van Luijk: *Applications in radiation therapy of a scintillating screen viewed by a CCD camera*. Nucl. Instr. Meth. A **477** (2002) 480-485

schmidt2002 D. Schmidt, B. Asselineau, R. Bottger, H. Klein, L. Leberton, S. Neumann, R. Nolte, G. Pichenot: *Characterization of liquid scintillation detectors*. Nucl. Instr. Meth. A **476** (2002) 186-189

selzer1977 P.M. Selzer, D.S. Hamilton, and W.M. Yen: *Nonradiative Spectral and Spatial Energy Transfer in Ruby*. Phys. Rev. Lett. **38** (1977) 858-861

sharonov1996 M.Yu. Sharonov, Z.I. Zhmurova, E.A. Krivandina, A.A. Bystrova, I.I. Buchinskaja, B.P. Sobolev: *Improved by Yb^{3+} sensitizer fluoride crystals, doped with Pr^{3+}, for 1.3 μm optical amplifiers*. Opt. Comm. **124** (1996) 595-601

siebold1980 H.Siebold, J.Heber: *"Discrete shell model" for analysing time-resolved energy transfer in solids*. J. Lumin. **22** (1981) 297-319

stroud1962 J.S. Stroud: *Color Centers in a Cerium-Containing Silicate Glass*. J. Chem. Phys. **37**, 4 (1962) 836-841

sveshnikov1962 Б.Я. Свешников, В.И. Широков: *О зависимости изменений средней длительности и выхода люминесценции в процессе тушения от закона взаимодействия молекул*. Опт. Спектроск. **12** (1962) 576-581

tachiya1983 M. Tachiya: *Theory of diffusion-controlled reactions: formulation of the bulk reaction rate in terms of the pair probability*. Radiat. Phys. Chem. **21** (1983) 167-175

tissue1989 B.M. Tissue, J.C. Wright: *Phonon-assisted energy transfer within dimers in Pr^{3+}:CaF_2*. J. Lumin. **44** (1989) 33-40

tonooka1991 K. Tonooka, N. Kamata, K. Yamada, K. Matsumoto, F. Moruyama: *A non-linear analysis of energy transfer in highly Tb^{3+}-doped glasses*. J. Lumin. **50** (1991) 139-151

ursu1989 I. Ursu, A. Lupei, S. Georgescu, V. Lupei, A.M. Prokhorov, V.I. Zhekov, T.M. Murina, M.I. Studenikin: *Energy transfer characteristics of the $^4S_{3/2}$ level of Er^{3+} in YAG*. Opt. Comm. **72** (1989) 209-213

vandeun1999 R. Van Deun, K. Binnemans, C. Gorller-Warland, J.L. Adam: *Judd-Ofelt intensity parameters of trivalent lanthanide ions in a $NaPO_3$-BaF_2 based fluorophosphate glass*. J. Alloys Compd. **283** (1999) 59-65

vliet1989a J.P.M. van Vliet, D. van der Voort, G. Blasse: *Luminescence and energy migration in Eu^{3+}-containing sheelites with different anions*. J. Lumin. **42** (1989) 305-316

voronko1976 Ю.К. Воронько, Т.Г. Мамедов, В.В. Осико, А.М. Прохоров, В.П. Сакун, И.А. Щербаков: *Исследование природы безызлучательной релаксации энергии возбуждения в конденсированных средах с высоким содержанием активатора*. ЖЭТФ **71** (1976) 478-496

vries1988 A.J.Vries, J.P.M.van Vliet, G.Blasse: *Mechanism of Concentration Quenching of Gd^{3+} and Eu^{3+} Emission in Perovskite-Like Aluminates*. Phys. Stat. Sol (b) **149** (1988) 391-401

vries1988a A.J. de Vries, B.P. Minks, G. Blasse: *Evaluation of the energy migration in $GdAl_3B_4O_{12}$*. J. Lumin. **39** (1988) 153-160

vries1988b A.J.De Vries, M.F.Hazenkamp, G.Blasse: *On the Gd^{3+} luminescence and energy migration in $Li(Y,Gd)F_4$-Tb^{3+}*. J. Lumin. **42** (1988) 275-282

walsh2000 B.M. Walsh, N.P. Barnes, B. Di Bartolo: *The temperature dependence of energy transfer between the Tm $^3F_4$ and Ho $^5I_7$ manifolds of Tm-sensitized Ho luminescence in YAG and YLF*. J. Lumin. **90** (2000) 39-48

weber1971 M.J. Weber: *Luminescence Decay by Energy Migration and Transfer: Observation of Diffusion-Limited Relaxation*. Phys. Rev. B **4**, 9 (1971) 2932-2939

wegh1997 R.T. Wegh, H. Donker, A. Meijerink, R.J. Lamminmaki, J. Holsa: *Vacuum-ultraviolet spectroscopy and quantum cutting for Gd^{3+} in $LiYF_4$*. Phys. Rev. B **56** (1997) 13841-13848

wegh1999 R.T.Wegh, A.Meijerink: *Spin-allowed and spin-forbidden $4f^n \leftrightarrow 4f^{n-1}5d$ transitions for heavy lanthanides*. Phys. Rev. B **60** (1999) 10820-10829

wietfeldt1986 J.R. Wietfeldt, D.S. Moore, B.M. Tissue, and J.C. Wright: *Mechanism of nonresonant energy transfer between ions in SrF_2:Er^{3+}*. Phys. Rev. B **33** (1986) 5788-5794

wright1976 J.C. Wright: *Up-Conversion and Excited State Energy Transfer in Rare-Earth Doped Materials*. In: Topics in Applied Physics, V.**15** (Radiation's Processes in Molecules and Condensed Phases), Springer (1976) 239-297

yokota1967 M. Yokota, O. Tanimoto: *Effects of Diffusion on Energy Transfer by Resonance*. J. Phys. Soc. Jap. **22**, 3 (1967) 779-784

zanella1994 G. Zanella, R. Zannoni, R. Dall'Igna, B. Locardi, P. Polato, M. Bettinelli, and A. Marigo: *A new cerium scintillating glass for X-ray detection*. Nucl. Instr. Meth. A **345** (1994) 198-201

zanella1995 G. Zanella, R. Zannoni, R. Dall'Igna, B. Locardi, P. Polato, M. Bettinelli: *Development of a terbium-lithium glass for slow neutron detection*. Nucl. Instr. Meth. A **359** (1995) 547-550

zarkouna2004 E.B. Zarkouna, A. Driss: $LiYb(PO_3)_4$. Acta Cryst. E **60** (2004) i102-i104

Publications

M. Nikl, K. Nitsch, E.Mihokova, N. Solovieva, J.A. Mares, P. Fabeni, G.P. Pazzi, M. Martini, A. Vedda, S. Baccaro: *Efficient radioluminescence of the Ce^{3+}-doped Na-Gd phosphate glasses*. Appl. Phys. Lett **77**, 2159-2161 (2000)

M.Nikl, J.A.Mares, E.Mihokova, K.Nitsch, N.Solovieva, V.Babin, A.Krasnikov, S.Zazubovich, M.Martini, A.Vedda, P.Fabeni, G.P.Pazzi, S.Baccaro: *Radio- and thermoluminescence and energy transfer processes in $Ce^{3+}(Tb^{3+})$-doped phosphate scnitillating glasses*. Rad. Measurements **33**, 593-596 (2001)

J.A.Mares, M.Nikl, K.Nitsch, N.Solovieva, A.Krasnikov, S.Zazubovich: *A role of Gd^{3+} in scintillating processes in Tb-doped Na-Gd phosphate glasses*. J.Lumin. **94-95**, 321-324 (2001)

A.Vedda, M.Martini, M.Nikl, E.Mihokova, K.Nitsch, N.Solovieva, F.Karagulian: *Optical absorption and thermoluminescence of Tb^{3+} -doped phosphate scintillating glasses*. J.Phys.: Cond.Matter **14**, 7417-7426 (2002).

G.P.Pazzi, P.Fabeni, C.Susini, M.Nikl, E.Mihokova, N.Solovieva, K.Nitsch, M.Martini, A.Vedda, S.Baccaro, A.Cecilia, V.Babin: *Defect states induced by UV-laser irradiation in scintillating glasses*. Nucl. Instr. Meth. Phys. Research B **191**, 366-370 (2002)

V. Babin, A. Krasnikov, J. A. Mares, M. Nikl, K. Nitsch, N. Solovieva, and S. Zazubovich: *Luminescence spectroscopy of the Gd-rich Ce^{3+}-, Tb^{3+}- and Mn^{2+}-doped phosphate glasses*. Phys. Stat. Sol. (a) **196**, 484-495 (2003)

M. Rodová, A. Cihlář, K. Knížek, K. Nitsch, and N. Solovieva: *Preparation and properties of Ce-doped Na-Gd phosphate glasses*. Rad. Meas. **38**, 489-492 (2004)

N. Solovieva, M. Nikl, K. Nitsch: *Energy migration in the Ce^{3+}-doped Na-Gd phosphate glasses*. Optical Materials, In Press

Other publications

M. Nikl, N. Solovieva, E.Mihokova, M.Dusek, A.Vedda, M.Martini, K.Shimamura and T. Fukuda: *Scintillation Decay of $LiCaAlF_6:Ce^{3+}$ Single Crystals*. Phys.stat.sol. (a) **187**, R1-R3 (2001)

M. Nikl, P. Bohácek, E. Mihóková, N. Solovieva, M. Martini, A. Vedda, P. Fabeni, G. P. Pazzi, M. Kobayashi, M. Ishii, Y. Usuki, D.Zimmerman: *Modification Of $PbWO_4$ Scintillator Characteristics By Doping*. J.Cryst. Growth **229**, 312-315 (2001)

M.Nikl, P.Bohacek, E.Mihokova, N.Solovieva, A.Vedda, M.Martini, G.P.Pazzi, P.Fabeni, M.Kobayashi: *Complete characterization of doubly doped $PbWO_4$:Mo,Y scintillators*. J.Appl.Phys. **91**, 2791-2797 (2002)

M.Nikl, P.Bohacek, E.Mihokova, N.Solovieva, A.Vedda, M.Martini, G.P.Pazzi, P.Fabeni, M.Ishii: *Enhanced efficiency of $PbWO_4$:Mo,Nb scintillator*. J.Appl.Phys. **91**, 5041-5044 (2002).

H.Sato, K.Shimamura, A.Bensalah, N.Solovieva, A.Beitlerova, A.Vedda, M.Martini, H.Machida, T.Fukuda, M.Nikl: *Induced Absorption Phenomena, Thermoluminescence and Colour Centres in $KMgF_3$, $BaLiF_3$ and $LiCaAlF_6$ Complex Fluorides*. Jpn.J.Appl.Phys. **41**, 2028-2033 (2002)

M.Nikl, J.A.Mares, J.Chval, E.Mihokova, N.Solovieva, M.Martini, A.Vedda, K.Blazek, P.Maly, K.Nejezchleb, P.Fabeni, G.P.Pazzi, V.Babin, K.Kalder, A.Krasnikov, S.Zazubovich, C.D'Ambrosio: *An effect of Zr^{4+} co-doping of YAP:Ce scintillator*. Nucl. Instr. Meth. Phys. Research A **486**, 250-253 (2002)

N. Chiodini, M. Fasoli, M. Martini, E. Rosetta, G. Spinolo, A. Vedda, M. Nikl and N. Solovieva, A. Baraldi and R. Capelletti: *High-efficiency $SiO_2:Ce_3$ glass scintillators*. Appl. Phys. Lett. **81**, 4374-4376 (2002)

J. A. Mares, M. Nikl, E. Mihokova, N. Solovieva, K. Blazek, K. Nejezchleb, P. Maly, J. Kejchal, V. Mucka, M. Pospíšil, A.Vedda, M. Martini, and S.Baccaro: *Radiation induced colour center and damane in $YAlO_3$:Ce and $YAlO_3$:Ce,Zr scintillators*. Rad. Eff. & Def. Sol. **157**, 677-681 (2002)

M.Nikl, P.Bohacek, E.Mihokova, N.Solovieva, A.Vedda, M.Martini, G.P.Pazzi, P.Fabeni, M.Kobayashi: *Influence of Y-codoping on the $PbWO_4$:Mo luminescence and scintillator characteristics*. Nucl.Instr.Meth. Phys.Research A **486**, 453-457 (2002)

A.Yoshikawa, T.Akagi, M.Nikl, N.Solovieva, K.Lebbou, C.Dujardin, C.Pedrini, T.Fukuda: *$\{Y_{3-x}Yb_x\}Ga_2Ga_3O_{12}$ and $Lu_2Yb_1Al_2Al_3O_{12}$ single crystals for scintillator application grown by the modified micro-pulling-down method*. Nucl.Instr.Meth. Phys.Research A **486**, 79-82 (2002)

M. Kobayashi, R. Nakamura, M. Ishii, N. Solovieva, M. Nikl: *Energy Transfer Phenomena in GdF_3:Mn Co-doped with Ce^{3+}, Pr^{3+} or Zr^{4+}*. Jpn. J. Appl. Phys. **42**, 1648-1654 (2003)

J. B. Shim, A. Yoshikawa, A. Bensalah, T. Fukuda, N. Solovieva, M. Nikl, E. Rosetta, A. Vedda, D. H. Yoon: *Luminescence, radiation damage, and color center creation in Eu^{3+}-doped $Bi_4Ge_3O_{12}$ fiber single crystals*. J. Appl. Phys. **93**, 5131-5135 (2003)

J.B.Shim, A.Yoshikawa, M.Nikl, N.Solovieva, J.Pejchal, D.H.Yoon, T.Fukuda: *Growth and characterization of Yb^{3+}-doped $YAlO_3$ fiber single crystals grown by the modified micro-pulling-down metod*. J. Cryst. Growth **256**, 298-304 (2003)

H.Ogino, A.Yoshikawa, J.-H.Lee, M.Nikl, N.Solovieva and T.Fukuda: *Growth and scintillation properties of Yb-doped $Lu_3Al_5O_{12}$ crystals*. J. Cryst. Growth **253**, 314-318 (2003)

N.Chiodini, M.Fasoli, M.Martini, F.Morazzoni, E.Rosetta, R.Scotti, G.Spinolo, A.Vedda, M. Nikl, N.Solovieva, A.Baraldi, R.Capelleti, R.Francini: *Rare-earth doped sol-gel silicate glasses for scintillator applications*. Rad.Eff. Defects Sol. **158**, 463-467 (2003).

A.Yoshikawa, H.Ogino, J.H.Lee, M.Nikl, N.Solovieva, N.Garnier, C.Dujardin, K.Lebbou, C.Pedrini, T.Fukuda: *Growth and optical properties of Yb-doped new scintillator crystals*. Optical Materials **24**, 275-279 (2003).

M.Nikl, N.Solovieva, M.Dusek, A.Yoshikawa, Yuji Kagamitani and T.Fukuda: *Concentration quenching of Tb^{3+} luminescence in $Tb^xA_{3-x}Al_5O_{12}$ (A=Yb,Y) single crystals*. J. Cer. Proc. Res. 4, 112-114 (2003)

J.A. Mares, M. Nikl, N. Solovieva, C. D'Ambrosio, F. de Notaristefani, K. Blazek, P. Maly, K. Nejezchleb, P. Fabeni, G.P. Pazzi, J.T. M. de Haas, C.W.E. van Eijk, P. Dorenbos: *Scintillation and spectroscopic properties of Ce^{3+}-doped $YAlO_3$ and $Lu_x(RE)_{1-x}AlO_3$ (RE = Y^{3+} and Gd^{3+}) scintillators*. Nucl. Instr. Meth. Phys. Research A **498**, 312-327 (2003).

M.Nikl, N.Solovieva, J.Pejchal, J.B.Shim, A.Joshikawa, T.Fukuda, A.Vedda, M.Martini, D.H.Yoon: *Very fast $Yb_xY_{1-x}AlO_3$ single-crystal scintillators*. Appl. Phys. Let. **84**, 882-884 (2004)

M. Nikl, J.A. Mares, N. Solovieva, J. Hybler, A.Voloshinovskii, K. Nejezchleb, K. Blazek: *Energy transfer to the Ce^{3+} centers in $Lu_3Al_5O_{12}$:Ce scintillator*. Phys.stat.sol. (a) **201**, R41-R44 (2004).

A.Yoshikawa, T.Satonaga, K.Kamada, H.Sato, M.Nikl, N.Solovieva and T.Fukuda: *Crystal growth of Ce: PrF_3 by micro-pulling-down method*. J. Cryst. Growth **270**, 427-432(2004)

G.Chen, M.Nikl, N.Solovieva, A.Beilerova, J.Rao, Y.Yang, Y.Zhang, X.Jiang, C.Zhu: *Photoluminescent properties of nanocrystallyzed zinc borosilicate glasses*. Rad. Meas. **38**, 771-774 (2004)

J.A.Mares, A.Beitlerova, M.Nikl, N.Solovieva, C.D'Ambrosio, K.Blazek, P.Maly, K.Nejezchleb and F.de Notaristefani: *Scintillation response of Ce-doped or intrinsic scintillating crystals in the range up to 1 MeV*. Rad. Meas. **38**, 353-357 (2004)

P. Bohacek, M. Nikl, N. Solovieva and B. Trunda: *Radioluminescence spectra of PWO crystals (co)doped by Ba*. Rad. Meas. **38**, 363-365 (2004)

H. Sato, A. Bensalah, N. Solovieva, A. Beitlerova, A. Vedda, M. Martini, M. Nikl and T. Fukuda: *X-ray damage characterization in $BaLiF_3$,$KMgF_3$ and $LiCaAlF_6$ complex fluorides*. Rad. Meas. **38**, 463-466 (2004)

A. Yoshikawa, H. Ogino, J. B. Shim, M. Nikl, N. Solovieva and T. Fukuda: *Growth and luminescent properties of Yb^{3+}—doped oxide single crystals for scintillator application*. Rad. Meas. **38**, 467-470 (2004)

A. Novosselov, A. Yoshikawa, M. Nikl, N. Solovieva, J. -H. Lee and T. Fukuda: *Shaped crystal growth and scintillating properties of Yb:$(Gd,Lu)_3Ga_5O_{12}$ solid solutions*. Rad. Meas. **38**, 481-483 (2004)

H.Ogino, A.Yoshikawa, J.-H.Lee, M.Nikl, N.Solovieva and T.Fukuda: *Scintillation properties of Yb^{3+}-doped garnet crystals*. Rad. Meas. **38**, 485-488 (2004)

A. Bensalah, M. Nikl, E. Mihokova, N. Solovieva, A. Vedda, H. Sato, T. Fukuda and G. Boulon: *Excited-state dynamics of Yb^{2+} in $LiCaAlF_6$ single crystal*. Rad. Meas. **38**, 545-548 (2004)

A. Vedda, D. Di Martino, M. Martini, J. Mares, E. Mihokova, M. Nikl, N. Solovieva, K. Blazek and K. Nejezchleb: *Trap levels in Y-aluminum garnet scintillating crystals*. Rad. Meas. **38**, 673-676 (2004)

A.Yoshikawa, H.Ogino, J.B.Shim, V.V.Kochurikin, M.Nikl, N.Solovieva, S.Ono, N. Sarakura, M.Kikuchi, T.Fukuda: *Growth and scintillation properties of Yb-doped aluminate, vanade and silicite single crystals*. Opt. Mater. **26**, 529-534 (2004)

H.Ogino, A.Yoshikawa, J.-H.Lee, M.Nikl, N.Solovieva, T.Fukuda: *Growth and characterization of Yb^{3+} doped garnet crystals for scintillator application*. Opt. Mater. **26**, 535-539 (2004)

A. Vedda, N. Chiodini, D. Di Martino, M. Fasoli, M. Martini, F. Moretti, E. Rosetta, G. Spinolo, M. Nikl, N. Solovieva, A. Baraldi, R. Capelletti: *Luminescence properties of rare-earth ions in SiO_2 glasses prepared by the sol-gel method*. J. Non-Cryst. Sol. **345&346**, 338-342 (2004)

A. Vedda, N. Chiodini, D. Di Martino, M. Fasoli, S. Keffer, A. Lauria, M. Martini, F. Moretti, G. Spinolo, M. Nikl, N. Solovieva, G. Brambilla: *Ce^{3+}-doped fibers for remote radiation dosimetry*. App. Phys. Lett. **85**, 6356-6358 (2004)

M.Nikl, A.Yoshikawa, T.Satonaga, K.Kamada, H.Sato, N.Solovieva, A.Beitlerová, T.Fukuda: *Scintillation characteristics of PrF_3:Ce single crystal*. Phys. Stat. Sol.(a) **201**, No.14 (2004) R108-R110

K. Kamada, A. Yoshikawa, T. Satonaga, H. Sato, A. Beitlerova, M. Nikl, N. Solovieva, and T. Fukuda: *Growth and scintillation properties of Ce-doped PrF_3 single crystals*. Opto-electronics Review **12**, 365-368 (2004).

J.A. Mareš, A. Beitlerová, P. Bohacek, M. Nikl, N. Solovieva, C. D' Ambrosio: *Influence of non-stoichiometry and doping on scintillating response of $PbWO_4$ crystals.* Phys. Stat. Sol. (c) **2**, No. 1, 73-76 (2005)

J.A. Mareš, M. Nikl, A. Beitlerová, N. Solovieva, C D'Ambrosio, K. Blazek, P. Maly, K. Nejezchleb, P. Fabeni, G.P. Pazzi: *Ce^{3+}-doped scintillators: status and properties of (Y, Lu) aluminium perovskites and garnets.* Nucl. Instr. Meth. Phys. Research A **537** (2005) 271-275.

A. Novoselov, A. Yoshikava, M. Nikl, N. Solovieva, and T. Fukuda: *Study on shaped single growth and scintillating properties of Bi-doped rare-earth garnets.* Cryst. Res. Technol. **40** (2005) 419-423.

A. Novoselov, A. Yoshikawa, M. Nikl, N. Solovieva, T. Fukuda: *Shaped single crystal growth and scintillation properties of Bi:$Gd_3Ga_5O_{12}$.* Nucl. Instr. Meth. Phys. Research A **537** (2005) 247-250.

A. Vedda, N. Chiodini, D. Di Martino, M. Fasoli, M. Martini, A. Paleari, G. Spinolo, M. Nikl, N. Solovieva, A. Baraldi, and R. : *Rare-eart aggregates in sol-gel silica and their influence on optical properties.* Phys. Stat. Sol. (c) **2** (2005) 620-623.

A. Yoshikawa, M. Nikl, H. Ogino, J.B. Shim, V.V. Kochurikhin, N. Solovieva, T. Fukuda: *Crystal growth and luminescence properties of Yb-doped aluminate, gallate, phosphate and vanadate single crystals.* Nucl. Instr. Meth. Phys. Research A **537** (2005) 76-80.

P. Bohacek, N. Solovieva and M. Nikl, *Formation of absorption and emission centers in $PbWO_4$ surface layers induced by mechanical processing.* Phys. Stat.sol. (c) **2**, 81-84 (2005).

M. Nikl, N. Solovieva, K. Apperson, D.J.S. Birch, A. Voloshinovskii, *Scintillators based on aromatic dye molecules doped in a sol-gel glass host.* Appl. Phys. Letters **86**, 101914 (2005).

M.Nikl, K Kamada, A Yoshikawa, A Krasnikov, A Beitlerova, N Solovieva, J Hybler and T Fukuda. *Luminescence characteristics and energy transfer in the mixed $Y_xGd_{1-x}F_3$:Ce, Me (Me = Mg, Ca, Sr, Ba) crystals.* J. Phys.: Condens. Matter **18** 3069-3079 (2006).

Acknowledgements

This dissertation would not be possible without the help and support of many people.

First and foremost, I would like to express my deep gratitude to my supervisor, Dr. M. Nikl, for introducing me to the exciting field of scintillation glasses, welcoming me in his laboratory, and guiding me through the whole process of my dissertation research. His expert advice was indispensable. He has taught me many things that can be taught only through personal communication and by personal example. In particular, I have learned much from him about the organization of experiment and the presentation of research results.

I am also very grateful to my other academic advisor, Dr. J. Mareš, for the useful comments on the dissertation text, and for his kind help in solving many logistical issues that I had to face.

Next I would like to thank Dr. K. Nitsch, M. Rodová, and A. Cihlář, who prepared all the samples studied in this dissertation, and willingly assisted in establishing their chemical and physical properties. I am especially thankful to Dr. K. Nitsch for fruitful discussions. I am also grateful to Dr. M. Dušek for the computation of the structure parameters of $NaNd(PO_3)_4$ crystals, A. Beitlerová for the measurement of the absorption spectra, and J. Pejchal for various help in the laboratory. My gratitude is extended to all my colleagues from the Department of Optical Crystals, who supported and encouraged me on the long way to the completion of this dissertation. It was a pleasure to work in such a friendly and responsive team.

The experimental results reported in this dissertation were obtained within Czech and international research projects: NATO Science for Peace grant No. 973510-Scintillators (2000-2003), Projects No. A 2010304 (2003-2005) and IAA200100626 (2006-2008) of the Grant Agency of the Academy of Sciences of the Czech Republic. I am grateful to my colleagues from Estonia and Italy for their cooperation. Special thanks go to Dr. S. Zazubovich for the low temperature measurements, Dr. G.-P. Pazzi and Dr. P. Fabene for the measurements of the laser excited decay kinetics, and Dr. A. Vedda for the measurements of the TSL spectra.

I gratefully acknowledge the financial and organizational support that I received from the Czech Academy of Sciences and the Charles University in Prague.

Last, although not the least, I am thankful to my husband A. Tyutin for emotional support and his professional help in the statistical analysis of the experimental data.